LONG-TERM SENSING SYSTEM FOR BRIDGE PIERS

A Thesis presented to the Faculty of the Graduate School of the

University of Missouri – Columbia

In Partial Fulfillment of the Requirements for the Degree

Master of Science

By

MARY KATHRYN MASTERSON

Dr. Glenn Washer, Graduate Advisor

MAY 2009

The undersigned, appointed by the Dean of the Graduate School, have examined the thesis entitled

LONG-TERM SENSING SYSTEM FOR BRIDGE PIERS

Presented by Mary Kathryn Masterson,

A candidate for the degree of Master of Science,

And hereby certify that, in their opinion, it is worthy of acceptance.

_____

Professor Glenn Washer

_____

Professor Hani Salim

_____

Professor Steven Neal

ACKNOWLEDGEMENTS

First, I would like to thank my advisor, Dr. Glenn Washer, Assistant Professor of the Department of Civil and Environmental Engineering at the University of Missouri–Columbia. Dr. Washer's guidance and support has enabled me to have success with this project.

I would also like to thank Paul Fuchs of Fuchs Consulting Inc. His technical expertise and development of the data acquisition system was critical to this project. Thanks to Caleb Phillips, who worked hard on the initial stages of the project and enabled me to take over with ease. In addition, I would like to thank Rich Oberto for his patience and willingness to help get the project underway. Finally, thanks to Patrick Earney for the use of his temperature chamber and his programming expertise.

TABLE OF CONTENTS

LIST OF FIGURES

LIST OF TABLES

ABSTRACT

Structural instability of bridge piers resulting from scour or other natural hazards can lead to bridge collapse. As a result, a method of monitoring bridge piers is needed to evaluate long-term changes in structural conditions. This research project examines the use of an array of tilt sensors to monitor the structural behavior of bridge piers.

This thesis presents the results of efforts to design and test a tilt sensor system. Testing equipment, as well as sensor characterization, will be presented. In addition, the development of multi-sensor algorithms will be discussed, including the concepts of sensor consistency, sensor correlation, and fuzzy thresholds. Results from five laboratory tests of the multi-sensor system, including both pier rotation and superstructure displacement, will be explained. Lastly, the work remaining in the project will be discussed.

1: Introduction

1.1. Overview

Scour and other natural hazards have the potential to undermine the stability of highway bridges and the piers that support them. Hazards such as erosion and unexpected settlement can result in a loss of subsurface support. Unexpected superstructure behavior such as locked bearing can manifest in unexpected structural movements that can lead to bearing failures and even collapse. These effects have caused bridge collapse in the past. Significant efforts have been undertaken to address the potential danger of scour, and a number of scour monitoring devices have been developed to address this need (Schall, 2004). However, there remains a lack of reliable, cost-effective, long-term monitoring devices capable of monitoring the condition of bridge piers when other events, such as unexpected settlement or bearing conditions, occur. These events typically affect a bridge over a long time period, perhaps years, and separating these conditions from normal structural movements is challenging.

Tilt sensors have been proposed and are currently utilized in systems intended to monitor short term events, such as a scour event that occurs during a time of flooding (Richardson, 2003). These systems frequently include a limited number of tilt sensors, due to cost and other considerations. As a result, the systems lack redundancy, and the

measurement configurations assume rigid body rotations along a specific axis will occur. Thus, the systems may be incapable of identifying unusual structural motions, such as vertical displacement. For example, systems which utilize sensors located on the pier may not detect a movement in which the pier itself does not tilt, such as sinking of the entire structure due to settlement. In addition, a long-term gradual tilt may remain undetected or assumed to be sensor drift characteristics rather than actual structural movements.

In order to address these issues a long-term multiple sensor system has been developed. The concept of this system is to utilize an array of low cost tilt sensors, deployed on both the pier and the superstructure of the bridge, to monitor the stability of a bridge pier. The system is being developed to measure both changes in rotation (tilt) as well as vertical displacement of a pier, allowing for a more complete understanding of the behavior of the pier than is available using currently available technologies. The sensors are deployed in a high-density array, such that multiple sensor outputs can be integrated to eliminate erroneous readings, provide systematic sensor redundancy, and increase signal to noise ratios. Signal processing correlation algorithms are being developed that use sensor density and location to better measure and understand long-term bridge rotations and displacements. The system is intended to provide a tool for long-term asset management, allowing owners to monitor remotely the behavior of a bridge over many years, and provide notification if long-term structural motions are occurring that may lead to structural collapse.

This thesis will present the results of efforts to design and test the proposed tilt sensor system. The equipment utilized for the project will be discussed, with added detail

placed on the sensor selection and sensor characterization. In addition, the development of multi-sensor algorithms will be presented, including the concepts of sensor consistency, sensor correlation, and fuzzy thresholds. Results from five laboratory tests of the system, including both pier rotation and superstructure displacement, will be described. Lastly, the work remaining in the project will be discussed.

1.2. Goals and Objectives

The goal of the research presented in this thesis is to develop and test a tilt monitoring system capable of detecting long-term rotations and displacements of bridge piers. Objectives include:

- Select suitable sensors
- Integrate sensors into arrays on a test bridge
- Develop algorithms to measure tilt
    - Initial filtration
    - Calibration and temperature compensation
    - Movement computation
- Develop algorithms to integrate sensor outputs to capitalize on array configuration
    - Determination of sensor consistency
    - Sensor correlation
    - Critical movement identification
- Test algorithms to verify ability and accuracy of sensor system
    - Verification of effectiveness of multiple sensors

- Verification of accurate pier rotation identification
- Verification of 3-D pier rotation detection
- Verification of superstructure displacement detection
- Verification of effectiveness of embedding sensors

This thesis will present the results of efforts to achieve the goals of this research project. The algorithms and verification testing required will be discussed in detail, as well as the sensor selection, sensor characterization, testing equipment, and remaining work for the project.

2: Background

2.1. Pier Movements

The potential of scour to result in bridge collapse has been documented. Scour is the erosion of supporting soil beneath a bridge substructure. In fact, the most common cause of bridge failures is from floods scouring bed material from around bridge foundations (Richardson 2001). Figure 2-1 shows a typical scour situation.

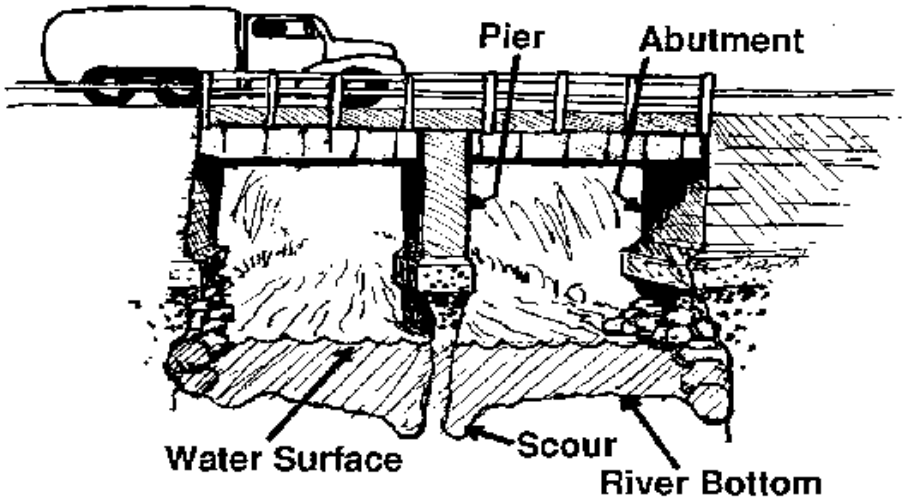

Figure 2-1. Typical scour beneath pier (Warren 2007).

Presently, there are more than 26,000 bridges in the U.S. identified as scour critical (Richardson 2003; Schall 2004). More than 3,700 bridges were damaged by scour during the period of 1985 to 1995 (Mueller 2005). There are several technologies available to

monitor the development of scour holes including both fixed and portable instruments (Schall 2004). Bridges over waterways are routinely evaluated to determine the risk of scour and mitigation practices, such as the installation of rip-rap, are applied to reduce the risk of scour development. Tilt monitoring devices to monitor the effects of scour on pier tilt have been applied in the field with some success. However, these systems are challenged by diurnal thermal effects, which can cause significant tilt of a pier under normal conditions. Additionally, the thermal effects on the sensor itself, which may be heating and cooling at a different rate than the pier it is monitoring, can result in uncertain and sometimes confusing results. Identifying critical movements of the pier in this environment can be challenging.

In addition to scour, tilting of piers can result from subsurface erosion or uncertain support conditions beneath a bridge pier. Unexpected settlement of bridge piers has occurred, resulting in a vertical settlement of the pier that may not be accompanied by tilt. In this case, a tilt system applied to the pier will not be capable of detecting the vertical motion, such that this critical motion may not be detected, even if the structure is under continuous monitoring. Additionally, vertical motion of a pier is difficult to detect with conventional instrumentation, and periodic survey of bridge elevation may be required to monitor this condition, greatly increasing inspection costs.

The effects of locked bridge bearings and expansion joints can manifest in pier displacements and tilt that can lead to the superstructure falling off of its bearings. In this case, the tilt of the piers may be occurring over long periods of time, several years in many cases. One example of such failure is the partial collapse of the Dunn Bridge Memorial Interchange on July 27, 2005 (NYSDOT 2005). The bridge, located in the city

of Albany, New York, experienced a partial collapse of the superstructure onto a pier. The rocker bearings that supported the superstructure and bore on the pier cap tipped, causing the collapse. This either caused or was caused by major deflection of a pier. After falling off the bearings, portions of the superstructure sheared the pedestal concrete and came to rest on the edge of a pier cap as shown in Figure 2-2.

Figure 2-2. Partial collapse of the Dunn Bridge in New York.

Special efforts are required to enable a monitoring system to recognize motions of this type, and to ensure that sensor failure that may occur over long monitoring periods do not undermine the ability of a system to recognize such changes in bridge condition. Bearings may also become misaligned due to thermal effects on the bridge and expansion joint behavior as shown in Figure 2-3.

Figure 2-3. Bearing misalignment.

Misaligned bearings exert lateral forces on the pier that were unanticipated in the design of the bridge, and may manifest in unexpected tilt of the pier. While these conditions may be stable over long time periods, a monitoring system that could recognize if this condition was progressing toward a potential collapse would be a useful tool for monitoring the health of the bridge.

2.2. Monitoring Systems

There are a significant number of technologies that have been developed to analyze the effects of natural hazards on pier foundations. Some of the technologies used for scour monitoring include sounding rods, fathometers and ground penetrating radar (GPR). Sounding rods consist of a rod with a large foot that rests on the streambed. As the streambed drops during a scour condition, so does the foot. This drop in height is

recorded to determine scour depth. Fathometers use seismic (acoustic) waves that propagate through the water. The time required for these waves to reflect off the streambed and travel back to the source provides a depth measurement if wave velocity in water is known. GPR uses electromagnetic signals that reflect from the interface of two different materials such as water and soil.

There are several reasons why the current scour monitoring systems are sometimes ineffective. These systems evaluate the potential causes of damage by detecting scour holes, but are not capable of determining if damage to the bridge pier has actually occurred. A large scour hole can develop without necessarily undermining the stability of the bridge pier. On the other hand, a small scour hole that may be undetected can cause structural instability under certain circumstances. Additionally, because many scour monitoring systems typically need to be partially submerged, these monitoring systems are susceptible to the high water flow and debris that is inevitable during a flood event. This can cause the systems to be damaged or destroyed at a time when their function is most critical. For these reasons, a system that can monitor structural behavior to determine any structural instability can have advantages over a system that detects scour.

Systems have also been developed to determine the tilt in bridge piers. These systems typically consist of very few, costly inclinometers. Because so few sensors are used, an overall structural behavior must be assumed with only the localized behavior measurements. This behavior may not be representative of the overall bridge pier. For this reason, the actual movements cannot be determined and rigid body behavior of the pier is assumed. The low number of sensors, typically placed on the pier alone, also

prevents the system from determining vertical pier displacement that may occur without significant tilt in the pier. In order to determine the vertical tilt of the structure, sensors would also need to be placed on the superstructure of the bridge to determine tilt in the bridge girders caused by vertical pier movement. Systems with a small number of sensors are also susceptible to deleterious effects from diurnal and seasonal temperature changes, sensor drift over long periods, and sensor failure.

Some states have used the measurement of tilt of an abutment or pier as an indication of scour conditions. A remote monitoring system consisting of inclinometers was tested on a bridge in California in 1999 (Marron 2000). This system consisted of two inclinometers mounted on each face of the pier, wired to a central data acquisition system that collected tilt data from each of the 18 piers on an hourly basis. This data was made available to State personnel by dialing into the system using the program *pc anywhere* (Marron 2000). Initial results from outputs of these sensors indicated that significant diurnal variations in inclinometer output were experienced, making interpretation of data difficult. A system that can compensate for these diurnal variations would make accurate interpretation of the structural behavior possible.

In addition to placing inclinometers on bridge piers, tiltmeters have also been used on a multistory underground parking structure in an effort to measure and understand structural movements (Iskander 2001). In this case, tiltmeters were mounted on walls where motion was expected, with the goal of converting tilt measurements to structural displacements. The temperature-dependant outputs of the tiltmeters resulted in significant scatter, and as a result, it was difficult to determine if the structural movements suggested by the data were actually occurring, or were simply temperature

effects. The authors also indicated that the relatively short monitoring time and small number of tiltmeters used in the project presented challenges in the analysis of data, and that all possible structural motions needed to be considered in an effective instrumentation plan (Iskander 2001). The effects of diurnal temperature variations on tiltmeter response was addressed by estimating temperature effects using a sine wave function, although this method has many limitations (Schuyler 2000). The fundamental problem is that the temperatures experienced by the sensors may be significantly different than the temperatures experienced within an instrumented structure. The thermal behavior of the sensors is dominated by the physical location of the sensor, i.e. in the sun, shade, adjacent to water etc. The thermal behavior of the structure is dominated by its tremendous mass, and as a result, the relationship between actual thermal movements and thermal behavior of the sensors is difficult to separate and model (Schuyler 2000).

These previous long-term monitoring systems have involved a limited number of tilt sensors on a pier and have not seen widespread use. A major shortcoming of this technique is the inability to detect the downward movement of a pier. For some cases, the downward movement of a pier undermined by scour may not be accompanied by tilt of the pier, or the tilt may occur between measurement periods. As a result, it is desirable to design a sensor system that is capable of measuring both the tilt of the piers and any vertical motion of the pier, i.e. settlement. The vertical displacement of a pier could be monitored using tilt sensors mounted on the superstructure of the bridge. Under this scenario, the relative displacement of a pier would result in overall tilt of the superstructure. This approach has been used in the past to monitor the effects of compaction grouting (Schuyler 2000). Again, temperature effects presented challenges to

this application, as noted above, and long-term measurements require a more sophisticated instrumentation scheme to become effective.

Another difficulty with previous implementations of tilt meters for structural monitoring is the high cost of the inclinometers used for determining the tilt of the structure. Due to the high cost of these precision sensors, a relatively small number of sensors have been used. As a result, the systems are susceptible to failure of a single sensor and have little redundancy to confirm sensor outputs through multiple measurements.

2.3. Project Approach

In order to address the issues presented in the previous section, the goal of this research project is to develop a long-term multiple sensor pier monitoring system. The concept of this system is to utilize an array of low cost tilt sensors, deployed on both the pier and the superstructure of the bridge as shown in Figure 2-4, to monitor the stability of a bridge pier.

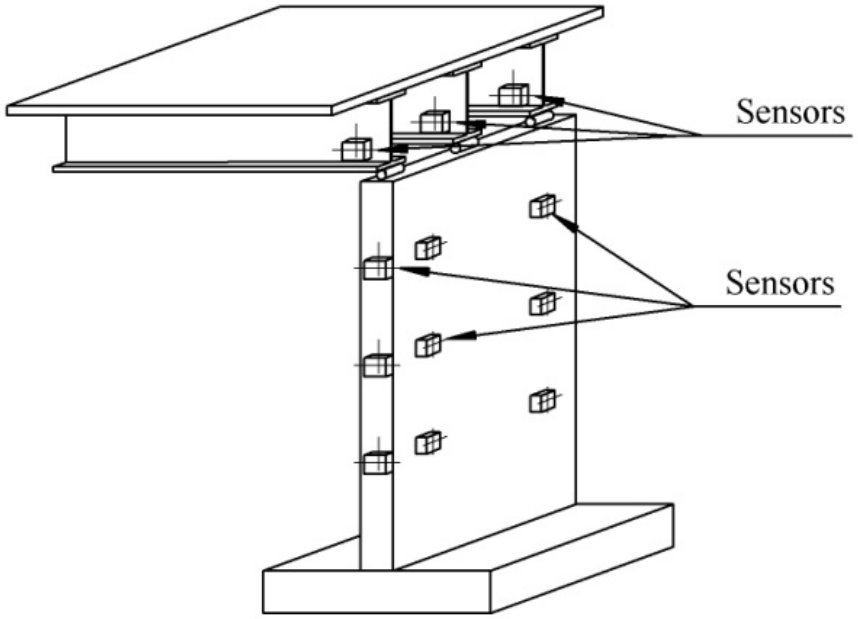

Figure 2-4. Schematic diagram of sensor system on a bridge.

The system was developed to measure both changes in rotation (tilt) as well as vertical displacement of a pier, allowing for a more complete understanding of the behavior of the pier than is available using currently available technologies. The sensors are deployed in a high-density array, such that multiple sensor outputs can be integrated to eliminate erroneous readings, provide systematic sensor redundancy, and increase signal to noise ratios. Signal processing correlation algorithms were developed that use sensor density and location to better measure and understand long-term bridge rotations and displacements. Laboratory testing was conducted in order to verify the ability and accuracy of the tilt monitoring system and the corresponding algorithms. Upon completion, the system will be implemented in the field on a bridge in New York State for final testing. The system is intended to provide a tool for long-term asset

management, allowing owners to monitor remotely the behavior of a bridge over many years, and provide notification if long-term structural motions are occurring that may lead to structural collapse.

3: Sensor Technology

3.1. Introduction

This section will provide an overview of the sensors chosen for the project. The selection of the sensors will be explained as well as the way in which the sensors operate. In addition, sensor characterization will be discussed, including calibration, temperature compensation, resolution, and noise classification.

3.2. Sensor Selection

A key component of the tilt monitoring system is the tilt sensors themselves. Ideal sensors for this application would be inexpensive, reliable, durable, and precise. The specific sensors chosen for this project are EZ-Tilt 3000 modules with DX-008 sensors. These sensors are manufactured by Advanced Orientation Systems Inc. (AOSI) and shown in Figure 3-1.

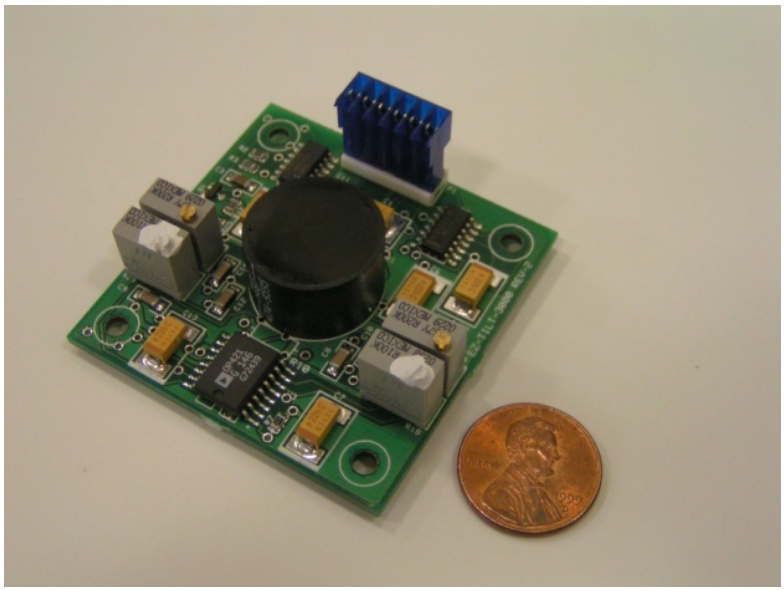

Figure 3-1. Photograph of an EZ-Tilt 3000 Module with a DX-008 Sensor.

This sensor provides a total range of +/- 20 arcdegrees, which includes a linear range of +/-8 arcdegrees. The large range allows for sensor placement without precision leveling of the module during the field installation process. The modules provide dual axis angle measurements with analog sensor outputs. The DX-008 sensor is a dual axis, five pin, electrolytic tilt sensor. The sensor, the black capsule in Figure 3-1, is designed to be removed from the module and mounted remotely in the field. In this way, the sensor can be directly grouted into a concrete structure, while the module is placed in an enclosure nearby. Mounting the sensor within a concrete structure allows the sensor to react in accordance to the structure with respect to temperature changes. A complete list of specifications for the sensor and module can be seen in Table 3-1.

Table 3-1. Specifications for EZ-TILT-3000 with a DX-008 Sensor.

Specification	Data	Description/units
RANGE	-20 to +20	Arcdeg monotonius
RANGE	-8 to +8	degrees Linear
SUPPLY	5 to 18	Vdc
CURRENT	2mA	@ 5Vdc Supply
RESPONSE TIME	40 mS	10% - 90% Output *#
NOISE	<1mVdc	Band Width 0Hz to 100Hz
LOAD (min. R)	3Kohm	On -X- and -Y- Outputs
REPEATABILITY	<0.02	arcdeg Typical
RESOLUTION	< 3 arcsec	Typical
SYMMETRY	<2% @4°	Typical
LINEARITY	<1% @ 8°	Typical
SENSING ELEMENT	Dual axis DX-008	(Included)
CONSTRUCTION	Shatter proof	Hi Temp Advanced Polymer
TEMPERATURE	-40 to +60	degC

3.3. Sensor Operation

Electrolytic tilt sensors produce precision measurements of tilt with respect to the gravity vector. The sensor operates on the principle that an enclosed bubble always orients its surface perpendicular to gravity. The bubble is enclosed within an electrolytic, or electrically conductive, fluid. As the enclosure tilts, the bubble orients itself with respect to the gravity vector as shown in Figure 3-2. A central pin conducts an alternating current between the outside four pins. Alternating current is necessary to prevent electrolysis of the sensor. The conductivity between the points is dependent upon the amount of fluid between them, and thus, an impedance variation results from the changes in the fluid level between pins. The changing angle of tilt produces an output voltage that is a function of the tilt angle of the sensor.

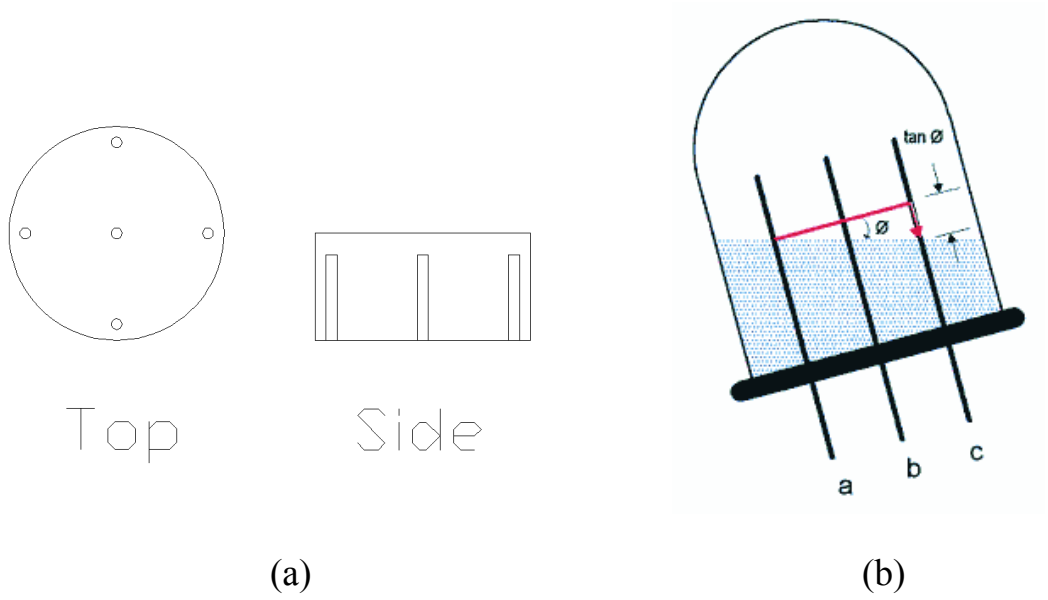

Figure 3-2. Diagrams of a five pin tilt sensor (a) and bubble orientation in electrolytic fluid (b) (Pheifer 2000).

3.4. Sensor Characterization

Initial laboratory testing was completed in order to characterize the electrolytic tilt sensors. Testing was completed in order to calibrate the sensors as well as determine temperature effects, resolution, and sensor noise. This section describes the initial testing of the sensors including the sensor characterization completed.

3.4.1 Calibration

The electrolytic tilt sensors output measurements in millivolts. In order to convert those measurements into degrees, the calibration factors for each axis of each sensor had to be determined.

Using the rotary stage shown in Figure 3-3, calibration of the sensors was completed by rotating each sensor in 23 arcminute (0.38°) increments through its linear range.

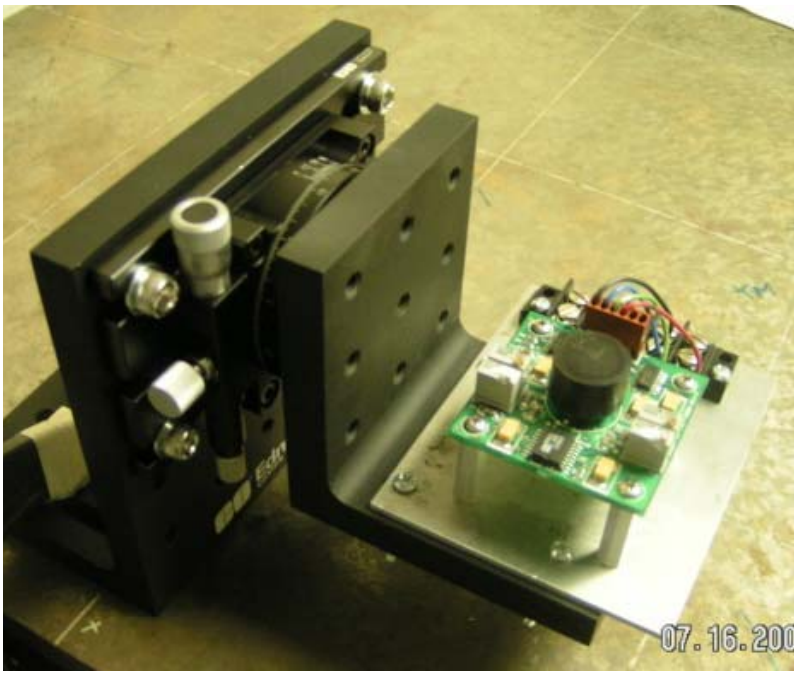

Figure 3-3. Photograph of rotary stage with mounted sensor used for sensor calibration.

The voltage output was recorded by a data acquisition system (to be described in Section 4.2.2), and calibration plots were created for each axis of the ten sensors. Figure 3-4 shows a typical calibration plot completed for one axis of an electrolytic tilt sensor. The figure shows the calibration data collected for the sensor for a portion of its linear range (~ ±5°). R^2 values for these calibration tests were typically greater than 0.99, thus showing the highly linear behavior of the electrolytic tilt sensors within the tested range. Similar calibration plots for both axes of all ten sensors can be seen in Appendix A – Calibration Numbers and Graphs.

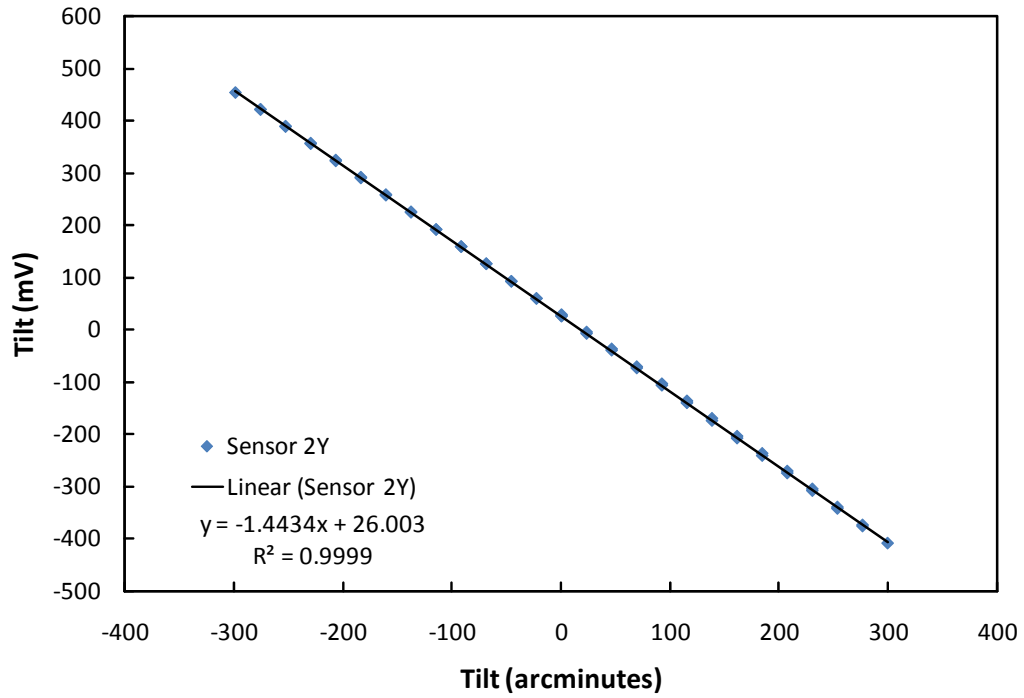

Figure 3-4. Graph showing calibration of Sensor 2, y-axis.

3.4.2 Temperature Effects

Along with calibration, tests have been run in order to determine temperature effects, specifically to verify the nominal temperature compensation factor. The temperature compensation factor accounts for the change in calibration factor as the temperature varies. The calibration factors for electrolytic tilt sensors vary linearly with temperature due to the changing viscosity of the fluid within the sensor. In order to verify this factor, a test was completed in which the rotary stage was placed in a temperature chamber as shown in Figure 3-5. While being kept at a constant temperature, the sensors were rotated through their linear range. This test was repeated at three different temperatures, 20°C, 30°C, and 40°C, in order to determine the calibration

factor at each temperature. The full set of data as well as calibration plots can be seen in Appendix B – Temperature Compensation Data.

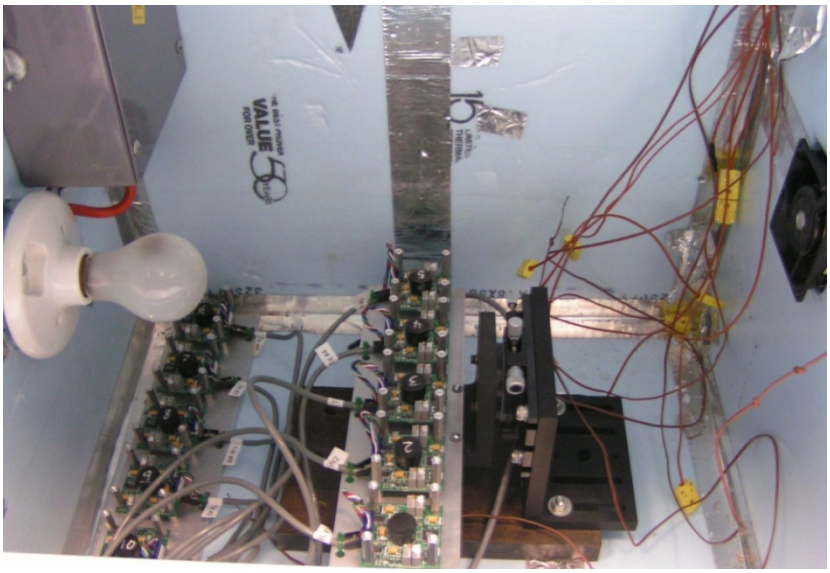

Figure 3-5. Photograph of set-up for temperature effects test.

The results for one axis of four sensors (Sensors 2 - 5) can be seen in Table 3-2. The first column of Table 3-2 specifies the sensor number, while the second column reports the original calibration factors determined in the lab at room temperature (22°C). The remaining columns present the calibration factors determined in the temperature chamber at their respective temperatures. These values were then compared with the expected calibration factors computed by applying the nominal temperature compensation factor of -0.08%/°C to the original calibration factors for each of the three temperatures. These expected values for each temperature are shown in Table 3-3. The error between the experimentally collected and the expected values was then computed, with the results shown in Table 3-4. As shown, the percent error ranges from 1% to 9%.

Because the error was found to be less than 10% in all cases, it was determined that the nominal temperature compensation factor of -0.08%/°C is acceptable for use in post-processing.

Table 3-2. Experimental calibration numbers (mV/min).

Table 3-3. Expected calibration numbers (mV/min).

Table 3-4. Percent Error in experimental calibration numbers.

	20 Degree Test	30 Degree Test	40 Degree Test
Sensor 2	3.95%	2.68%	2.77%
Sensor 3	8.38%	2.13%	1.66%
Sensor 4	4.14%	4.27%	5.82%
Sensor 5	9.21%	3.80%	4.01%

3.4.3 Resolution

The resolution of the system is dependent on several components, including the A/D converter, the test setup, and the sensors themselves. The specifications from the sensors report that the sensors have a resolution of less than 3 arcseconds. The A/D converter is capable of resolving 0.67 millivolts over a ten volt range. This is with a 13 bit conversion plus a differential measurement scheme, as reported by the manufacturer.

In the measurements from calibration, the data was collected over a ten arcdegree range, which covers nearly 1 volt and corresponds to approximately 1.5 millivolts/arcminute. If the A/D converter can resolve 0.67 millivolts and the calibration factor is 1.5 millivolts/arcminute, then there are 1.5 / 0.67 = 2.239 intervals per arcminute. This is equal to 26.8 arcseconds per interval as the max resolution of the A/D converter.

In order to determine the actual resolution, it was necessary to find the smallest change in tilt that the sensors could detect. This was done by conducting a test in which data was collected every 1.5 seconds. Five sensors were mounted on an aluminum plate and tilted with a rotary stage. The sensors were started at a five degree position, and then moved in 28 arcsecond intervals, which was the smallest interval possible with the rotary stage. The results of this test for one sensor are shown in Figure 3-6.

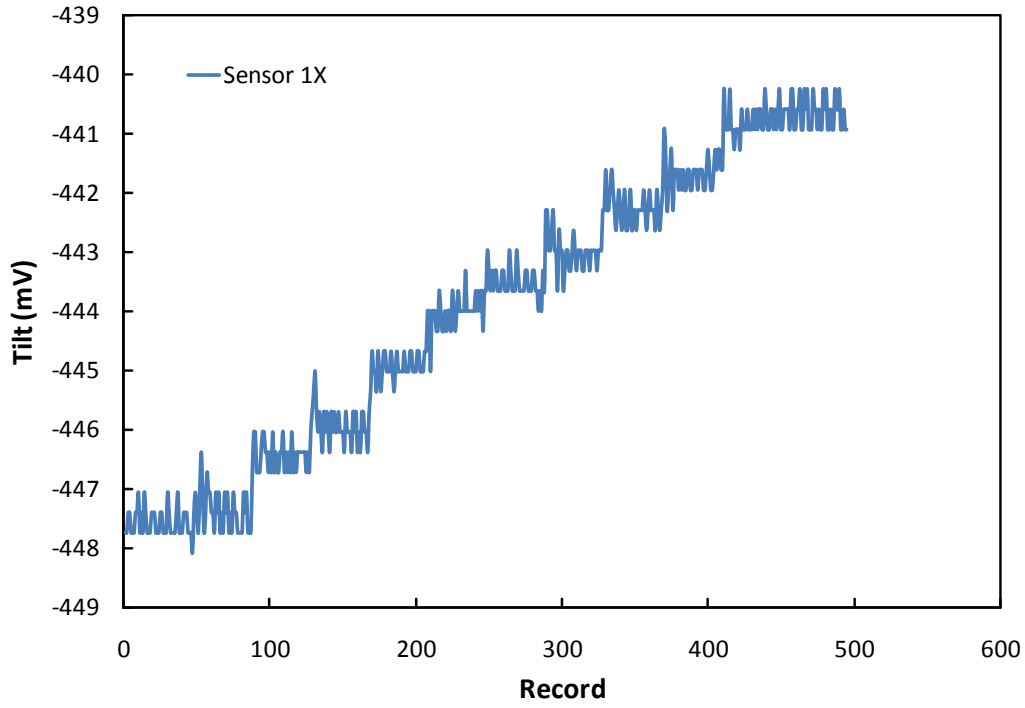

Figure 3-6. Graph of resolution test for x-axis of Sensor 1.

Looking at the data in Figure 3-6, the 28 arcsecond steps are easily identifiable. Thus, the resolution that was achieved in the laboratory, which was controlled by the test setup, was 28 arcseconds or 0.0077°. Although a smaller resolution may have been possible under different conditions, the resolution achieved is sufficient for this project's application.

3.4.4 Noise

Along with calibration and resolution testing, testing was also completed in order to identify types of noise. These tests consisted of leaving the sensors stationary for an extended period of time in a configuration shown in Figure 3-7.

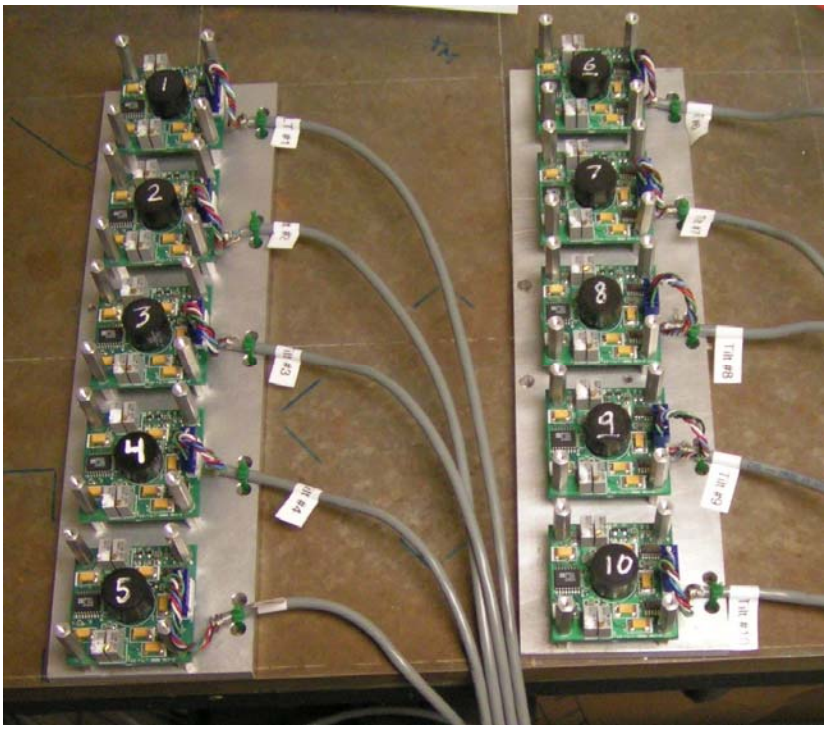

Figure 3-7. Setup for stationary noise tests.

Figure 3-8 shows the results from one axis of one sensor and exhibits the two types of noise experienced.

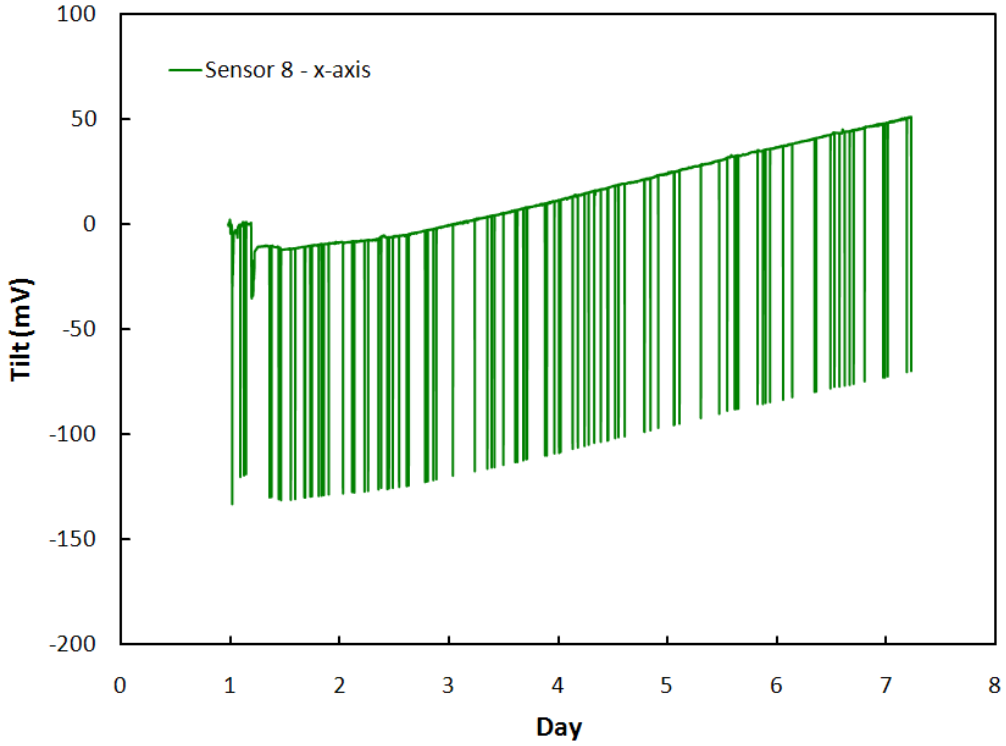

Figure 3-8. Results from Sensor 8 x-axis for stationary noise test.

Figure 3-8 shows the voltage output from the x-axis of Sensor 8 during a stationary test. The motion displayed in the graph consists of two types of noise. One type of noise seen in the voltage output is the interment noise spikes, which in this case look like 100 mV jumps. It has been determined that this noise is due to intermittent data collection errors and will be eliminated in the field system. The second and more important type of noise displayed in Figure 3-8 is the drift. As shown, the voltage steadily increases from 0 mV to around 50 mV over the course of 7 days. More extensive drift data can be seen in Appendix C – Data from Stationary Drift Tests. Appendix C contains the drift per day results from a 13 day stationary drift test. This drift could become a major issue when

trying to identify small movements that have occurred over a long period of time; for, the actual movement of the pier may be similar to the drift. This issue was addressed in post-processing algorithms discussed in Section 4.3.

3.5. Conclusion

Sensor selection and characterization was an important part of the project. It was necessary to choose appropriate sensors and conduct initial testing in order to determine calibration factors, verify temperature compensation factors, determine resolution, and quantify noise levels. Once completed, the sensors were used in laboratory testing in order to develop and test the multi-sensor monitoring system.

4: Experimental

4.1. Introduction

The following sections will explain the laboratory equipment used for testing the tilt monitoring system. This section also discusses in detail the algorithms developed for post-processing of the sensors' dual axis tilt output. The method for combining the outputs from sensor arrays will be presented, as well as the fuzzy thresholds utilized for movement identification. Along with algorithm development, five laboratory tests aimed to verify the system will be discussed.

4.2. Project Equipment

The equipment needed for development and laboratory testing of a tilt monitoring system includes three things, sensors, a data acquisition system, and a test bridge. The sensors chosen have already been discussed in a previous section. This section will describe the data acquisition system developed to collect data from the sensors as well as the test bridge constructed on which to test the sensor system.

4.2.1 Sensors

The sensors used for the system are dual axis, electrolytic tilt sensors. The selection and specifications for the sensors was discussed in Section 3.

4.2.2 Data Acquisition System

Laboratory testing has been conducted using a custom-designed 32 channel data acquisition system developed by Fuchs Consulting, Inc. (FCI). A photograph of the instrument is shown in Figure 4-1. The system supplies the power to the tilt sensors, logs the output from the sensors at a specified rate, provides temperature measurements, and offers a computer interface for analyzing data.

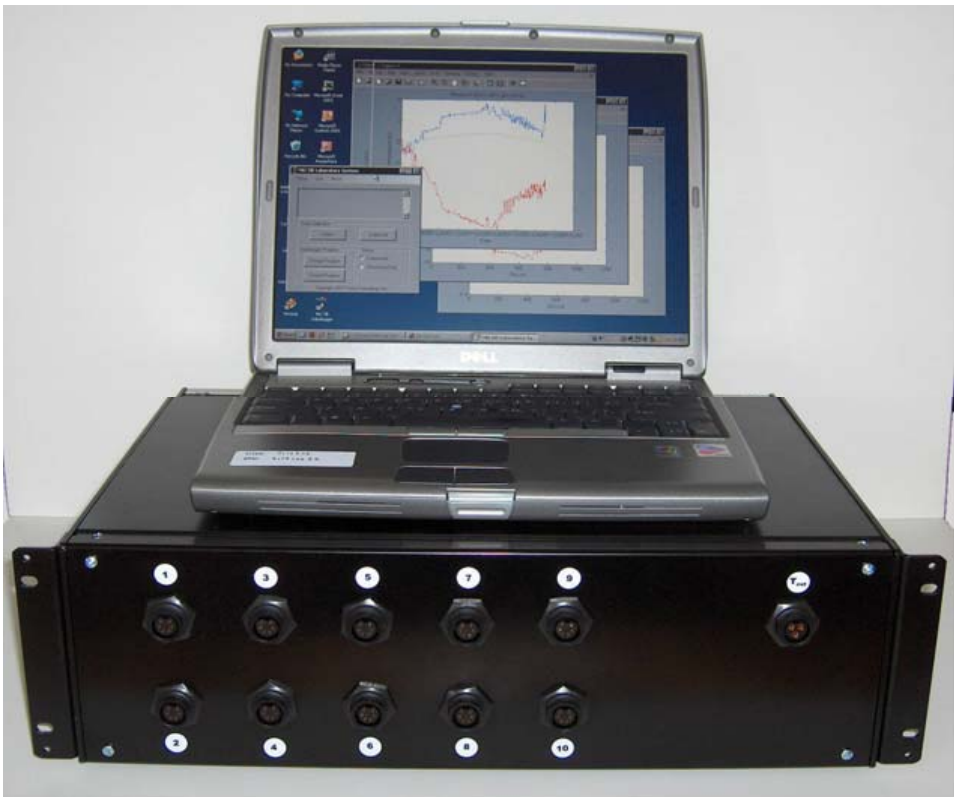

Figure 4-1. Photograph of data acquisition system.

The 32 channels of data consist of the x-axis, y-axis, and temperature output from each of the ten sensors, as well as an internal and external temperature of the system. Included with the system were 20 ft sensor cables with connectors for the tilt modules and a 20 ft temperature sensor cable with a temperature sensor. Associated software was also designed by FCI. This software allows the user to collect data at various rates. These data collection rates range from as fast as every 1.5 seconds to every 120 minutes. The collected data is stored in a stand-alone mode within the instrument, which is independent of an external computer.

4.2.3 Test Bridge

In order to test the sensors and data acquisition system in the lab, a test bridge has been designed and constructed on which the sensors can be mounted. A photograph of the bridge can be seen in Figure 4-2. Both the pier and three girder lines are composed of extruded aluminum parts from 80/20™ Inc. The pier has a triangular base with three spring-loaded feet containing wing nuts that can be adjusted to tilt the pier in all directions as shown in Figure 4-3(a). Testing has been completed in order to calibrate the turning of the wing nuts with respect to the actual tilt of the pier in two dimensions. It is estimated that the test bridge can be tilted within a tolerance of $1/8^{th}$ turn of a wing nut or ±0.0132°.

Figure 4-2. Photograph of test bridge.

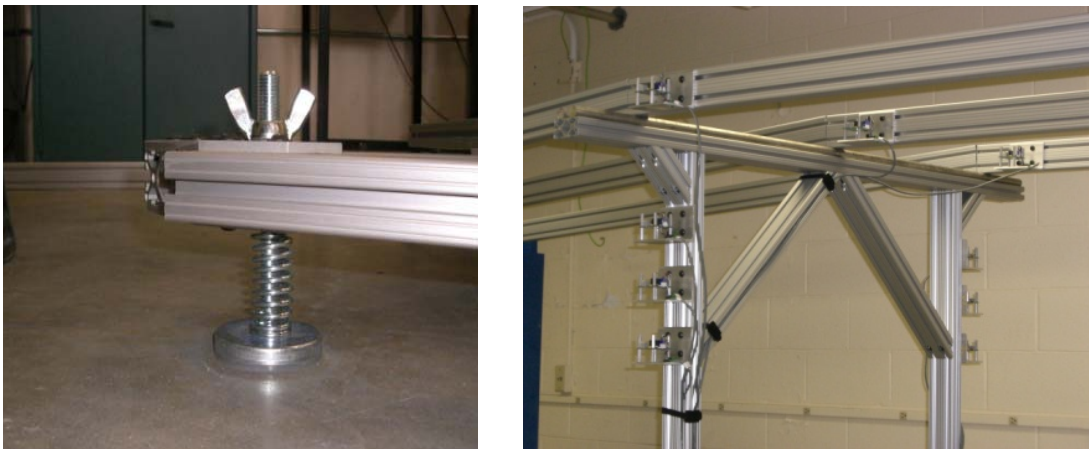

(a) **(b)**

Figure 4-3. Photograph of spring-loaded feet (a) and sensors mounted on test bridge (b).

The test bridge is designed in order to mount the sensors in three arrays, one on each side of the pier and one on the superstructure as shown in Figure 4-3(b). For laboratory testing the sensors are mounted to aluminum brackets with standoff and plastic washers. A close-up of the sensor mount is shown in Figure 4-4.

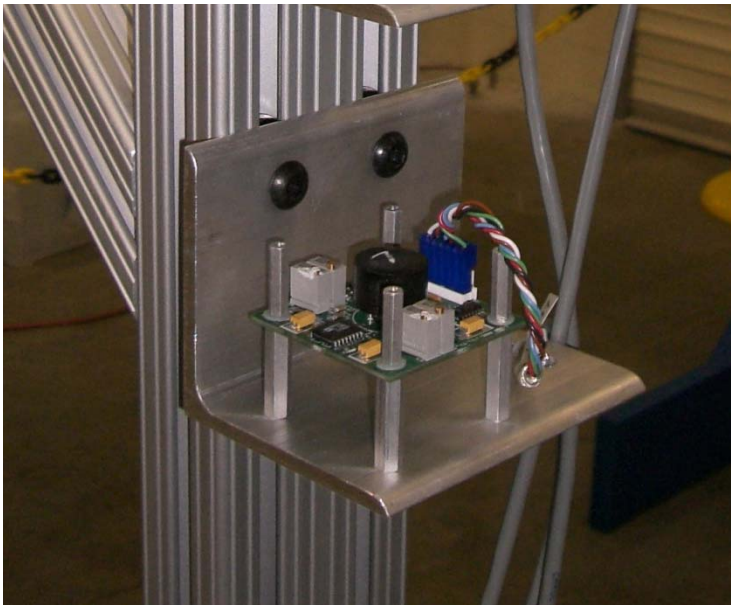

Figure 4-4. Photograph of sensor mount on test bridge.

4.3. Algorithm Development

One aspect of this system that sets it apart from currently available monitoring systems is the use of multiple sensors. The use of multiple sensors allows one to achieve measurement redundancy, increase signal to noise ratios, identify inconsistent sensors, and utilize signal correlation to better define overall movements. These areas were the focus of algorithm development. Numerous algorithms were developed, programmed and tested. Algorithms have been developed to achieve the following: initial filtration, calibration and temperature compensation, movement computation, determination of sensor consistency, sensor correlation, and critical movement identification.

In order to program the above mentioned algorithms, a combination of constant and fuzzy thresholds has been utilized. Constant thresholds, those that are independent of the data to which they are applied, are used to determine sensor consistency, while fuzzy thresholds, those that vary depending on the data to which they are applied, are used as an initial filter as well as to identify critical movements. Here, critical movements are identified as those that are unusual or do not follow the normal pattern of the data. In this way, critical movements can be distinguished from normally occurring motion from temperature variations. In addition, movement computation has been completed using vector comparison. A method of averaging allows the program to compute the overall movement of the bridge based on the outputs of the sensor arrays. Overall, the program is capable of taking the raw data from the data acquisition system, filtering it, converting it to degrees, computing the change in tilt for each sensor over six different time periods, determining if sensor outputs are consistent, combining sensor array outputs, computing

overall movements of the bridge pier and superstructure, and ultimately, identifying critical movements of both the pier and superstructure.

4.3.1 Initial Filtration

To address potential noise sources or error in field measurements, an initial filter has been developed that screens raw data for errant noise spikes that may occur across all data channels. If left untreated, these noise spikes may cause inaccurate movements to be calculated in future post-processing. The filter is immediately applied to the raw data during post-processing. The data file from the data acquisition system consists of 32 channels, including 2 axes of tilt and 1 temperature output for each of 10 sensors as well as an internal and external temperature reading. The initial filter has been developed to address errant readings that are consistent among all of the channels. As a result, the filter is designed to consider only one of the 32 channels for filtering. This channel may be a temperature or tilt channel, and is typically chosen as the channel with the most consistent data whose noise spikes deviate far from the mean. Errant data points that occur in individual channels are addressed in algorithms to test sensor consistency within the sensor array, as described in a later section.

The filter was developed by utilizing the "3 Sigma Edit Rule" in which an outlier in a data set is that which deviates more than three times the standard deviation from the mean of the set. In order to increase the filter's ability to detect multiple outliers, thus making it more robust, the Hampel identifier was added (Näsi, 2005). This method

replaces the mean with the median, and the standard deviation with the median absolute deviation from the median.

Another important aspect of the filter is the amount of data considered. In order to account for potentially variable data, the filter considers only the nearest points when computing the median and median absolute deviation from the median. Thus, the filter is able to account for large variations in the data, such as may occur with diurnal temperature variations, and still accurately detect outliers. Detected outliers are then replaced in the data set using a median value from nearby points.

In order to show the effectiveness of the filter, the following figure contains direct output from the initial filter applied to a temperature channel. In this case, approximately 10% of the data are noise points generated from intermittent data collection errors.

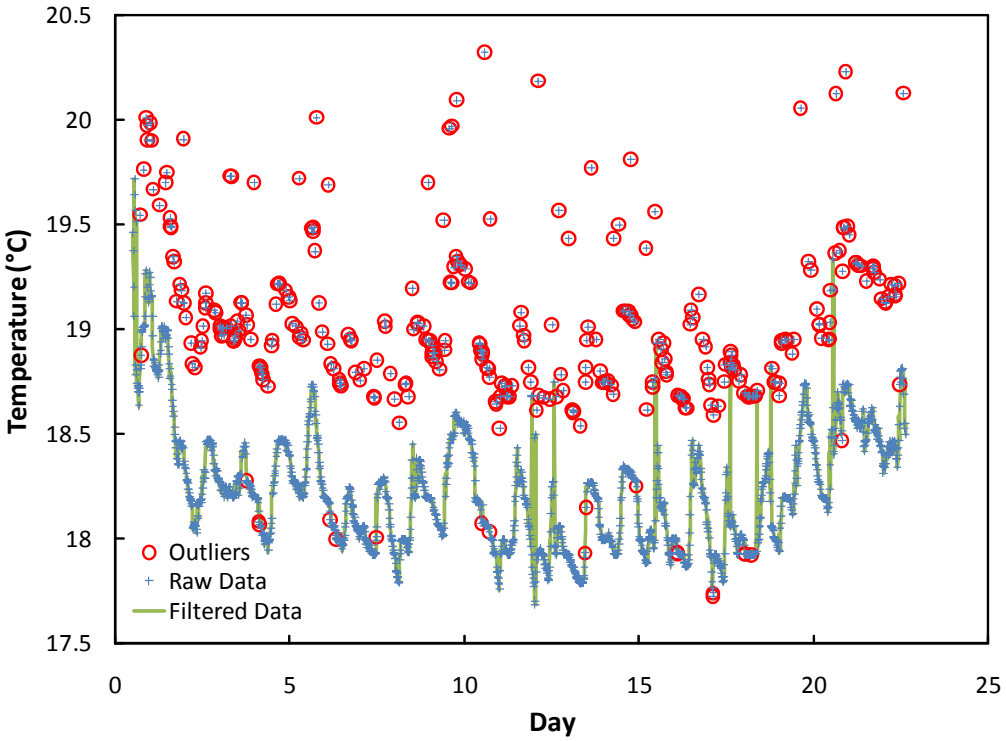

Figure 4-5. Results from initial filter applied to temperature output.

Figure 4-5 shows the results of the filter on a set of data collected over the course of three weeks in which the temperature varied daily. As shown with the red circles, the filter detects the errant points and replaces them with median points. The green line represents the filtered data set. The filter has been shown to detect more than 95% of the noise spikes. In this way, the noise spikes are eliminated, thus reducing inaccurate movement calculations in future post-processing.

4.3.2 Calibration & Temperature Compensation

Along with the initial filter, algorithms have been developed to convert the raw voltage output of the sensors to angular measurements in degrees. Included in this conversion are the calibration scale factors, the temperature at calibration, and the temperature compensation factors determined during sensor characterization. These factors can be seen in Table 4-1.

Table 4-1. Calibration factors and the sensor temperatures during calibration.

Sensor	mV/degree		Temperature (°C)	
	X	Y	X	Y
1	94.07	90.94	18.0	20.9
2	95.31	86.61	19.0	21.1
3	91.47	94.56	17.4	21.0
4	93.67	86.89	17.7	21.0
5	99.66	103.97	18.3	21.5
6	91.98	89.78	18.2	21.4
7	91.13	91.98	18.6	21.1
8	73.99	96.88	18.0	21.4
9	98.30	92.09	18.4	21.2
10	90.62	90.16	18.0	21.2

Table 4-1 reports the calibration factors as well as the temperatures recorded at the time of the calibration. These values are used with the temperature compensation factor of -0.08%/°C. In order to use these factors to convert the sensors' voltage output into degrees, equation (1) was used ("Tiltmeter" 2008).

$$S = S_{cal}[1+K_S(T-T_{cal})] \quad (1)$$
$$\theta = V/S$$

where S_{cal} = Calibration factor, mV/degree
K_S = Temperature compensation factor
T_{cal} = Temperature at calibration, °C
T = Temperature at time of measurement, °C
S = Temperature compensated calibration factor, mV/degree
V = Sensor output, mV
θ = True tilt angle, degrees

4.3.3 Movement Computation

One of the goals of this project is to develop a system that can detect long term movements, in addition to short term movements. In order to do this, a method was developed in which the change in tilt is computed over several different time periods. In order to detect instantaneous movements or movements that occur quickly such as scour events, short time periods are used. On the other hand, in order to monitor long-term gradual movements or tilt that occurs gradually over a period of months due to subsurface erosion or locked bearings, longer time periods are utilized. In this way, the system will be sensitive to both instant and gradual tilts. Algorithms have been completed to assess tilt data over 1 hr, 12 hrs, 24 hrs, 7 days, 28 days and 90 days.

In order to determine the magnitude and direction of pier movements, the programmed algorithms compute the change in tilt over a set time integral using vector comparison. The output from the x and y axis of each sensor is used to compute two 2-dimensional unit vectors in the x-z and y-z directions, respectively. These unit vectors are then translated 90° so that they lie within the plane of the base of the sensor module. Once completed, the normal vector to the module base is determined by computing the cross product of the two unit vectors. Figure 4-6 and equation (2) show how this is completed.

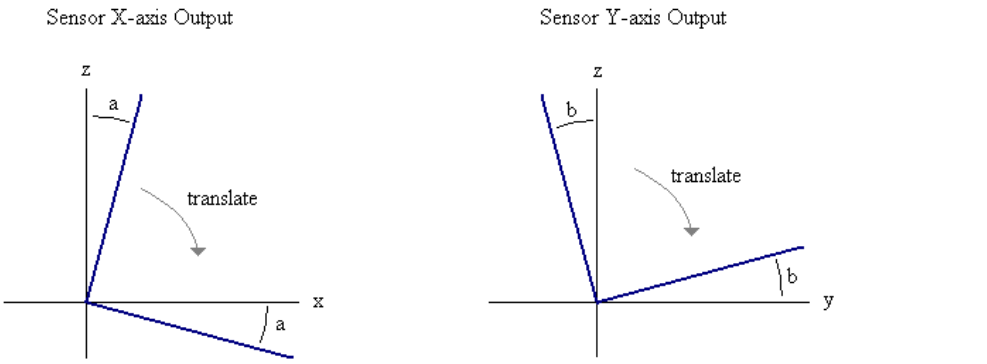

a ≡ tilt output for x-axis (degrees)
$x_a = \cos(a)$
$y_a = 0$
$z_a = \sin(a)$

b ≡ tilt output for y-axis (degrees)
$x_b = 0$
$y_b = \cos(b)$
$z_b = \sin(b)$

Figure 4-6. Method for converting sensor output into unit vectors.

$$\text{normal vector} = n1 = \begin{bmatrix} i & j & k \\ x_a & y_a & z_a \\ x_b & y_b & z_b \end{bmatrix} \quad (2)$$

With equation (2), the 3-dimensional vector normal to the sensor module is computed, which completely describes the orientation of the sensor. This process is repeated for

each data point in time. To determine the movement over a set time period, a normal vector from the beginning of the time period, n1, is compared to that from the end of the time period, n2. The angle between the two normal vectors is computed based on equation (3).

$$\cos\theta = \frac{n1 \bullet n2}{|n1||n2|} \tag{3}$$

Thus the resulting angle is the magnitude of the change in tilt over that time period in degrees. In addition, the direction of that movement is also computed. The file is programmed to compute the change in tilt over each of the time integrals under consideration.

4.3.4 Sensor Consistency

The use of multiple sensors allows for invalid sensor measurements to be identified and excluded from post-processing. In this way, a sensor can malfunction without jeopardizing the entire system, and users can be notified of the sensor failure without having to monitor system performance on a daily basis. This concept differs from currently available technologies, which count on individual sensors to report accurate data at all times.

The system was assembled in the laboratory such that Sensors 2, 3, and 4 form an array (A) on one side of the pier, while Sensors 5, 6, and 7 form an array (B) on the

opposite side, and sensor 8, 9 and 10 form array C on the superstructure, as shown schematically in Figure 4-7.

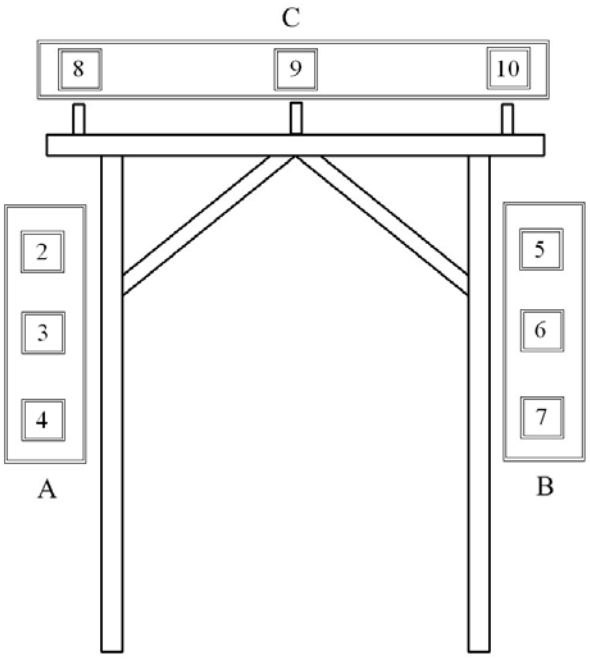

Figure 4-7. Diagram of sensor array configuration.

The sensors are configured in this way so that each side of the pier has three sensors mounted directly on the test bridge to achieve sensor redundancy. Because of this, each set of three sensors can be considered in order to pinpoint an errant sensor. By comparing the outputs from the sensors within a particular array, a dissimilar output can be detected and disregarded.

The algorithms developed first check for errant readings in each sensor individually. Once each sensor is checked individually, sets of sensors are considered. Within each array, an average movement is determined for each record. Each sensor's tilt movement is then compared with that average. If any movement varies more than a set threshold from that average, a sensor inconsistency exists. The output furthest from

the average belongs to the inconsistent sensor. If a sensor is shown to be inconsistent, its output is excluded in future post-processing for that record.

In the case that a sensor is deemed inconsistent and its output is disregarded, the program checks the remaining sensors in the array in order to ensure consistency between them. This method is repeated for each record, and if another inconsistency is detected a message is sent to the user stating that the sensors in the array are inconsistent and further review is necessary.

Figure 4-8 shows direct output in which one sensor in the array is inconsistent.

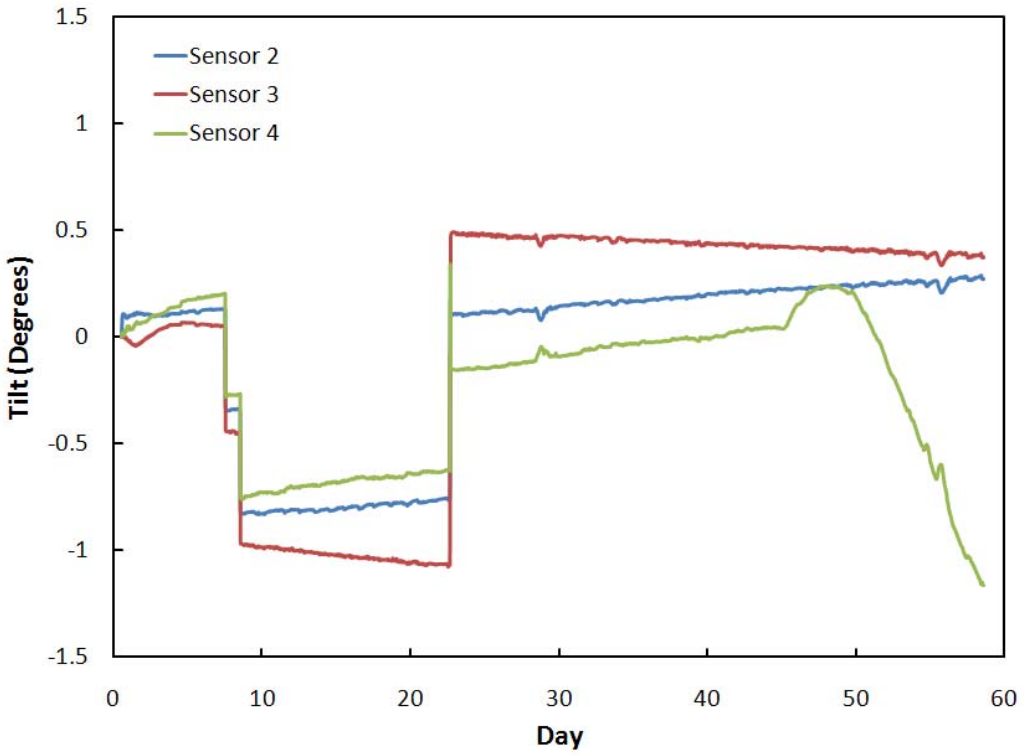

Figure 4-8. Example of data in which Sensor 4 becomes inconsistent.

Figure 4-8 shows the zeroed y-axis output from one array of sensors. During this test, the test bridge was tilted three times resulting in the three jumps shown in the figure. As

shown, Sensor 4 unexpectedly began to output irregular data after Day 45. The algorithms detect that irregularity and a message is given to the user reporting that Sensor 4 is inconsistent at each point after Day 45. Thus, the output from Sensor 4 will be disregarded for those records in further processing. Although the sensor failure is not desired, it is important to know that due to sensor redundancy in the system, the failure of Sensor 4 will not cause a loss in the effectiveness of the system.

Once all inconsistencies are identified, the remaining sensors in the array are averaged in order to determine one value for the movement of the array. This process is completed for each record of each array. Thus, once this portion of the program is completed, one value of tilt movement for each array remains for each time step. These values can then be used for sensor correlation.

4.3.5 Sensor Correlation

While sensor consistency algorithms were developed to identify inconsistent sensors, sensor correlation algorithms were developed to more accurately interpret the movement of the pier. Here, the concept of signal correlation is used both as a check of sensor outputs as well as a tool to more thoroughly model the behavior of the pier. The system is designed with two sensor arrays, one on each side of the pier. Once the movement for each array of sensors is determined through sensor consistency, sensor correlation is used to compare these values and combine them into an overall movement of the bridge pier with respect to a universal coordinate system.

In order to ensure consistency between the arrays, a method is used in which the difference between the two array outputs is computed and compared to a predetermined threshold. If above the threshold, the arrays are deemed inconsistent. Each inconsistency is reported to the user so that further review can be completed if necessary.

Once the arrays are shown to be consistent with one another, they are combined to determine an overall movement of the bridge pier. To do this, the magnitude of the movement from each array is averaged. In addition, the directions from each array are transformed to a universal coordinate system and averaged. Thus, an overall direction of the tilt of the pier is recorded for each time step as well as the magnitude of that movement.

4.3.6 Critical Movement Identification

The final aspect of algorithm development is identifying critical movements. Due to diurnal temperature changes, a bridge typically experiences some tilt daily. The goal is to isolate movements that are unusual or do not follow the normal pattern that the bridge experiences. Because the system computes movements over six different time periods, different methods of identifying critical movements are necessary. For the shorter time periods of 1 hour, 12 hours, and 1 day, instantaneous movements will appear as spikes in the movement data. In order to do detect these, a method of applying a fuzzy threshold has been utilized. The method is similar to that in "Sensor Validation and Outlier Detection Using Fuzzy Limits" by Jari Näsi, Aki Sorsa, and Kauko Leiviskä. The algorithms entail the application of a fuzzy threshold to the overall pier movements

determined during the sensor correlation portion of the program. For each record, the appropriate threshold is computed based on neighboring points of pier movement data. The threshold for each record is set as the median plus three times the modified standard deviation. The modified standard deviation is computed based on equation (4).

$$\sigma_m = \sqrt{\frac{1}{N}\sum_{i=1}^{N} \alpha\left(x_i - m\right)^2} \tag{4}$$

where $\alpha = e^{-a\left(b(x_i - m)\right)^2}$, a = 0.5, b = 50, N = 48, $m = \frac{1}{n}\sum_{i=1}^{n} x_i$.

Upon the application of this threshold, outliers are detected. In order to determine if the detected outlier is an actual movement rather than a noise spike, the direction of the movement is considered. The direction of the movement is recorded as a unit vector. Due to the combination of six sensors in order to determine the overall pier movement, if the movement is a noise spike, the recorded direction will not be valid. In other words, the resultant direction will not be of magnitude 1.0. If the detected movement is an actual movement, the resultant direction will be close to 1.0, thus making it a valid direction. In this way, critical movements are detected for the shorter time period programs for both the pier and the superstructure.

When a critical movement is detected and verified by the direction, it is reported to the user. Figure 4-9 shows the fuzzy threshold being applied to pier movement data from the 1hr program.

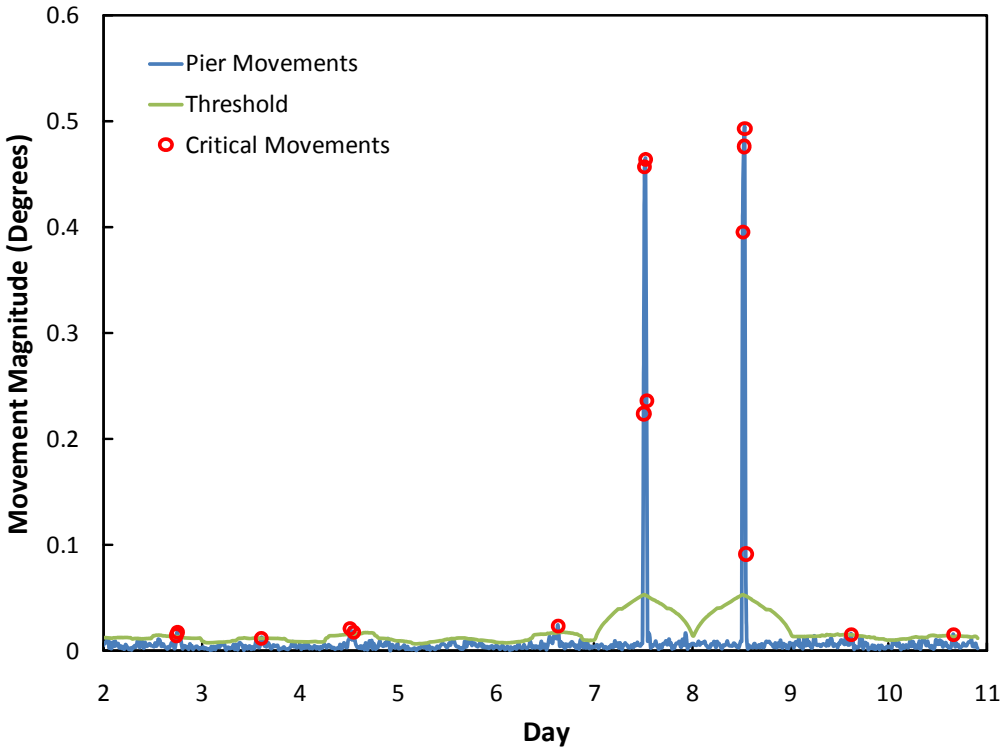

Figure 4-9. Application of fuzzy threshold on data in which 2 movements occurred.

Figure 4-9 shows the results from a test in which the bridge pier was moved twice in 0.529° ± 0.013° increments along the y-direction of the bridge. The blue line represents the overall pier movement magnitudes computed over a 1 hour time period for each record, while the green line is the applied fuzzy threshold. The red circles are those points that were detected as outliers with the threshold, and whose directions will be checked for validity. Upon this check, the following message is reported to the user.

> Critical movement occurred for a 1 hour period at..01-14-2008 12:30:00
> Pier moved..0.45214 degrees in the direction x=-0.063271, y=-0.99351
> Critical movement occurred for a 1 hour period at..01-15-2008 12:45:00
> Pier moved..0.46542 degrees in the direction x=-0.070703, y=-0.99683

Thus the program effectively detected to the two movements that the bridge pier experienced during this test.

For longer time periods, diurnal variations will not be evident in the data and gradual movements will not appear as spikes, but rather as gradual increases in movement magnitude. As a result, constant thresholds can be used based on tolerable movements for bridge piers. According to the *Manuals for the Design of Bridge Foundations,* horizontal movements of 2 in. and vertical settlements of 4 in. are "usually intolerable" to bridge structures (Barker 1991). For the test bridge, a horizontal movement of 2 in. at the pier base corresponds with a pier tilt of 1.8°. In addition, a vertical settlement of 4 in. corresponds to a superstructure tilt of 2.6°. Thus, the constant thresholds used for the critical movement identification algorithms for the system located on the test bridge are set at 1.8° for the pier and 2.6° for the superstructure. These thresholds are bridge specific, and will have to be determined for each bridge structure on an individual basis. Once the constant thresholds are applied to the movement data, critical movements are identified and validated the same way as with the shorter time periods.

4.3.7 Algorithm Summary

The previous sections discussed the algorithms that were developed in order to process the data from the sensors. In order to summarize these algorithms, this section will present one set of data, and show how it goes from raw data to final results. The data used was collected over the course of 10 days and contains several pier movements.

The first step in post-processing is to filter the data to removed errant data spikes. Figure 4-10 shows the results of the filter applied to one of the tilt channels.

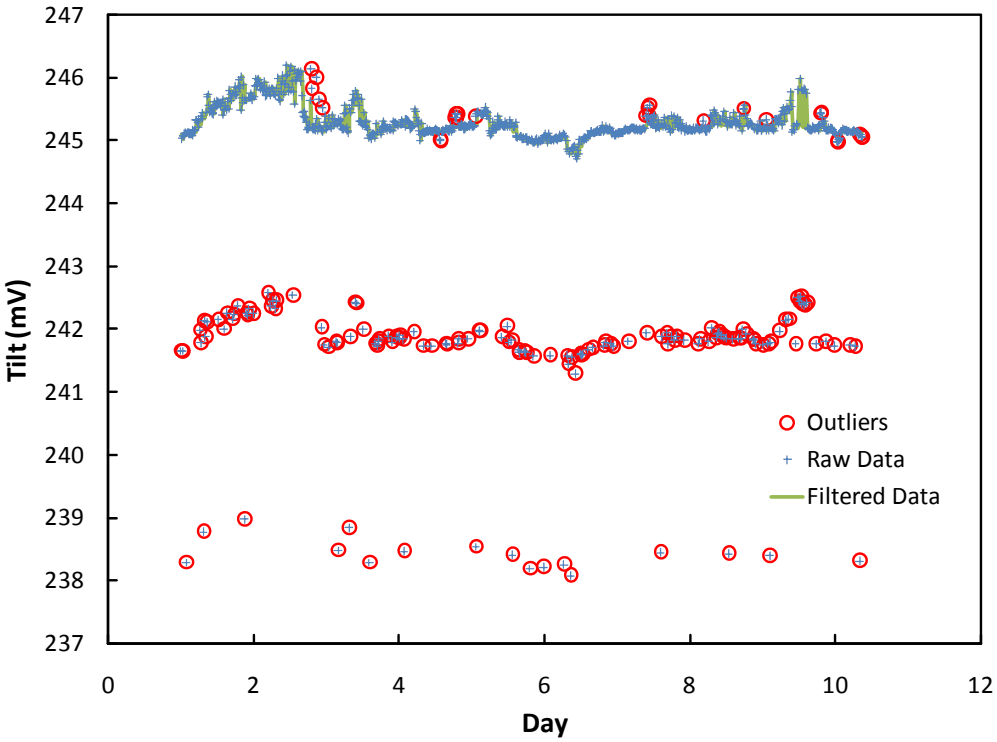

Figure 4-10. Results from initial filter applied to data set.

Figure 4-10 shows the results of the filter being applied to one axis of one sensor. Because the errant data points are consistent among all of the data channels, these errant points are identified in one channel and removed from all.

The data is then converted from millivolts to degrees with the calibration and temperature compensation algorithms. The converted data is shown in Figure 4-11.

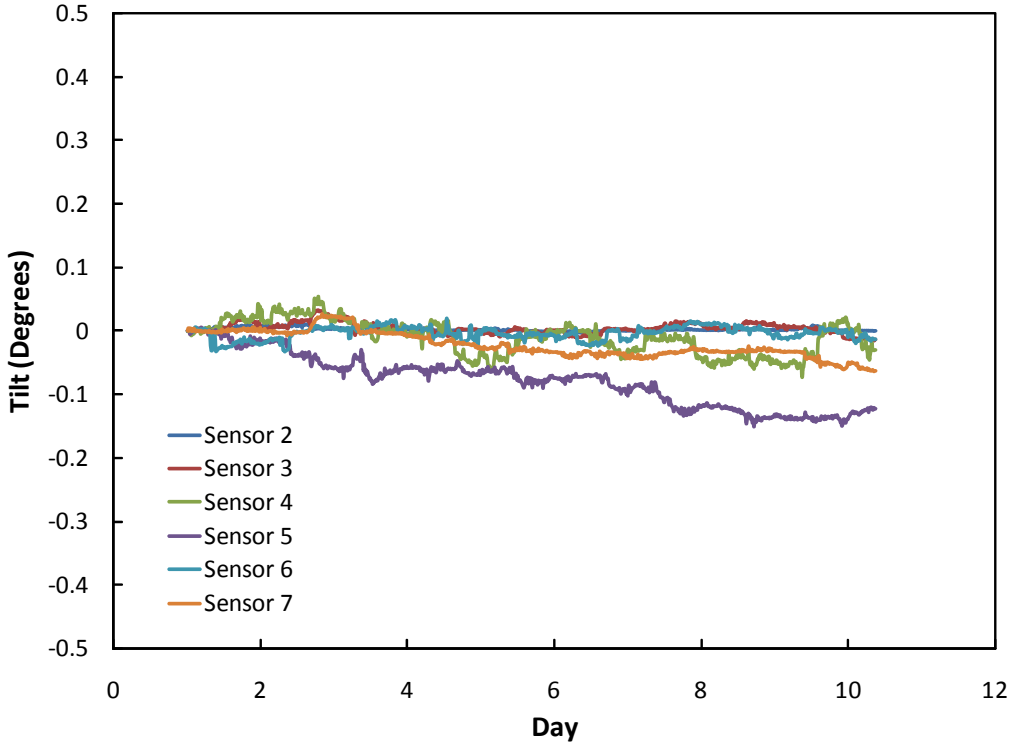

(a)

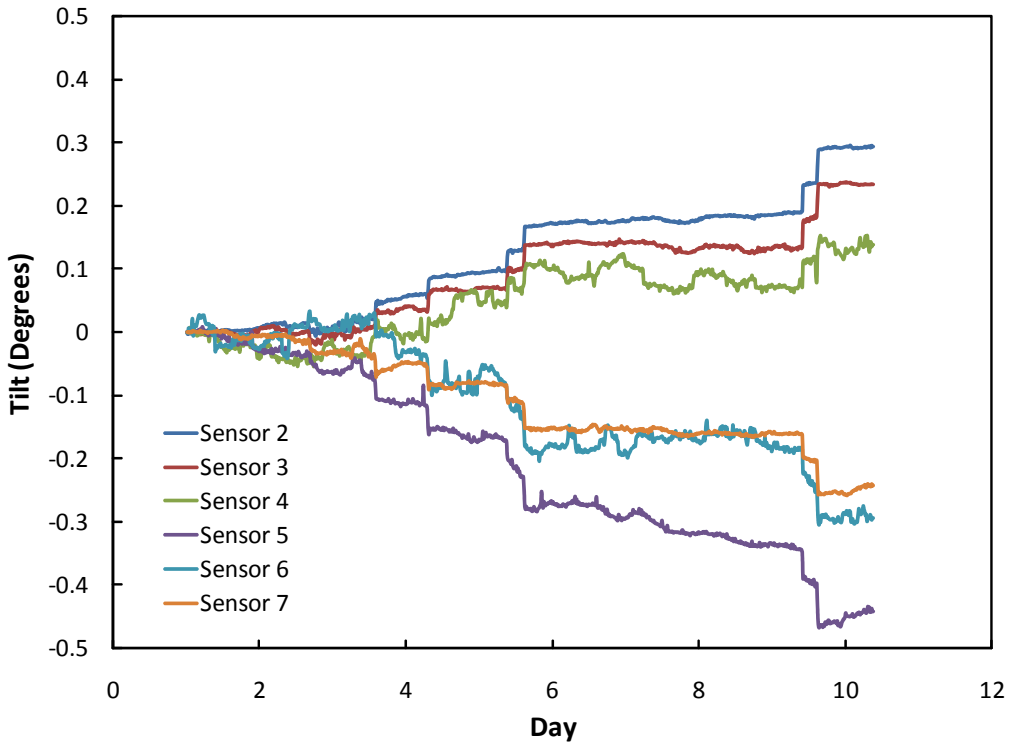

(b)

Figure 4-11. X-axis (a) and Y-axis (b) data in degrees.

Figure 4-11 shows the x-axis and y-axis data in degrees. The next step is to use this data in order to compute the short-term and long-term movements that occurred in time. In order to do this, the algorithms use the x-axis and y-axis data of each sensor and vector comparison in order to determine the change in tilt between two records in time. Figure 4-12 shows the resulting movements computed over a one hour time period from the data shown in Figure 4-11.

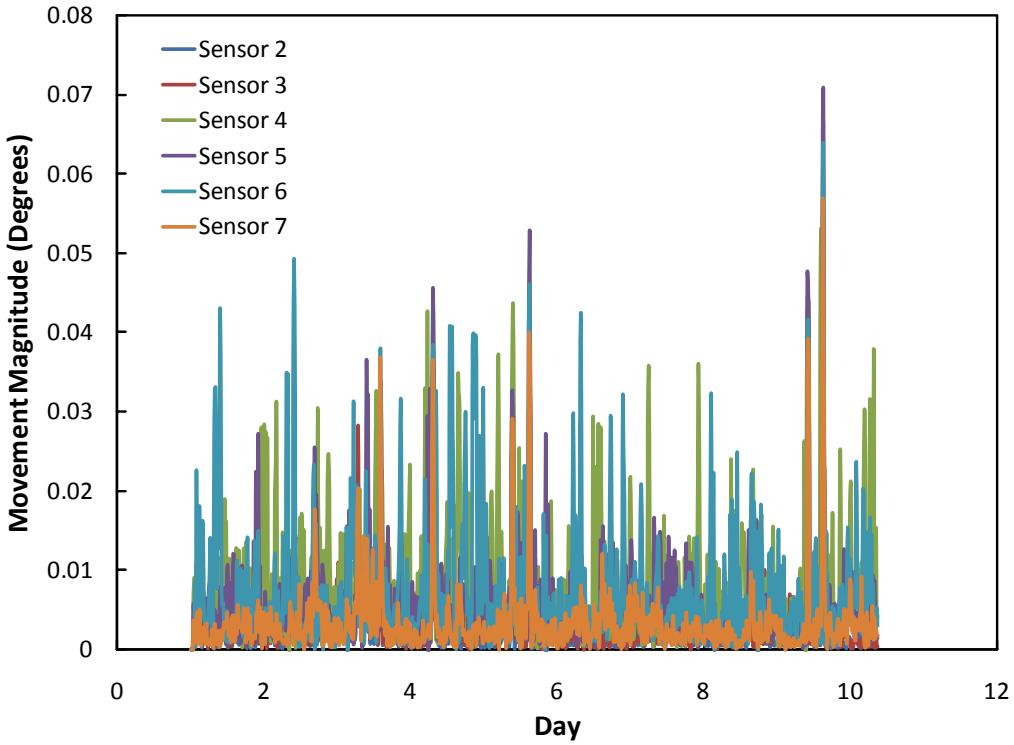

Figure 4-12. Movement from each pier sensor computed over a 1 hour time period.

Figure 4-12 shows the magnitudes of the movements computed for each sensor over a 1 hour period for each record in time.

Once the movements have been determined for each sensor individually, sensor consistency and sensor correlation algorithms are utilized in order to combine sensor

outputs from each array. This is done in order to identify and disregard inconsistent sensors as well as improve signal-to-noise ratios. First, the sensors within each array are compared and combined. Then, the two arrays on the pier are compared, their directions are translated into a universal coordinate system, and the magnitudes of their movements are averaged, resulting in the overall movement of the pier. Figure 4-13 shows the results of combining the sensors into the overall pier motion.

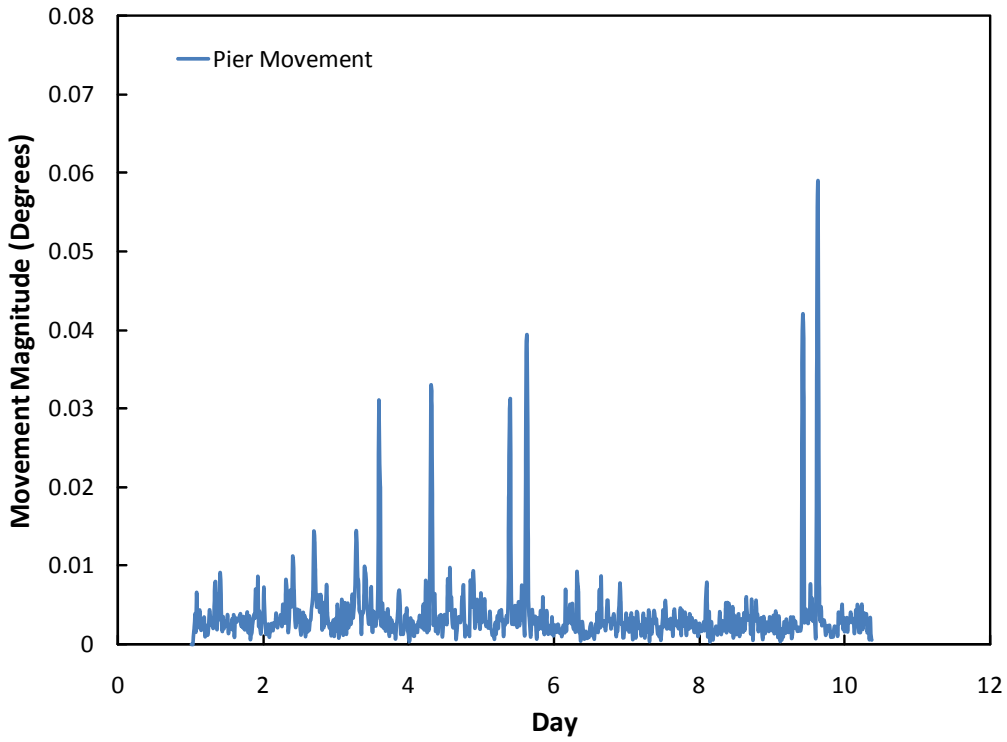

Figure 4-13. Overall pier movements from sensor combination.

In order to identify critical movements, a fuzzy or constant threshold is applied to the overall pier motion shown in Figure 4-13. A fuzzy threshold is used for the short time period algorithms, while a constant threshold is used for the longer time periods. Figure 4-14 shows the results from the fuzzy threshold.

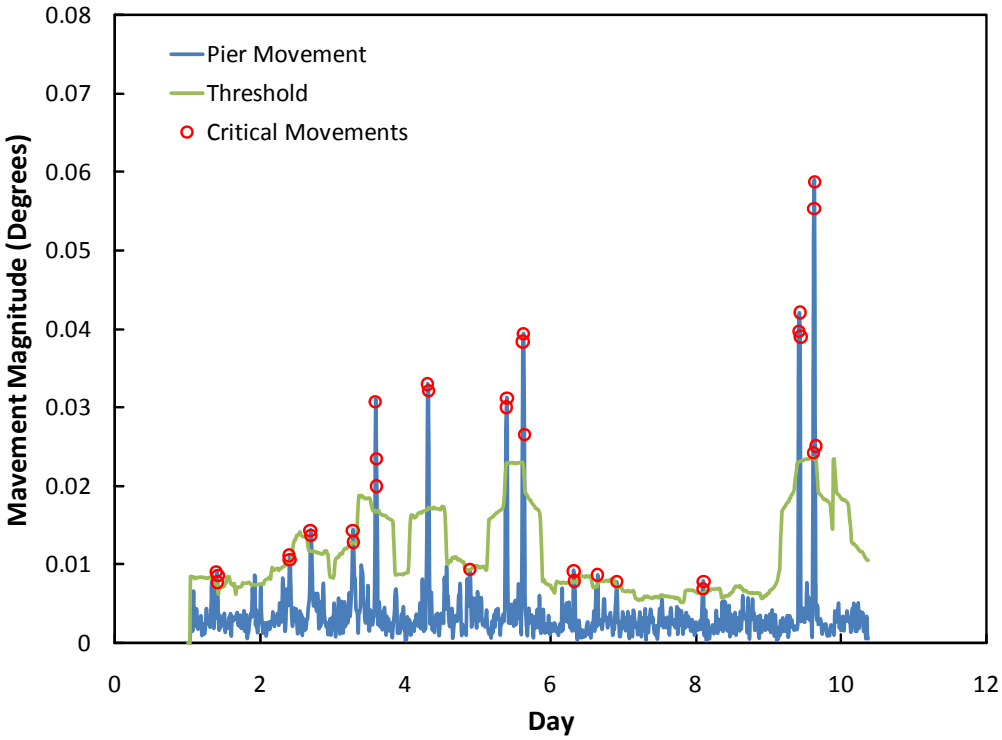

Figure 4-14. Results from applying fuzzy threshold to overall pier movements.

In Figure 4-14, the red circles are the movements identified above the threshold. The critical movement algorithms then check the validity of the directions of the movements identified, and the resulting valid movements are reported to the user. Thus, the algorithms have taken the raw data, filtered it to remove noise spikes, converted it into degrees, computed movements from each sensor's output using vector comparison, identified and removed inconsistent outputs using sensor consistency, combined movement magnitudes using sensor correlation, and identified and reported critical movements using critical movement determination.

4.3.8 Threshold Descriptions

The algorithms developed include seven constant thresholds and two variable thresholds. These thresholds are currently set somewhat randomly in order to allow the program to function. In the field, it is expected that the system will be installed and data will be collected for an initial period of time. This initial data set will be used in order to determine the constant thresholds. The variable thresholds will be computed continuously using the data as it is being collected. The following is a description of each, including what they are used for and how they will be determined.

4.3.8.1 Constant Thresholds

Six constant thresholds are used in order to determine sensor consistency and identify critical movements for the long time periods as discussed in the prior sections. They will be computed based on an initial data set collected upon installation in the field and the bridge structure itself.

4.3.8.1.1 Threshold "THR"

The first threshold used is "THR". This threshold is used as a preliminary check for validity of each sensor individually. The first check of sensor consistency entails comparing the movements of each sensor individually to the threshold THR. If above the threshold, a message is sent to the user. This threshold is different for each time period utilized in the program. The longer the time period, the higher the threshold is set due to the expectation of larger magnitudes of movements over longer periods of time.

Currently, this threshold is set at 1 degree. In the field system, this threshold will be computed using the initial data set. The initial set of data will be collected with the assumption that no critical movements are occurring during collection. Upon collection, the movements over each time period will be computed as usual. The mean and standard deviation of the movement data will then be computed. THR will be computed as the mean plus four times the standard deviation. This threshold will be computed for each sensor and each time period independently. Assuming the movement output closely follows a normal distribution, this will set the threshold to include 99.99% of the data. Any spike in data that falls above this threshold, will be detected as a possible errant or inconsistent point. If the spike is detected in every sensor, then this potential movement will be identified in additional processing.

4.3.8.1.2 Threshold "THR2"

THR2 is a constant threshold that is used with Sensors 2 thru 7. In order to determine if the sensors are consistent with one another, each set of three sensors are considered as an array. If the sensor outputs are more than THR2 away from the average output of the array, then an inconsistency exists. This inconsistency will then be identified and resolved. Once again, this threshold is different for each time period, due to the differing lengths and noise levels.

This threshold is currently set at a level that appears adequate for current data sets. In the field system, this threshold will be computed based on the initial data set. It is assumed that the initial data set is representative of data with no inconsistencies, in

which the sensors reported accurately at all times with no unusual movements occurring. Thus, the difference between each sensor and the average of the array will be computed for each record. The average and standard deviation of these differences will be computed for each sensor for each time period. The mean average and standard deviation for all six sensors will then be computed for each time period. The threshold THR2 will then be set as the mean plus two times the standard deviation for each time integral separately. Assuming a somewhat normal distribution, this method will include 95.45% within the threshold, with the outliers being deemed inconsistencies.

4.3.8.1.3 Threshold "THR3"

The third constant threshold used in the program is THR3. THR3 is also used for Sensors 2 thru 7 when one sensor in an array is found to be inconsistent. If the application of THR2 results in the detection of a sensor inconsistency, then the errant sensor is identified and excluded from processing for that particular data record. The remaining two sensors in the array are then compared using THR3 to determine if they are consistent with each other. If the remaining two sensors are more than THR3 from each other, then an inconsistency is present and an error message is reported to the user. In this case, the program continues with all three sensors from the array, but the user is notified that something is not correct and a closer review may be necessary.

As with THR and THR2, this threshold will be computed using the initial data set. The difference between each sensor and the other sensors in its array will be computed for each record for each time period. The average and standard deviation for each sensor

set will then be computed for each time period. The mean average and standard deviation will then be computed resulting in one value for these statistics for each sensor array for each time period. THR3 will be set as the mean plus two times the standard deviation. Similar to THR2, this threshold will be different for each time period due to varying levels of noise.

4.3.8.1.4 Threshold "THR4"

THR4 is used to compare the results from each array. Once any inconsistent sensors are identified and removed, an average movement from each array is computed for each record for each time period. The difference between the resulting movements from each array is then compared to the threshold THR4. If above the threshold then a message in sent to the user stating that the sensor arrays do not agree with one another and further review may be necessary.

THR4 is currently set at 0.2 degrees. It is important to note that the application of this threshold does not result in any action, but rather only an error message is given. In the field system, this threshold will be computed based on the initial data set. The difference between the arrays will be computed for each record. The average and standard deviation of the differences will then be computed for each time period independently. The threshold THR4 will then be set as the mean plus 3 times the standard deviation. Assuming a normal distribution, this will include 99.73% of the data within the threshold. The outliers will be deemed inconsistencies.

4.3.8.1.5 Threshold "THR5"

THR5 is the equivalent of THR2 for Sensors 8, 9, and 10. It is used and determined in the same way.

4.3.8.1.6 Threshold "THR6"

THR6 is the constant threshold used to identify critical pier rotations for the longer term periods of 7 days, 30 days, and 90 days. This threshold is applied to the overall pier movement in order to pinpoint movements that are large enough to be deemed as critical.

THR6 is determined based on the bridge dimensions. According to the *Manuals for the Design of Bridge Foundations,* lateral movements of 2 in. are "usually intolerable" to bridge structures (Barker 1991). For the test bridge, a horizontal movement of 2 in. corresponds with a tilt of 1.8°. Thus, the constant threshold used for the critical pier movement identification algorithms for the system located on the test bridge is set at 1.8°. This threshold is bridge specific, and will have to be determined for each bridge structure on an individual basis. The height of the bridge structure in combination with the 2 in. of tolerable lateral movement will be used to compute the tolerable tilt. The tolerable tilt determined will be set as the constant threshold.

4.3.8.1.7 Threshold "THR7"

THR7 is a constant threshold, similar to THR6, which is used to identify critical superstructure displacements for the longer term periods. It is determined based on the

bridge dimensions. According to the *Manuals for the Design of Bridge Foundations,* vertical settlements of 4 in. are "usually intolerable" to bridge structures (Barker 1991). For the test bridge, a vertical displacement of 4 in. corresponds with a superstructure tilt of 2.6°. Thus, the constant threshold used for the critical superstructure movement identification algorithms for the system located on the test bridge is set at 2.6°. Similar to THR6, this threshold is bridge specific, and will have to be determined for each bridge structure on an individual basis. The height of the bridge structure in combination with the 4 in. of tolerable vertical settlement will be used to compute the tolerable superstructure tilt. The tolerable tilt determined will be set as the constant threshold.

4.3.8.2 Variable Thresholds

The two variable thresholds are used in the initial filter and the critical movement identification. These thresholds are independent of the initial data set. This section describes the two variable thresholds and explains how they are computed.

4.3.8.2.1 Filter Threshold

The initial filter is used in order to eliminate errant data spikes that are consistent among all 32 channels of data. Due to intermittent data collection errors in the current system, up to 10% of the raw data are errant points. The first process that is applied to the raw data before calibration is to run it through the initial filter. This filter is designed to detect outliers with its variable threshold then replace these points with median values.

The threshold used in the initial filter is based on the "3 sigma edit rule" in combination with the Hampel identifier. This approach was developed based on Näsi, Sorsa, and Leiviskä, 2005. Focusing on one data channel, the median and median absolute deviation from the median of the nearest 48 points are computed for each record. The threshold for each record is then set as the median plus three times the median absolute deviation from the median. This threshold is applied to the data channel of focus and outliers are identified. Because these outliers are typically consistent among all 32 channels, they are replaced in every channel with median values from nearby points.

4.3.8.2.2 Movement Identification Threshold

The identification of critical movements for the short time period programs is done by applying a fuzzy threshold to the movement data. This process is done for both the pier movement determination as well as the superstructure movement determination. In the case of the pier movement identification for the one hour program, this threshold is applied to the overall movement data from the pier (the result of averaging the two arrays of data) and outliers are detected. If two outliers in a row are detected, and the direction of the identified movement is valid, then the highest magnitude movement value of the nearest three points is reported to the user, including the direction and time of that movement.

The threshold utilized is computed using a modified standard deviation. This method is based on Näsi, Sorsa, and Leiviskä, 2005. For each record, the appropriate threshold is computed from the nearest 48 points of pier movement data. The threshold

for each record is set as the median plus three times the modified standard deviation. The modified standard deviation is computed based on equation (3) in section 4.3.6. Outliers are those which lie above the threshold.

4.4. Test Descriptions

Testing has been conducted in order to verify the effectiveness and accuracy of the algorithms developed. Several tests have been completed in order to determine if the program can accurately identify pier rotations and superstructure displacements. Testing has also been completed in order to show the effectiveness of the multi-sensor system over single sensor systems. In addition, embedded sensors have been tested in order to determine their viability for the field system. The following sections will describe the laboratory tests in detail. The first shows the benefits of the multi-sensor system. The second and third tests were completed in order to verify the system's ability to identify pier rotations. Along with pier rotations, it was also important to verify the system's ability to identify superstructure displacements, which was completed in the fourth test. Lastly, the fifth test involved testing an embedded sensor and comparing its results to non-embedded sensors.

4.4.1 Multi-Sensor Test

The use of multiple sensors allows for sensor redundancy, increases signal to noise ratios, and helps to create a clearer depiction of the motion of the bridge. In order to verify that the multi-sensor system is more effective than individual sensors, a test was

conducted in which the pier was tilted in 0.0176° ± 0.0132° increments. The tolerance in the tilt movements comes from the estimated accuracy in manually tilting the bridge pier. In total, the pier was tilted 7 times over the course of one day along the y-axis of the bridge. Figure 4-15(a) shows the test bridge setup while Figure 4-15(b) shows the placement of the sensors.

(a)

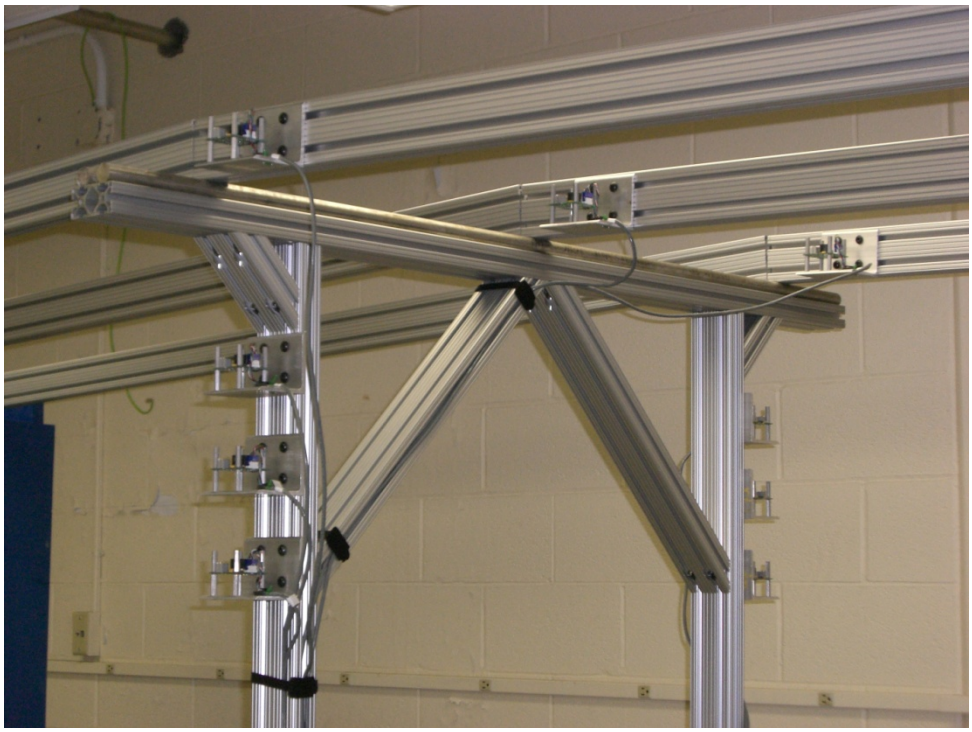

(b)

Figure 4-15. Test bridge setup (a) and sensor placement (b) for multi-sensor test.

For this test, a 1 minute sample rate was utilized. The results for this test will show the difference between the sensors when considered individually as opposed to combined as a multi-sensor system.

4.4.2 Pier Threshold Test

In order to verify the accuracy of the program as well as determine the lower limit of detectable pier rotations when using a 15 minute sample rate, a test was conducted over the course of two weeks in which the pier was tilted in increasing increments from 0.8 arcminutes to 3.2 arcminutes. The test setup can be seen in Figure 4-15.

Table 4-2 shows the movements that were applied to the bridge pier as well as the time of each movement.

Table 4-2. Applied pier movements for pier threshold test.

Movement	Time	Magnitude (degrees)
1	5/19/08 10:46 AM	0.0132 ± 0.0132
2	5/20/08 8:22 AM	0.0132 ± 0.0132
3	5/20/08 12:39 PM	0.0176 ± 0.0132
4	5/21/08 8:53 AM	0.0176 ± 0.0132
5	5/21/08 1:40 PM	0.0265 ± 0.0132
6	5/22/08 6:50 AM	0.0265 ± 0.0132
7	5/23/08 8:49 AM	0.0353 ± 0.0132
8	5/23/08 2:25 PM	0.0353 ± 0.0132
9	5/27/08 9:43 AM	0.0529 ± 0.0132
10	5/27/08 2:45 PM	0.0529 ± 0.0132

The results will discuss the movements that were identified and the accuracy of the system with the post-processing algorithms.

4.4.3 3-D Pier Rotation Tests

In addition to the test to determine the lower limit of detectable pier rotations, other tests were also completed in order to verify the system's ability to identify 3-

dimensional pier rotations. These tests entailed tilting the pier along multiple axis, thus testing the full three dimensional capability of the system. The test setup is identical to the previous two tests and is shown in Figure 4-15.

One of these tests was completed by turning each screw jack one full revolution, thus lowering each corner of the pier base, one at a time. This test was completed over the course of ten minutes with a 1.5 second sample rate. The second of these 3-dimensional tests was completed in order to verify magnitudes and directions of rotation. For this test, each screw jack was turned down, then back up to its initial position. Once each screw completed this task, they were each raised up in sequence. This test was conducted over the course of two hours and utilized a 1 minute sample rate. Table 4-3 reports the magnitude and direction of the applied movements.

Table 4-3. Applied pier rotations for 3-D pier test.

Movement	Magnitude (degrees)	Direction
1	0.1058 ± 0.0132	<0,->
2	0.1058 ± 0.0132	<0,+>
3	0.1058 ± 0.0132	<-,+>
4	0.1058 ± 0.0132	<+,->
5	0.1058 ± 0.0132	<+,+>
6	0.1058 ± 0.0132	<-,->
7	0.1058 ± 0.0132	<0,+>
8	0.1058 ± 0.0132	<+,->
9	0.1058 ± 0.0132	<-,->

4.4.4 Superstructure Displacement Test

Along with pier rotation, it was also important to test the system's ability to identify vertical displacements of the superstructure. In order to do this, a test was

conducted in which the pier was raised incrementally over the course of a week. This was done by turning all three screw jacks the same amount, thus raising the pier. For this test, a 15 minute sample rate was used. Once again, the setup for this test is shown in Figure 4-15. Table 4-4 shows the movements that the pier actually experienced, including the displacement of the pier as well as the corresponding change in tilt of the superstructure sensors. The tolerances reported correspond to the ability to manually tilt the pier within 1/8th turn of each wing nut.

Table 4-4. Applied superstructure movements for vertical displacement test.

Movement	Time	Pier Displacement (in)	Change in Tilt (degrees)
1	6/9/08 8:30 AM	0.045 ± 0.011	0.029 ± 0.007
2	6/9/08 4:20 PM	0.045 ± 0.011	0.029 ± 0.007
3	6/10/08 8:45 AM	0.091 ± 0.011	0.058 ± 0.007
4	6/10/08 4:30 PM	0.091 ± 0.011	0.058 ± 0.007
5	6/11/08 8:35 AM	0.136 ± 0.011	0.087 ± 0.007
6	6/11/08 4:40 PM	0.136 ± 0.011	0.087 ± 0.007
7	6/12/08 8:40 AM	0.182 ± 0.011	0.117 ± 0.007
8	6/12/08 4:45 PM	0.182 ± 0.011	0.117 ± 0.007
9	6/13/08 8:40 AM	0.227 ± 0.011	0.145 ± 0.007
10	6/13/08 4:00 PM	0.227 ± 0.011	0.145 ± 0.007

The results for this test will compare the applied and measured movements in order to show the effectiveness of the system while utilizing the post-processing algorithms. Only the results from the superstructure sensors were considered.

4.4.5 Embedded Sensor Test

An important issue in the field application of the tilt sensor technology is the effects of normal ambient temperature variations on the tilt measurements of a bridge pier. Because the pier heats and cools at a much different rate than the surrounding environment, including the sensors intended to measure the pier motion, the measured motions and actual piers motions can be inconsistent. One approach to addressing this issue would be to embed the sensor within the concrete, such that it heats and cools at the same rate as the concrete. To evaluate this innovative concept, laboratory tests were conducted with the tilt sensor module embedded in concrete. Figure 4-16 shows a schematic diagram of the laboratory test configuration, with the sensor module disconnected from the supporting electronics and embedded in a 2 in. diameter block-out in a concrete slab set on-end.

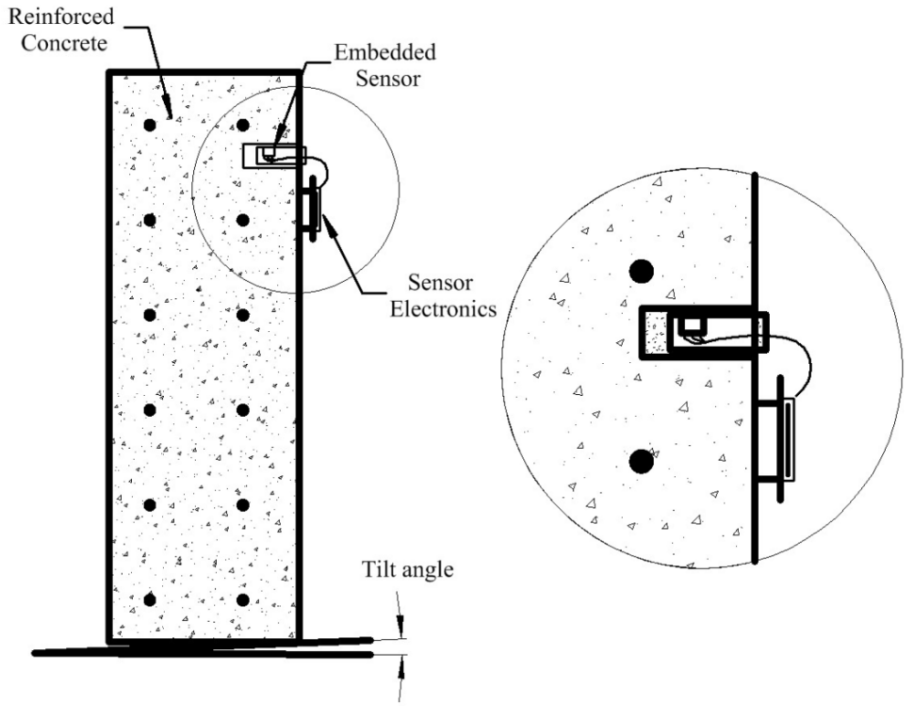

Figure 4-16. Diagram of embedded sensor design used for laboratory testing.

The sensor module was mounted in a 1 in. square plastic tube, and then grouted into the block-out. Two tilt sensors in a normal, board-mounted configuration were mounted on the surface of the concrete slab and utilized for comparison. Figure 4-17 is a photograph of the actual test setup.

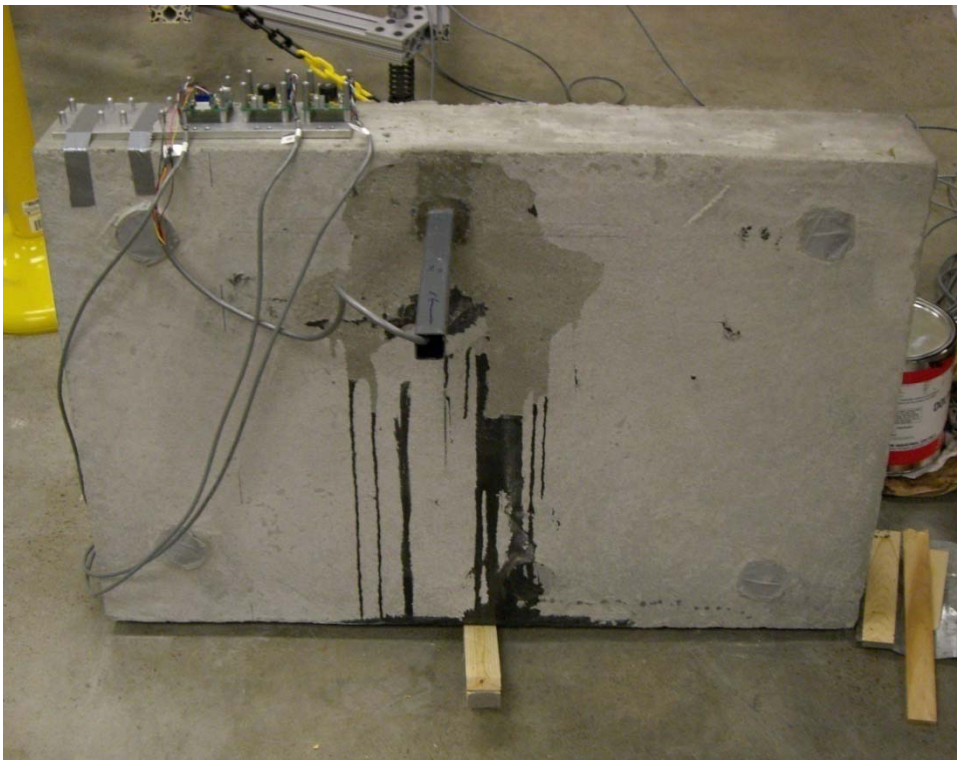

Figure 4-17. Photograph of test setup for embedded sensor tilt test.

Laboratory testing included a long term drift/noise test to evaluate the sensor performance while embedded in concrete, and a tilt test to compare sensor outputs from the embedded sensor with a normal configuration. The long term test was conducted over a five day period of time, while utilizing a 15 minute sample rate. The tilt test consisted of using a series of shims in order to cause tilt to the concrete slab. In total, the slab was tilted five times in one direction, and then five times back to its initial position. This test was conducted over the course of an hour and utilized a 1.5 second sample rate.

5: Results

5.1. Introduction

The following includes the results from the five laboratory tests discussed in the prior section. These tests were conducted in order to verify the ability of the algorithms developed for the multi-sensor system as well as to show the effectiveness of using multiple sensors embedded in the bridge pier. The results will include individual sensor outputs in addition to the output resulting from the combination of all of the sensors. Figures and tables are included in order to demonstrate the accuracy of the system.

5.2. Multi-Sensor Test

The multi-sensor test was completed in order to verify that a system of multiple sensors is more effective than individual sensors operating independently. Figure 5-1 shows the data from two arrays of sensors containing the seven movements which occurred.

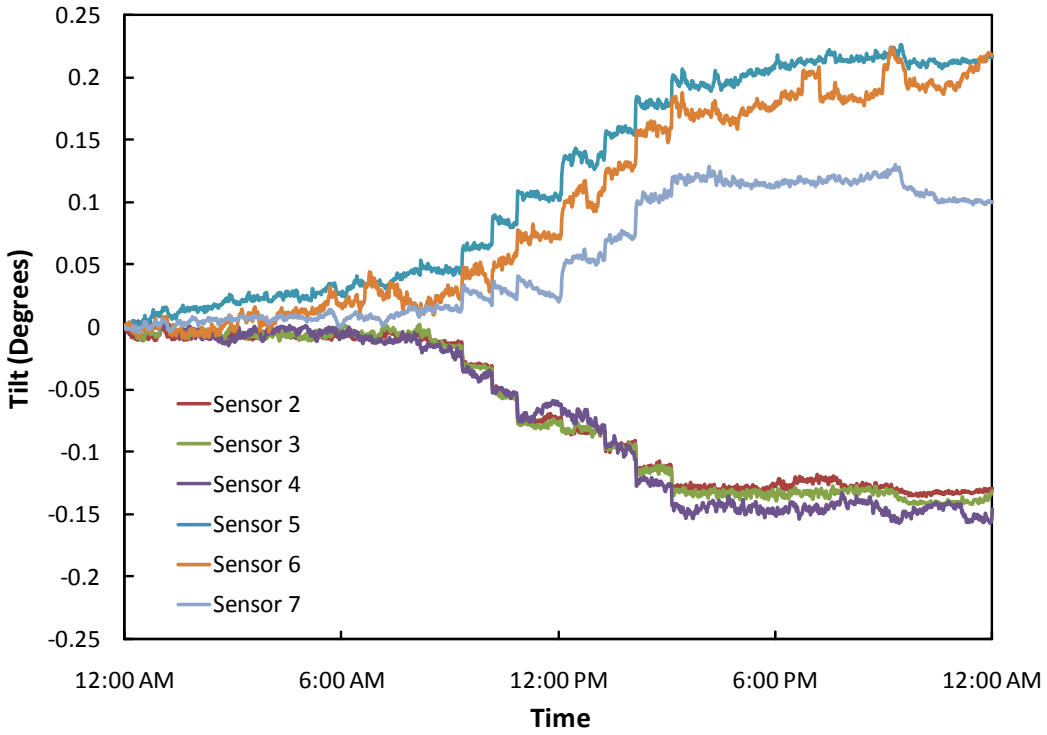

Figure 5-1. Data from y-axis of six sensors from multi-sensor test.

In Figure 5-1 the six lines represent the tilt output of the y-axis of six sensors. For this test, those six sensors were arranged in two arrays of three sensors each. The arrays were placed on opposite sides of the pier. Thus, the opposite direction of movement displayed in Figure 5-1 corresponds to the placement of the sensor arrays on the pier.

For a closer view at the individual movements, the data from two sensors can be seen in Figure 5-2.

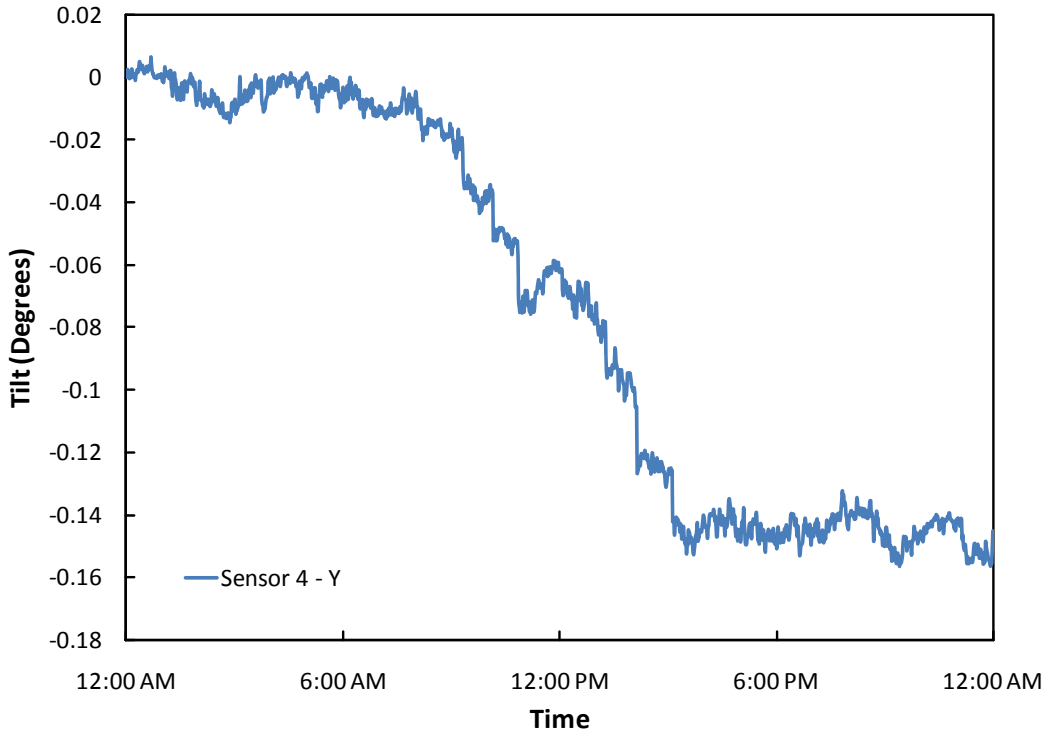

(a)

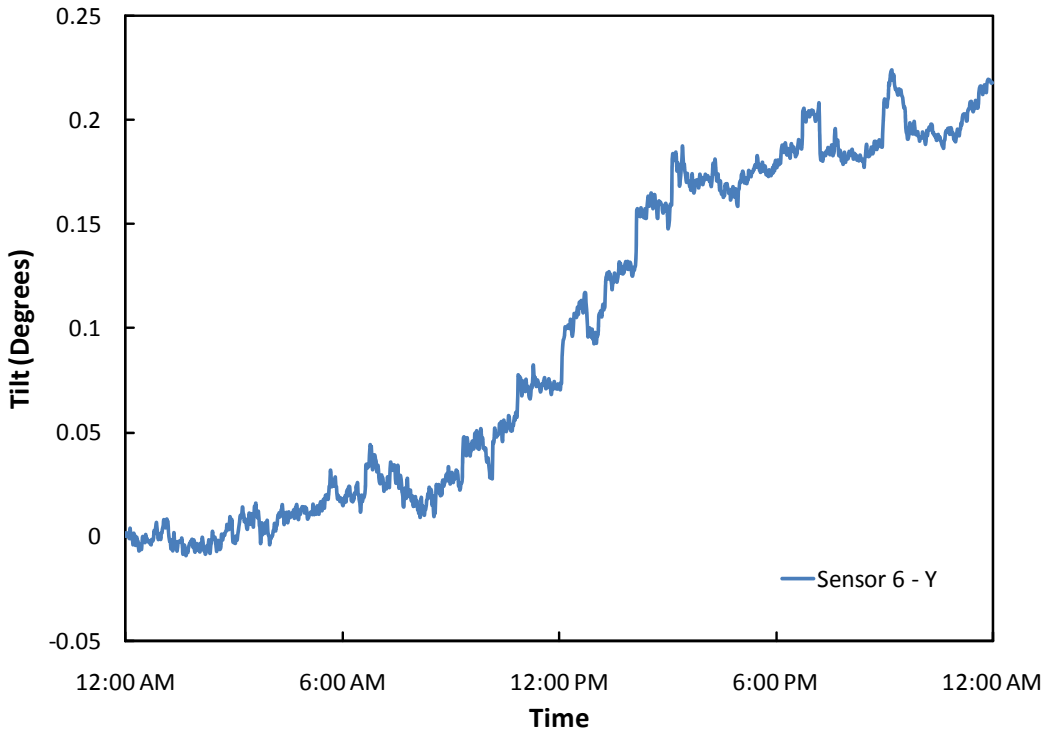

(b)

Figure 5-2. Data from Sensors 4 (a) and 6 (b) showing y-axis movements that occurred.

Figure 5-2(a) contains data from the y-axis of Sensor 4, while Figure 5-2(b) contains data from the y-axis of Sensor 6. Examining the data shown in the graphs, it is difficult to isolate movements within the noisy data set. This is likely due to individual sensor noise as well as drift. The data collected was then run through the 1hr program in order to pinpoint instantaneous movements. The results of this program on each individual sensor's output are shown in Figure 5-3 and Figure 5-4.

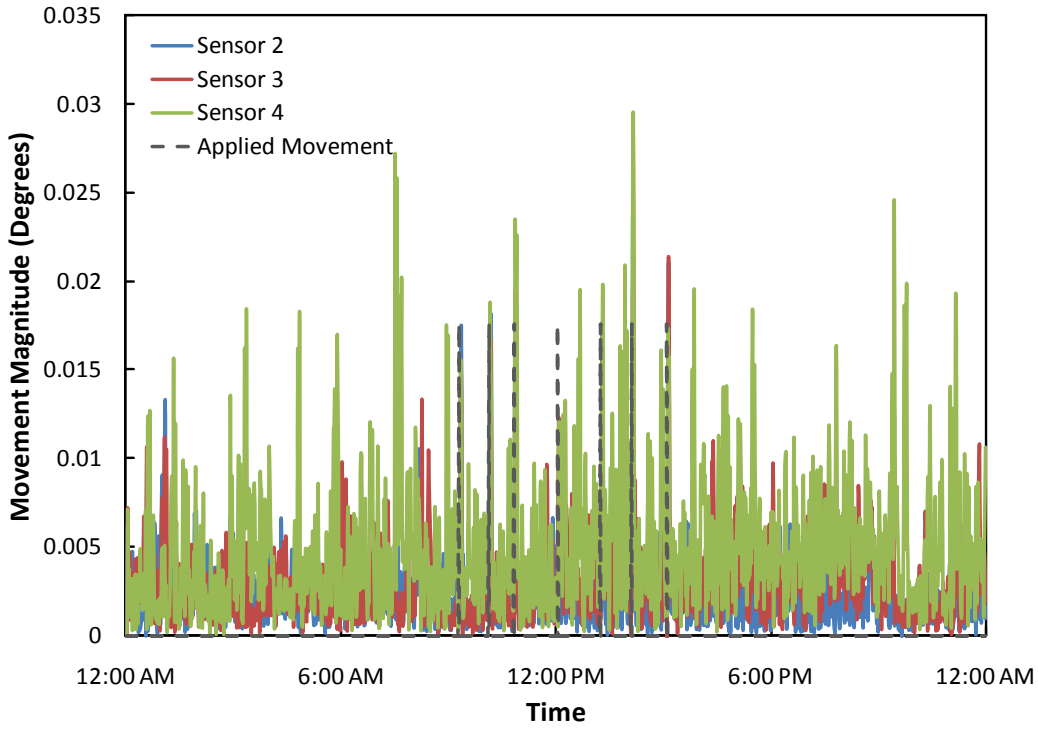

Figure 5-3. Movement results from Sensors 2, 3, and 4 individually.

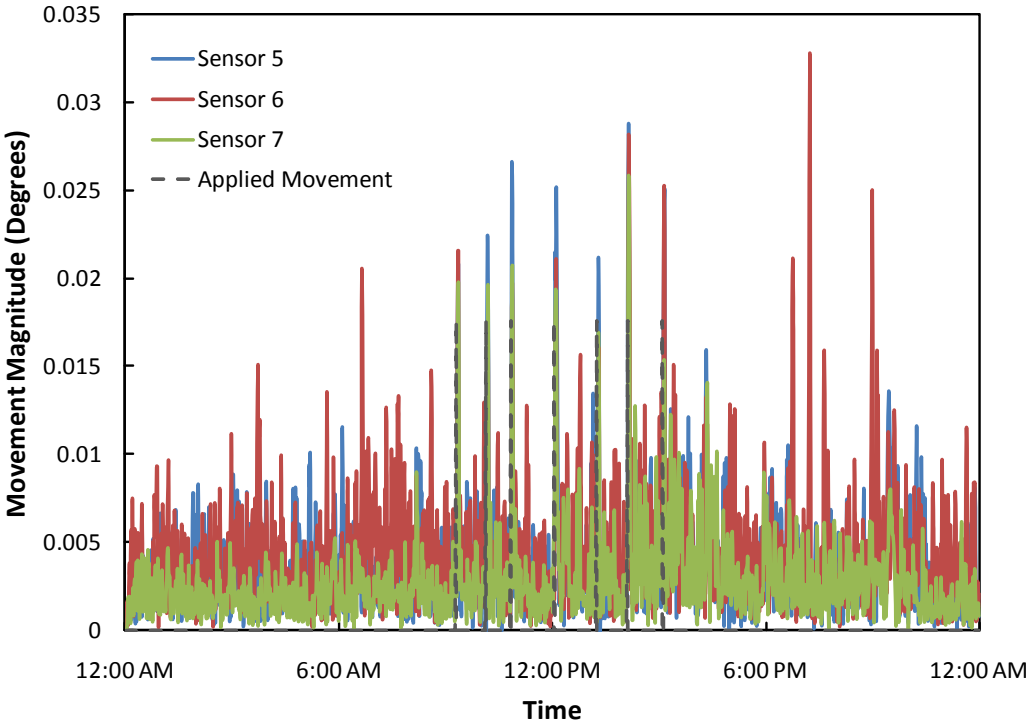

Figure 5-4. Movement results from Sensors 5, 6, and 7 individually.

Figure 5-3 and Figure 5-4 display the movements computed over a 4 minute time period. In a similar way, if the data had been collected using a 15 minute sample rate, than the resulting movements from the 1hr program would be computed over a period of one hour. From Figure 5-3 and Figure 5-4, it is somewhat difficult to identify the movements that occurred, as the signal to noise ratio for these results is ~1.0. When the sensors are combined into a multiple sensor system in which the sensors work together, this signal to noise ratio is improved significantly. Once the sensors are considered as an array, inconsistent outputs can be excluded from processing and signal correlation can be completed in order to pinpoint precise movements. Figure 5-5 shows the same portion of data as what is shown in Figure 5-3 and Figure 5-4, except it is a result of combining sensor outputs.

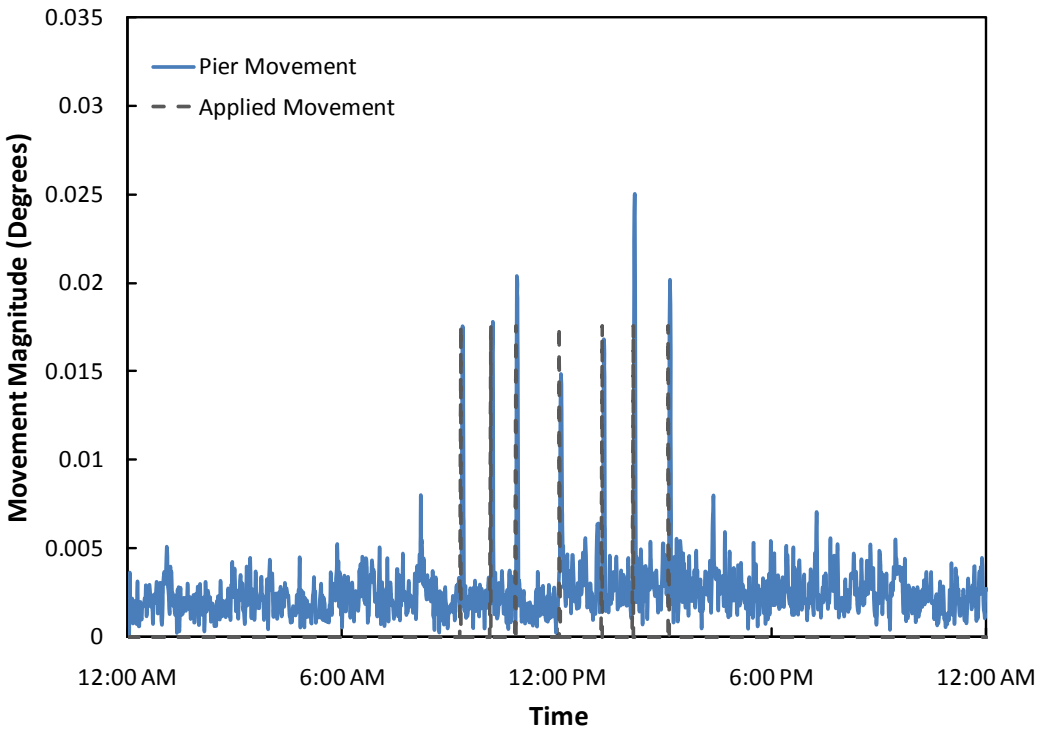

Figure 5-5. Overall pier movement from sensor combination showing 7 distinct movements.

Figure 5-5 shows the movement magnitudes in time from the combination of all six sensors, as well as the applied movements. It clearly shows the seven distinct movements that the bridge experienced. The signal-to-noise ratio has increased from ~1.0 when considering each sensor individually to ~3.0 when utilizing multi-sensor logic. This clearly shows the beneficial effect of using multiple sensors. The program reported the following data to the user:

> Critical movement occurred for a 1 hour period at..04-09-008 09:21:0
> Pier moved..0.017552 degrees in the direction x=0.0094345, y=-0.99977
> Critical movement occurred for a 1 hour period at..04-09-008 10:12:0
> Pier moved..0.017627 degrees in the direction x=-0.03945, y=-0.99668
> Critical movement occurred for a 1 hour period at..04-09-008 10:52:0
> Pier moved..0.02037 degrees in the direction x=0.066184, y=-0.97728

Critical movement occurred for a 1 hour period at..04-09-008 12:06:0
Pier moved..0.01485 degrees in the direction x=-0.26125, y=-0.92801
Critical movement occurred for a 1 hour period at..04-09-008 13:18:0
Pier moved..0.016797 degrees in the direction x=-0.20917, y=-0.96908
Critical movement occurred for a 1 hour period at..04-09-008 14:10:0
Pier moved..0.024997 degrees in the direction x=-0.13919, y=-0.97939
Critical movement occurred for a 1 hour period at..04-09-008 15:09:0
Pier moved..0.020183 degrees in the direction x=0.17185, y=-0.97765
Critical movement occurred for a 1 hour period at..04-09-008 09:22:0

The magnitude and time for each measured movement corresponds directly with the applied movements as shown in Table 5-1.

Table 5-1. Applied and measured movements for the multiple sensor test.

Movement	Magnitude (degrees)		Error (%)
	Applied	Measured	
1	0.0176 ± 0.0132	0.0176	0.3
2	0.0176 ± 0.0132	0.0176	0.2
3	0.0176 ± 0.0132	0.0204	13.6
4	0.0176 ± 0.0132	0.0149	18.5
5	0.0176 ± 0.0132	0.0168	4.8
6	0.0176 ± 0.0132	0.0250	29.6
7	0.0176 ± 0.0132	0.0202	12.8

Table 5-1 reports the magnitudes of the movements identified by the sensor system. In addition, the percent error is reported for each of the movements measured. At first glance, the errors reported appear too high for the measurements to be deemed accurate. However, each of the identified movements is within the tolerance of the applied movement. In addition, the size of the movement, being less than 2 hundredths of a degree, makes the reported errors somewhat unimpressive.

Another way of comparing the results from individual sensors to the results of the sensor system is to examine the mean and standard deviation of the movements that were recorded when the bridge experienced no actual movement. Ideally, both the mean and standard deviation should be zero when no movements are occurring. By computing these statistics over a one day period for each sensor individually as well as the two sensor sets and the combination of all six sensors, it is clear that the combination of all six sensors provides the best results. The mean of the individual sensors ranges from 0.0020° to 0.0044°, while the standard deviation ranges from 0.0013° to 0.0033°. The average mean of the six sensors is 0.0034°, with the average standard deviation being 0.0023° for the six individual sensors. Once the sensors have been combined into two sets of three, the mean lowers to between 0.0020° and 0.0028°, while the standard deviation lowers to between 0.0013° and 0.0016°. Finally, when all six sensors are combined into one system, the resulting mean and standard deviation lower to 0.0024° and 0.0010°, respectively. Thus, the system of six sensors provides much better results than isolated individual sensors.

The results discussed above were from a test in which data was collected every minute. The sample rate that will likely be used in the field is 15 minutes. Thus, while the data from a 1 minute collection rate can be used to clearly measure movements on the order of 0.0176° (1 arcminute), testing has been completed in order to determine the lower limit of movement magnitudes that can be effectively detected when using a 15 minute collection rate. Due to noise and drift, this limit is above 1 arcminute. The results from this test will be discussed in the following section.

5.3. Pier Threshold Test

In order to determine the lower limit of identifiable movements as well as verify the accuracy of the algorithms developed, a 1-dimensional pier threshold test was conducted. In this test, ten movements were applied to the test bridge along the y-axis of the sensors. Figure 5-6 shows the outputs from the y-axis of each of the sensors in the arrays located on the pier.

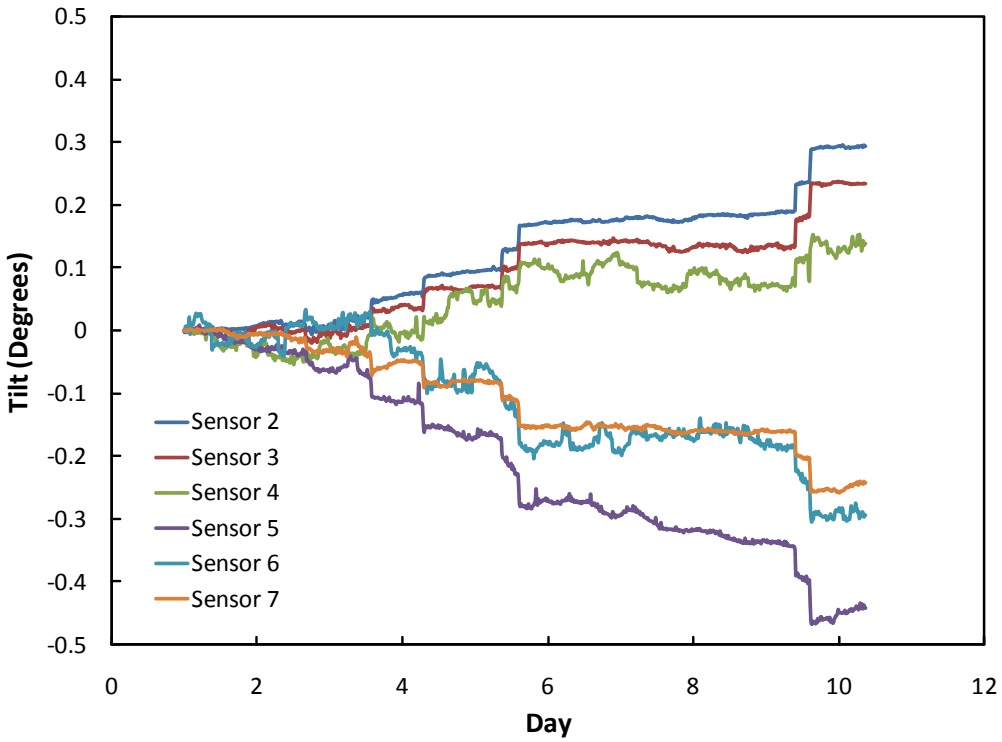

Figure 5-6. Sensors' y-axis output in which 10 movements of incremental magnitudes occurred.

The data shown in Figure 5-6, as well as the x-axis data, was then used in order to compute the movements over a 1 hour period. The resulting movements can be seen in Figure 5-7.

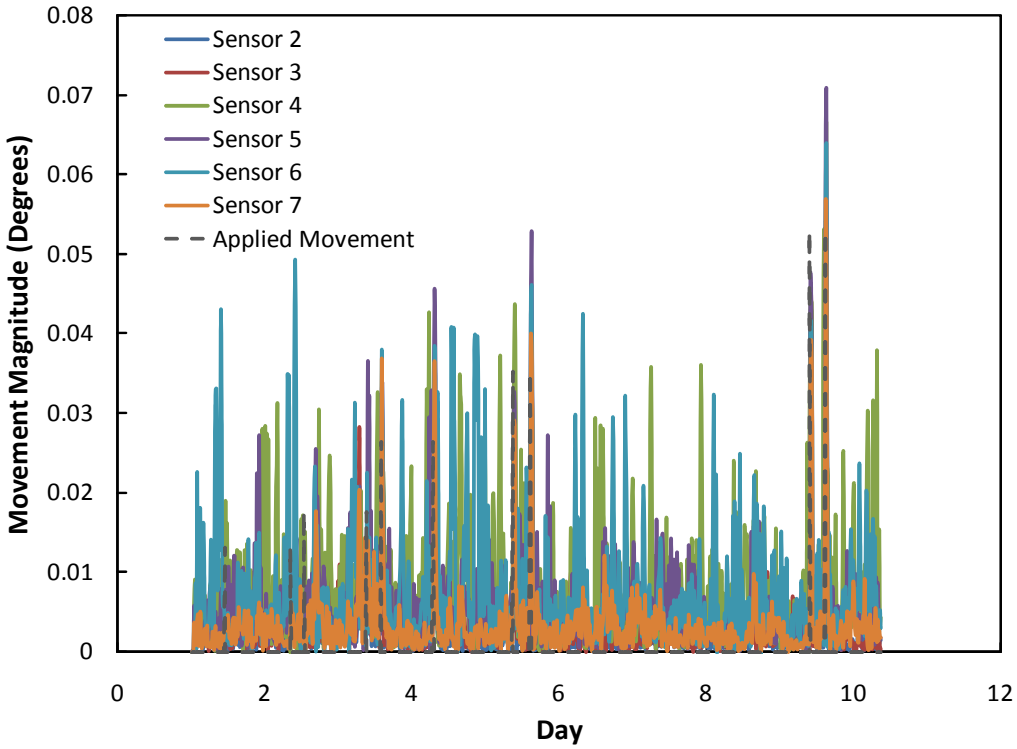

Figure 5-7. Movements from each sensor on pier computed over 1 hour period.

Figure 5-7 shows the movements that occurred in each sensor on the pier, as well as the applied movements. In other words, the movement of each sensor was computed at each record by determining the resultant change in tilt between the current record and the record from 1 hour prior. The graph is a good representation of the level of noise experienced during testing. It is hard to identify distinct movements when considering all of the sensors separately as shown in Figure 5-7.

After the individual movements of each sensor were computed, these movements were compared to others in their appropriate array, inconsistent outputs were disregarded, and an overall movement of the pier was determined for each record in time. The resulting overall pier movement from this test is shown in Figure 5-8.

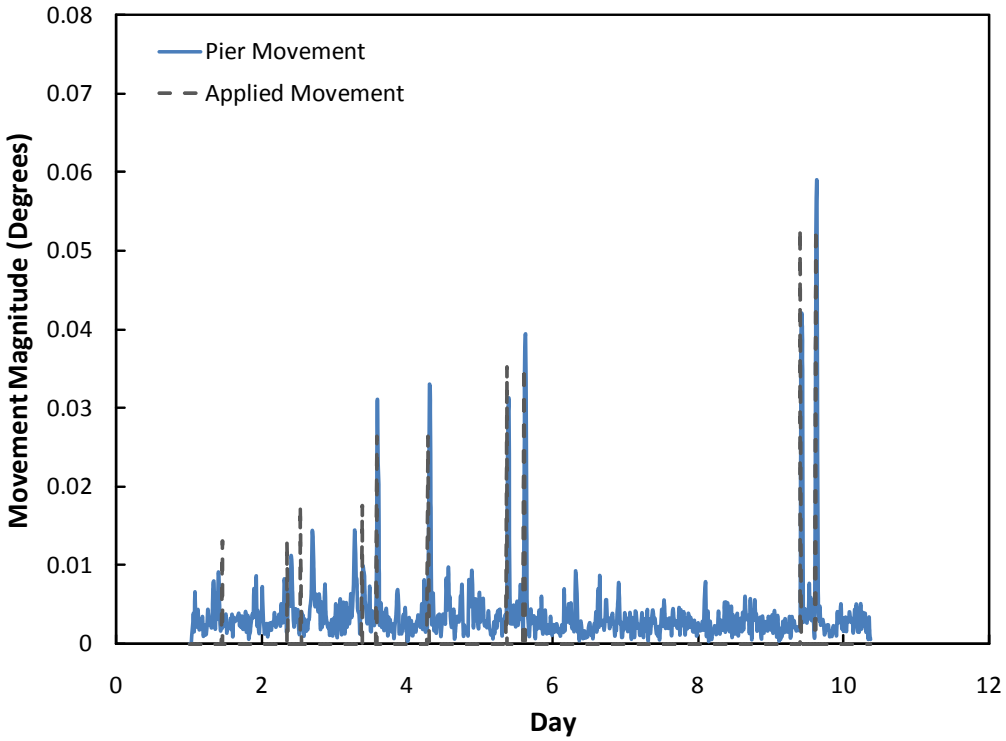

Figure 5-8. Overall pier movement computed over a 1 hour time period.

Figure 5-8 is a result of combining the outputs from the two arrays located on the pier into one overall pier movement. In comparison with Figure 5-7, movements are much easier to identify and correspond closely to the applied movements after combining sensor outputs.

In order to pinpoint the critical movements, the program applied a fuzzy threshold and considered the directions of the identified movements. The results from applying this threshold can be seen in Figure 5-9.

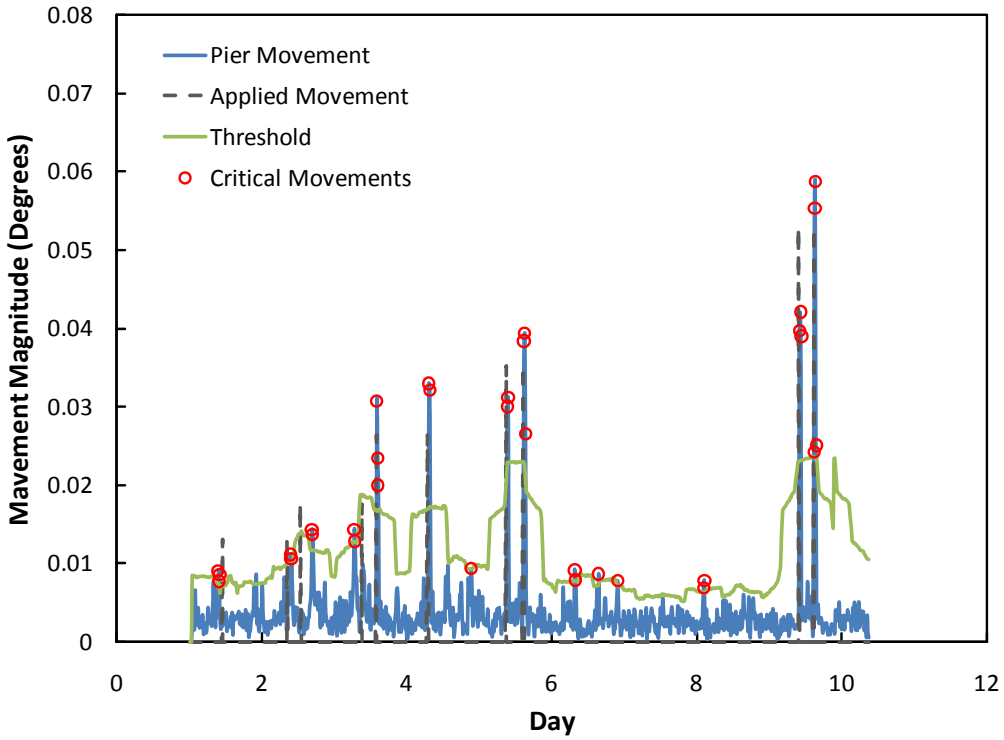

Figure 5-9. Graph of overall pier movement with fuzzy threshold applied.

In Figure 5-9, the red circles denote movements that were identified above the fuzzy threshold. The directions of these movements were then reviewed, and valid critical movements were reported to the user as follows:

Critical movement occurred for a 1 hour period at..05-21-008 14:00:0
Pier moved..0.030684 degrees in the direction x=-0.040707, y=0.99908
Critical movement occurred for a 1 hour period at..05-22-008 07:15:0
Pier moved..0.032966 degrees in the direction x=0.025831, y=0.99867
Critical movement occurred for a 1 hour period at..05-23-008 09:30:0
Pier moved..0.03117 degrees in the direction x=0.072059, y=0.99701
Critical movement occurred for a 1 hour period at..05-23-008 15:00:0
Pier moved..0.039397 degrees in the direction x=-0.015614, y=0.99174
Critical movement occurred for a 1 hour period at..05-27-008 10:15:0
Pier moved..0.042108 degrees in the direction x=0.042002, y=0.99773
Critical movement occurred for a 1 hour period at..05-27-008 15:15:0
Pier moved..0.058682 degrees in the direction x=-0.0086628, y=0.99982

The movements measured by the program correspond directly to the movements that the bridge pier experienced. Table 5-2 shows the movements that occurred as well as those measured.

Table 5-2. Applied and measured pier movements for pier threshold test.

Movement	Time		Magnitude (degrees)		Error (%)
	Applied	Measured	Applied	Measured	
1	5/19/08 10:46 AM	---	0.0132 ± 0.0132	---	---
2	5/20/08 8:22 AM	---	0.0132 ± 0.0132	---	---
3	5/20/08 12:39 PM	---	0.0176 ± 0.0132	---	---
4	5/21/08 8:53 AM	---	0.0176 ± 0.0132	---	---
5	5/21/08 1:40 PM	5/21/08 2:00 PM	0.0265 ± 0.0132	0.0307	13.7
6	5/22/08 6:50 AM	5/22/08 7:15 AM	0.0265 ± 0.0132	0.0330	19.7
7	5/23/08 8:49 AM	5/23/08 9:30 AM	0.0353 ± 0.0132	0.0312	13.1
8	5/23/08 2:25 PM	5/23/08 3:00 PM	0.0353 ± 0.0132	0.0394	10.4
9	5/27/08 9:43 AM	5/27/08 10:15 AM	0.0529 ± 0.0132	0.0421	25.7
10	5/27/08 2:45 PM	5/27/08 3:15 PM	0.0529 ± 0.0132	0.0587	9.9

According to Table 5-2, every movement above 0.0265° was detected and measured within a 30% error. Although the errors in the measurements seem high, the size of the measurements, being less than 5 hundredths of a degree, makes the error acceptable. Thus, it is clear that the lower limit of detectable pier movements is no more than 0.0265° ± 0.0132° or 1.6 arcminutes. In addition, the program is capable of detecting movements within 45 minutes of their occurrence. The results in Table 5-2 support that, showing that every measured movement was detected within 45 minutes of occurrence. Thus, this test was successful in verifying the program's ability to identify movements as well as determining the threshold of detectable pier rotations.

5.4. 3-D Pier Rotation Tests

In addition to the 1-dimensional pier threshold test, 3-dimensional pier rotation tests were conducted to verify the algorithms ability to identify 3-D motions. The first of these tests was conducted in order to qualitatively see the output of the sensors. Figure 5-10 shows the output from each axis of the sensors.

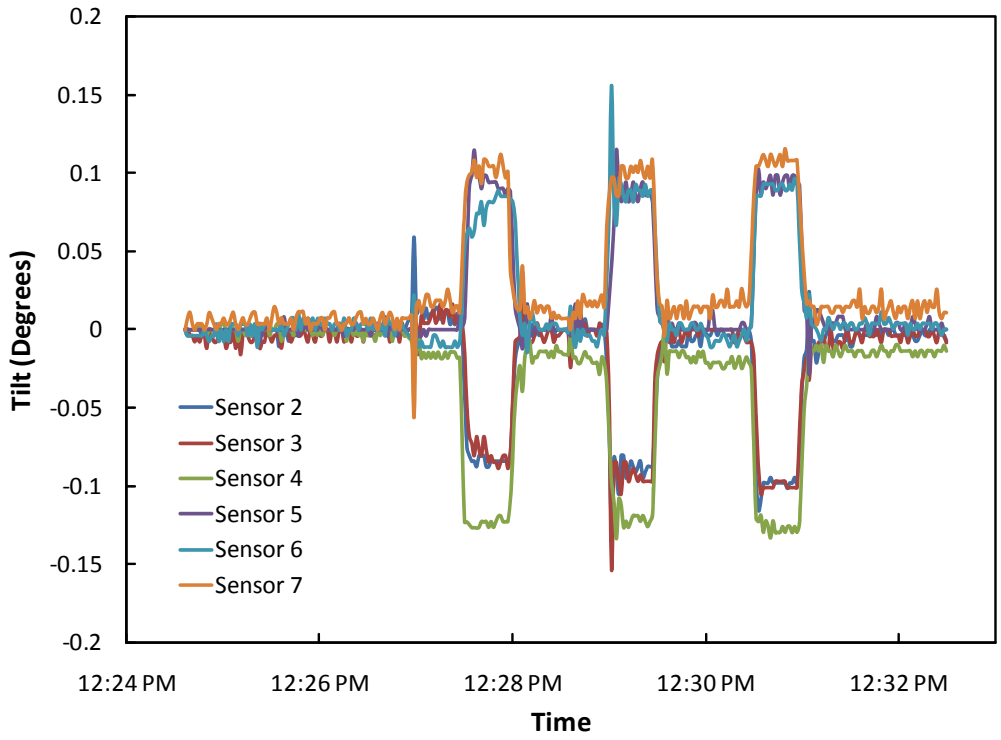

(a)

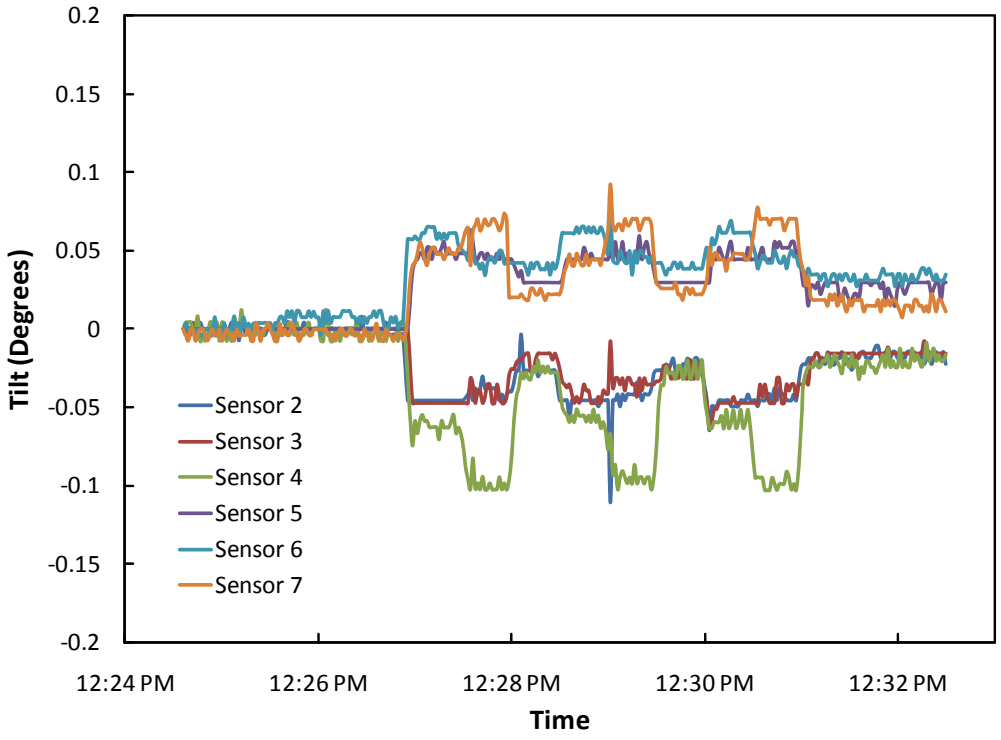

(b)

Figure 5-10. Sensor output from x-axis (a) and y-axis (b) for 3-D pier rotation test.

Upon combining the outputs from the sensor arrays, the overall motion of the pier was determined. Figure 5-11 is a 3-dimensional representation of the motion of the pier.

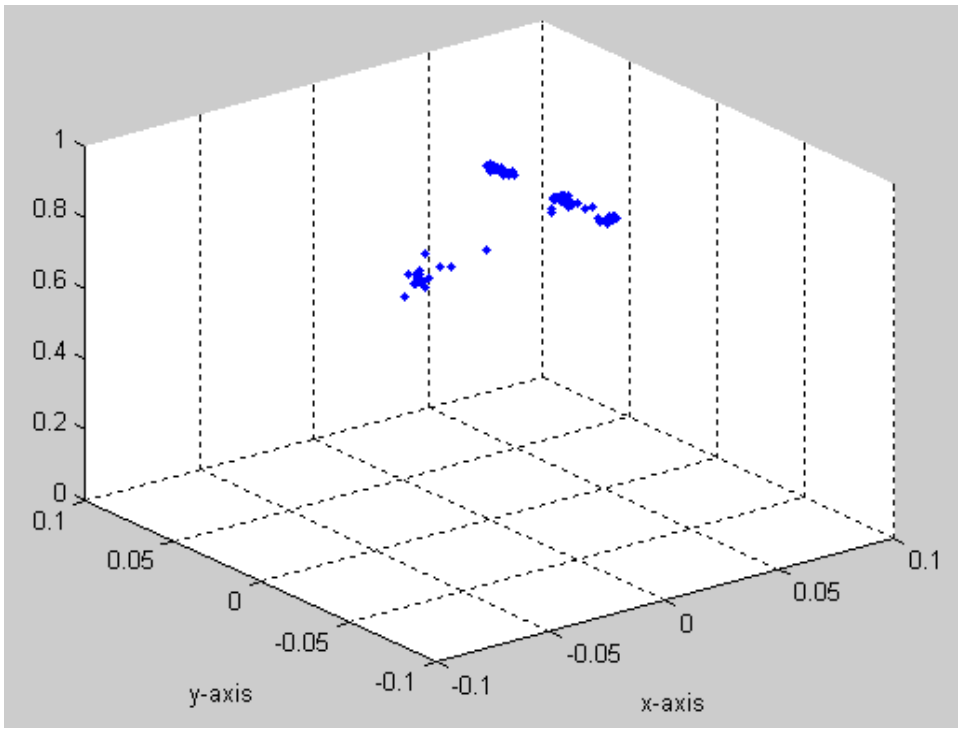

Figure 5-11. 3-D representation of pier rotation.

In Figure 5-11, the three clusters of points represent the locations of the top center portion of the pier. The single point in the center is the initial position. As each screw jack was tightened, the top of the pier tilted in the direction of the screw jack. The above graph shows that the 3-dimensional motion of the pier was effectively detected with the post-processing algorithms.

The second of the 3-dimensional tests was completed in order to quantitatively verify magnitudes and directions of rotation. Upon completion of the test, the data was run through the post-processing algorithms. Figure 5-12 shows the identified pier movements.

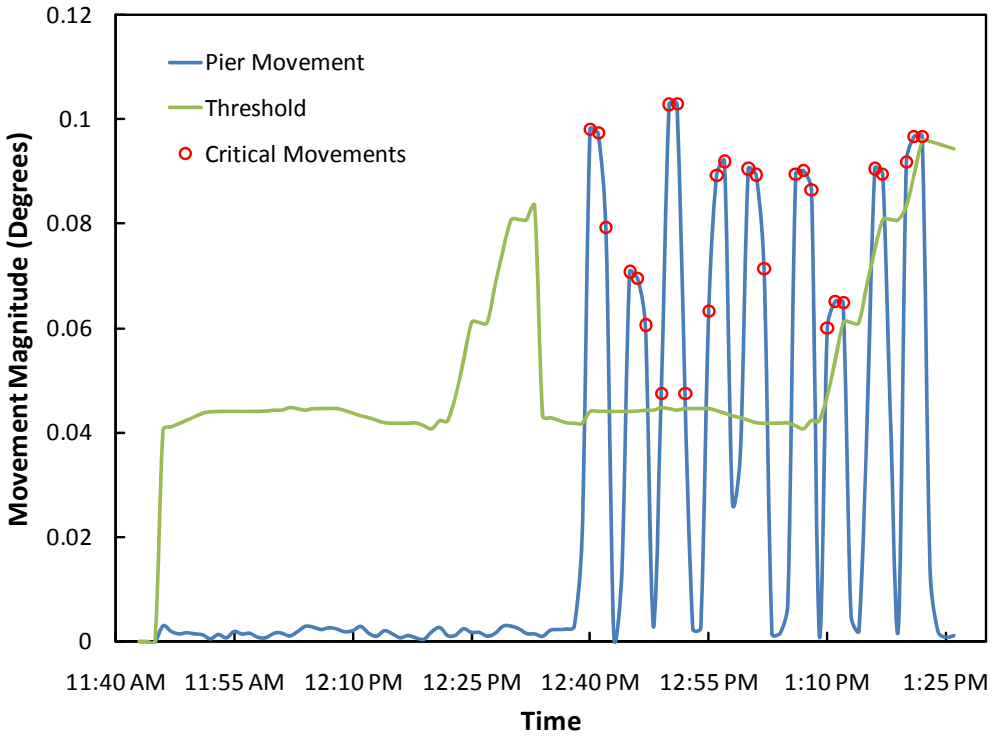

Figure 5-12. Identified pier rotations for 3-D pier test.

During the test, an initial period of time was allotted for the sensors to "warm-up". This is shown in the graph above; for, all of the movements occurred during the last half of the test. Table 5-3 shows the movements that were applied as well as those measured and reported to the user.

Table 5-3. Applied and measured pier rotations for 3-D pier test.

Movement	Direction		Magnitude (degrees)		Error (%)
	Applied	Measured	Applied	Measured	
1	<0,->	<0.034,-0.999>	0.1058 ± 0.0132	0.0982	7.7
2	<0,+>	<-0.083,0.994>	0.1058 ± 0.0132	0.0708	---
3	<-,+>	<-0.866,0.500>	0.1058 ± 0.0132	0.1030	2.7
4	<+,->	<0.990,-0.140>	0.1058 ± 0.0132	0.0920	15.0
5	<+,+>	<0.978,0.197>	0.1058 ± 0.0132	0.0906	16.8
6	<-,->	<-0.975,-0.207>	0.1058 ± 0.0132	0.0903	17.2
7	<0,+>	<-0.067,0.997>	0.1058 ± 0.0132	0.0652	---
8	<+,->	<0.996,-0.088>	0.1058 ± 0.0132	0.0906	16.8
9	<-,->	<-0.898,-0.437>	0.1058 ± 0.0132	0.0969	9.2

As shown in Table 5-3, each of the nine pier movements was measured with an appropriate direction. In addition, the measured magnitudes of the movements are all within a 20% error of what the pier actually experienced. Considering the amount of variability in the test setup as well as the magnitude of the movements being measured, an error less than 20% is respectable.

The shaded lower magnitudes that are exhibited with movements 2 and 7 are the result of errors in the test bridge motion at the time this test was conducted. Both movements correspond to the raising of the same screw jack, which was jammed and not allowing normal motions. When turning the wing nut, instead of purely raising the corner of the pier, the entire foot of the pier was turning at the ground surface, thus resulting in an unknown pier tilt. The problem has since been resolved. Nonetheless, the algorithms were successful in pinpointing each of the 3-dimensional movements that occurred during this test, reporting them effectively to the user.

5.5. Superstructure Displacement Test

The superstructure displacement test consisted of raising the bridge pier incrementally. The output from each axis of the sensors located on the superstructure is shown in Figure 5-13.

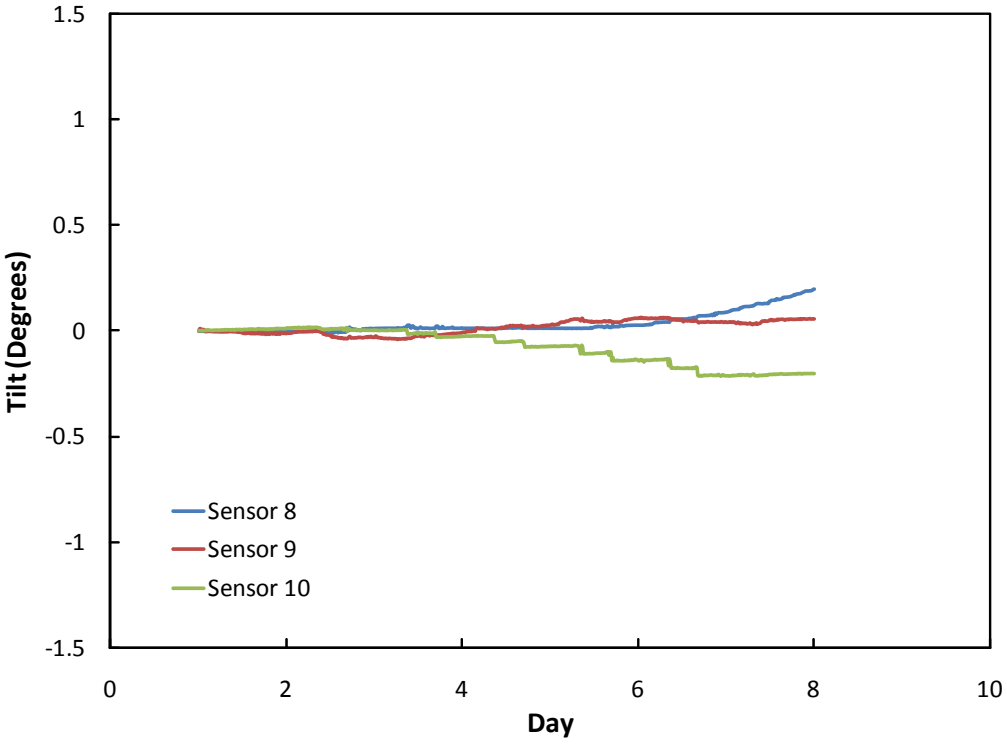

(a)

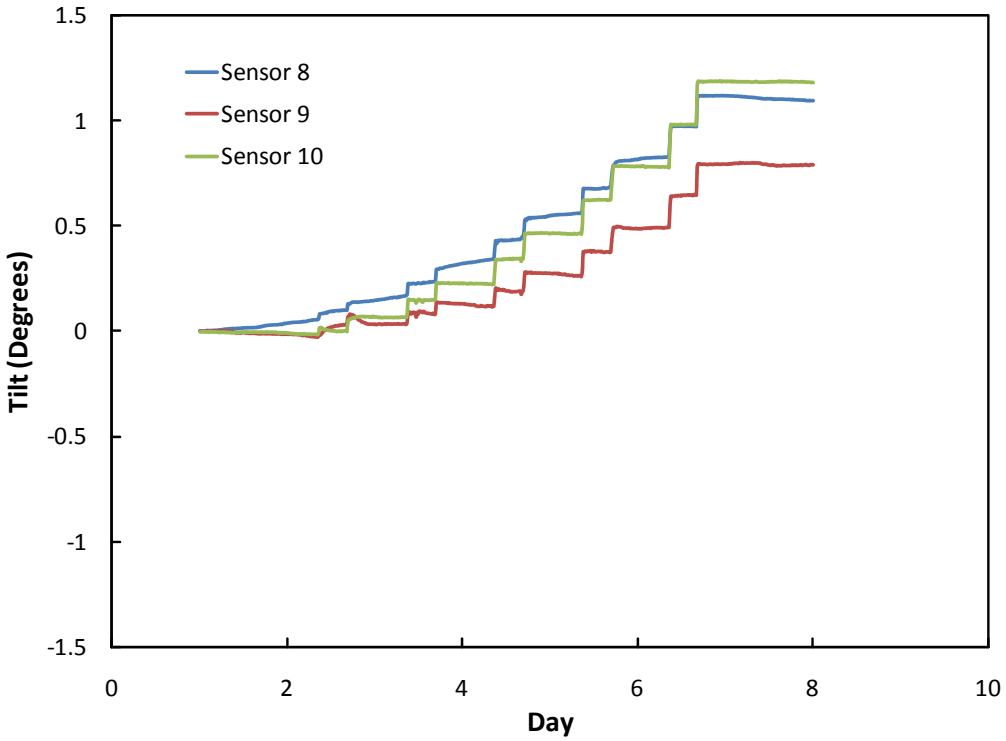

(b)

Figure 5-13. Output from x-axis (a) and y-axis (b) of sensors on superstructure.

From Figure 5-13, it can be seen that the movement was mostly directed along the y-axis of the sensors. The sensor outputs were then used in order to determine the movement of the bridge pier, specifically the displacement of the superstructure. Figure 5-14 shows the applied movements as well as those that were identified using the fuzzy threshold applied to the superstructure array of sensors.

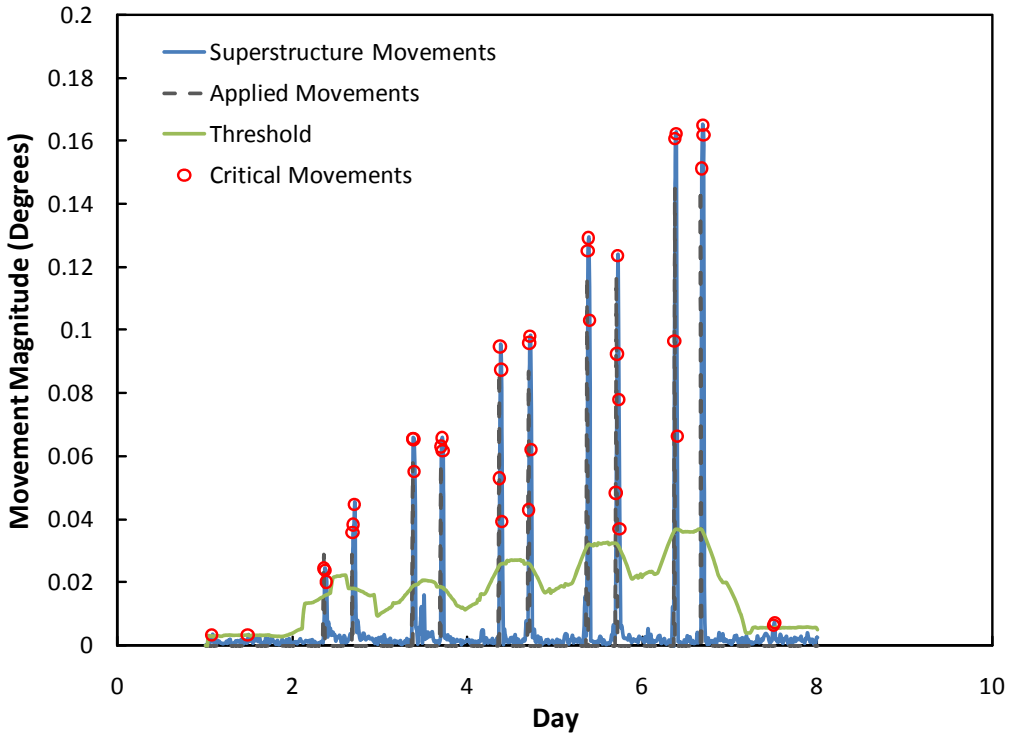

Figure 5-14. Superstructure displacements identified with post-processing algorithms.

Figure 5-14 shows the application of the fuzzy threshold on the output from the superstructure array. The directions of the movements circled in red were then checked for validity. Below are the results as reported to the user.

Critical movement occurred for a 1 hour period at..06-09-008 08:45:0
Superstructure moved..0.024349 degrees in the direction x=-0.10498, y=0.99447
Critical movement occurred for a 1 hour period at..06-09-008 16:45:0
Superstructure moved..0.038356 degrees in the direction x=0.064468, y=0.99792
Critical movement occurred for a 1 hour period at..06-10-008 09:00:0
Superstructure moved..0.06576 degrees in the direction x=-0.028669, y=0.99959
Critical movement occurred for a 1 hour period at..06-10-008 17:00:0
Superstructure moved..0.065843 degrees in the direction x=-0.073935, y=0.99726
Critical movement occurred for a 1 hour period at..06-11-008 09:00:0
Superstructure moved..0.094927 degrees in the direction x=-0.10768, y=0.99419
Critical movement occurred for a 1 hour period at..06-11-008 17:15:0
Superstructure moved..0.098092 degrees in the direction x=-0.06341, y=0.99799
Critical movement occurred for a 1 hour period at..06-12-008 09:15:0
Superstructure moved..0.12937 degrees in the direction x=-0.13763, y=0.99048
Critical movement occurred for a 1 hour period at..06-12-008 17:15:0

Superstructure moved..0.12376 degrees in the direction x=-0.11526, y=0.99333
Critical movement occurred for a 1 hour period at..06-13-008 09:00:0
Superstructure moved..0.16087 degrees in the direction x=-0.01676, y=0.99986
Critical movement occurred for a 1 hour period at..06-13-008 16:30:0
Superstructure moved..0.16516 degrees in the direction x=-0.10265, y=0.99472

Table 5-4 shows the time and magnitude of the applied and measured displacements.

Table 5-4. Applied and measured movements from vertical displacement test.

Movement	Time		Pier Displacement (in)		Change in Tilt (degrees)		Error (%)
	Applied	Measured	Applied	Measured	Applied	Measured	
1	6/9/08 8:30 AM	6/9/08 8:45 AM	0.045 ± 0.011	0.037	0.029 ± 0.007	0.024	20.8
2	6/9/08 4:20 PM	6/9/08 4:45 PM	0.045 ± 0.011	0.059	0.029 ± 0.007	0.038	23.7
3	6/10/08 8:45 AM	6/10/08 9:00 AM	0.091 ± 0.011	0.103	0.058 ± 0.007	0.066	12.1
4	6/10/08 4:30 PM	6/10/08 5:00 PM	0.091 ± 0.011	0.103	0.058 ± 0.007	0.066	12.1
5	6/11/08 8:35 AM	6/11/08 9:00 AM	0.136 ± 0.011	0.148	0.087 ± 0.007	0.095	8.4
6	6/11/08 4:40 PM	6/11/08 5:15 PM	0.136 ± 0.011	0.153	0.087 ± 0.007	0.098	11.2
7	6/12/08 8:40 AM	6/12/08 9:15 AM	0.182 ± 0.011	0.202	0.117 ± 0.007	0.129	9.3
8	6/12/08 4:45 PM	6/12/08 5:15 PM	0.182 ± 0.011	0.194	0.117 ± 0.007	0.124	5.6
9	6/13/08 8:40 AM	6/13/08 9:00 AM	0.227 ± 0.011	0.251	0.145 ± 0.007	0.161	9.9
10	6/13/08 4:00 PM	6/13/08 4:30 PM	0.227 ± 0.011	0.258	0.145 ± 0.007	0.165	12.1

As shown in Table 5-4, every movement was detected by the system and measured within a 25% error. It is worth noting that, in general, as the applied movements increase in magnitude, the error in the measurements decreases, as expected. The times of detection were all within 45 minutes of occurrence. In addition, the smallest displacement tested, 0.045 ± 0.011 inches corresponding to 0.029 ± 0.007 degree change in tilt of the superstructure sensors for the test bridge, was identifiable with the system. Overall, the test was successful in verifying the effectiveness of the superstructure array and the corresponding algorithms.

5.6. Embedded Sensor Test

The testing of the embedded sensor consisted of a long-term stationary drift test and a tilt test. The results of the drift/noise test were better than expected. Figure 5-15 shows the x-axis and y-axis outputs of the embedded sensor relative to the board-mounted sensors.

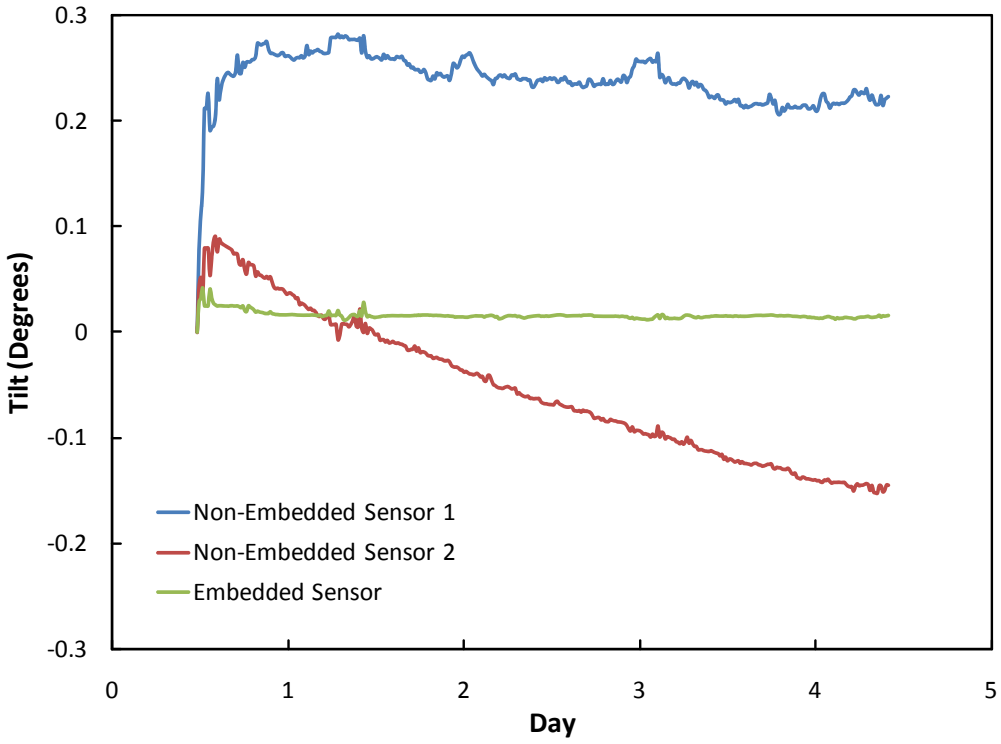

(a)

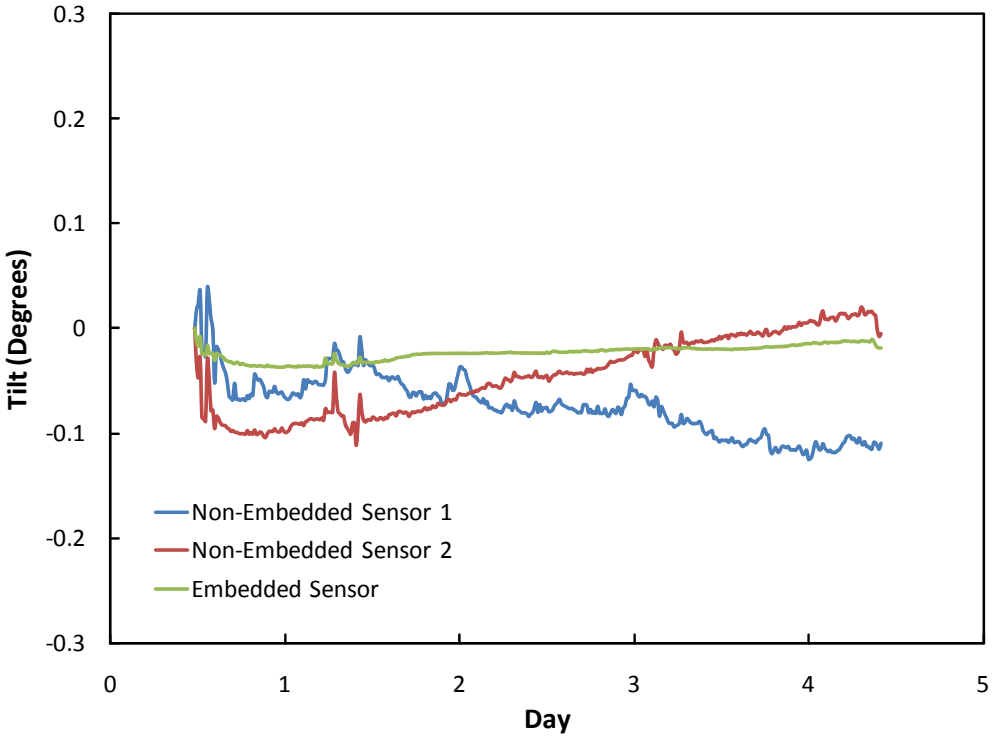

(b)

Figure 5-15. Output from x-axis (a) and y-axis (b) of embedded and non-embedded sensors.

As shown, the noise and drift level of the embedded sensor is significantly lower than that from the non-embedded sensors. This is due to the sensor not being affected by the warm-up of electronic components typical of the board-mounted configuration. The thermal environment when grouted into the concrete is very stable, leading to reduced noise and drift.

The second portion of the test was a tilt test, in which the block was tilted incrementally using wooden wedges. Table 5-5 shows the resulting movement magnitudes for both the embedded and non-embedded sensors as well as the percent

difference between the two. The results for the non-embedded sensors are the average of the two non-embedded sensors' outputs.

Table 5-5. Movement magnitudes for embedded sensor test.

Movement	Movement Magnitude (degrees)		Percent Difference
	non-embedded	embedded	
1	1.830	1.797	1.83%
2	1.753	1.784	1.80%
3	1.560	1.602	2.68%
4	1.570	1.520	3.16%
5	2.601	2.505	3.69%
6	2.373	2.319	2.26%
7	1.844	1.880	1.98%
8	1.592	1.549	2.69%
9	1.779	1.778	0.01%
10	1.704	1.667	2.21%

As Table 5-5 indicates, the difference between the embedded and non-embedded sensors for every movement was less than 3.69%. Thus, it can be concluded that the embedded sensor is consistent with non-embedded sensors.

In addition to the movement magnitudes, the direction results were also of interest. Table 5-6 shows the unit directions calculated from each motion during the embedded sensor test. The table shows the results from both non-embedded sensors, which are mounted directly on the surface of the block and the detached sensor that is embedded in concrete.

Table 5-6. Unit directions for embedded sensor test.

Movement	Movement Unit Direction (<x,y>)		
	non-embedded 1	non-embedded 2	embedded
1	<-0.970,0.243>	<-0.957,-0.291>	<-0.997,-0.075>
2	<-0.976,0.220>	<-0.944,-0.331>	<-0.996,-0.093>
3	<-0.978,0.210>	<-0.943,-0.334>	<-0.996,-0.089>
4	<-0.984,0.177>	<-0.973,-0.232>	<-0.996,-0.090>
5	<-0.998,0.055>	<-0.963,-0.270>	<-0.996,-0.093>
6	<1.000,-0.029>	<0.966,0.257>	<0.996,0.092>
7	<0.987,-0.158>	<0.964,0.265>	<0.996,0.088>
8	<0.977,-0.213>	<0.963,0.269>	<0.996,0.087>
9	<0.976,-0.219>	<0.940,0.341>	<0.996,0.092>
10	<0.972,-0.235>	<0.956,0.294>	<0.998,0.070>

During the test, the first five movements tilted the block in one direction, while the next five movements returned it to its initial position. Thus, the different signs on the last five movements are as expected. In addition to the embedded sensor results being more aligned with its axis, in other words, closer to <1.000, 0>, the results are also much more consistent than those from the non-embedded sensors. The variability in the non-embedded sensors, resulting from their placement on pins as well as other outside sources of movement, is not an issue for the embedded sensor. Thus, due to its consistency in reporting the movement magnitude as well as its direction, it appears that embedding the sensors into the concrete is an excellent installation technique that will be utilized in the field system.

6: Conclusion

6.1. Conclusion

Scour and other natural hazards have the potential to undermine the stability of bridge piers. The goal of this research was to develop and implement a system of tilt sensors capable of monitoring the long-term motion of bridge piers. Motion of bridge piers can result from scour, subsurface erosion, bearing malfunctions, and other unexpected events. In order to monitor these motions and detect motions that could be problematic to the bridge stability, a system of low-cost tilt sensors has been developed to monitor the rotation of the bridge pier as well as its vertical displacement.

Initial tests were completed in order to determine sensor characteristics such as calibration factors, temperature compensation factors, resolution, and drift effects. Algorithm development included utilizing multi-sensor reasoning in order to program initial filtration, calibration and temperature compensation, movement computation, determination of sensor consistency, sensor correlation, and critical movement identification. Within algorithm development, an initial filter was developed in order to eliminate noise spikes that, if left untreated, would result in inaccurate movement computations. Calibration and temperature compensation were completed in order to convert the voltage output into units of degrees. Movements were computed over several

different time integrals in the movement computation algorithms in order that the system can detect instantaneous events such as scour, as well as long-term gradual movements due to subsurface erosion or locked bearings. Because of sensor redundancy in the system, sensor consistency algorithms were developed in order to identify and disregard failed sensors without inhibiting the effectiveness of the system. In addition, the placement of sensors in arrays allows for a more accurate model of the pier movement to be determined through sensor correlation. Finally, critical movement identification algorithms have been developed in order to pinpoint the movements that require notification.

In order to verify the ability and accuracy of the tilt system and corresponding algorithms, several laboratory tests were conducted using a custom test bridge and data acquisition system. Results have shown the following

- The system is capable of effectively detecting 0.0265° ± 0.0132° pier movements within 45 minutes of their occurrence.
- The post-processing algorithms are fully capable of measuring and reporting 3-dimensional rotations of the bridge pier.
- The multi-sensor system is much better in terms of signal-to-noise ratio and deviation from the mean than a system utilizing single sensors.
- The sensor array on the superstructure can pinpoint displacements as small as 0.045 ± 0.011 inches for the test bridge setup.
- Embedded sensors have reduced noise and drift when compared with non-embedded sensors and accurately detect rotations with more consistent directional output.

6.2. Future Work

Appropriate constant thresholds need to be integrated into the program. Currently, a program capable of determining adequate constant threshold values has been completed. This program utilizes an initial set of data from an initial installation period on each individual bridge in order to compute the required thresholds. Thus, upon installation in the field, adequate thresholds values for the bridge at hand will be used in post-processing.

In addition, more work is required in order to verify the program. Model data will be required in order to test the program's ability to detect long-term gradual movements. In addition, data that exhibits the diurnal temperature changes expected in the field is also needed in order to verify that the program is capable of isolating unusual or critical movements from normal temperature related movements. This data will either be modeled or replicated using the test bridge.

Once programming and verification are complete, a field system will be developed, including the enclosures, software and installation scheme for the sensors. This field system will be implemented on a bridge in New York State for final testing.

Appendix A. Calibration Numbers and Graphs

Table A-1. Scale factors from the calibration of Sensors 1-10, x and y-axis.

	mV/arcmin		mV/degree	
Sensor	**X**	**Y**	**X**	**Y**
1	1.568	1.516	94.07	90.94
2	1.588	1.443	95.31	86.61
3	1.525	1.576	91.47	94.56
4	1.561	1.448	93.67	86.89
5	1.661	1.733	99.66	103.97
6	1.533	1.496	91.98	89.78
7	1.519	1.533	91.13	91.98
8	1.233	1.615	73.99	96.88
9	1.638	1.535	98.30	92.09
10	1.510	1.503	90.62	90.16

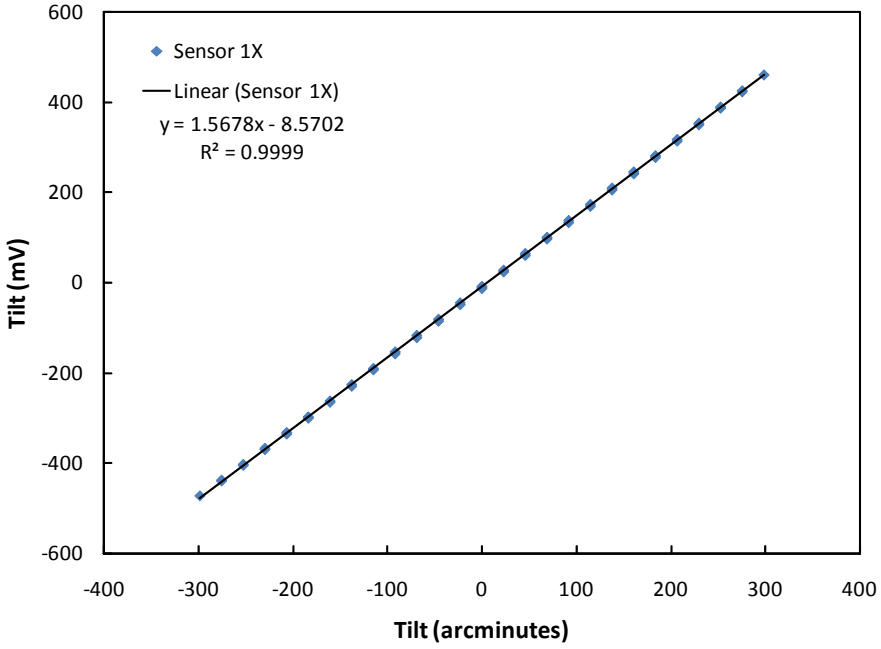

Figure A-1. Graph showing the calibration for Sensor 1, x-axis.

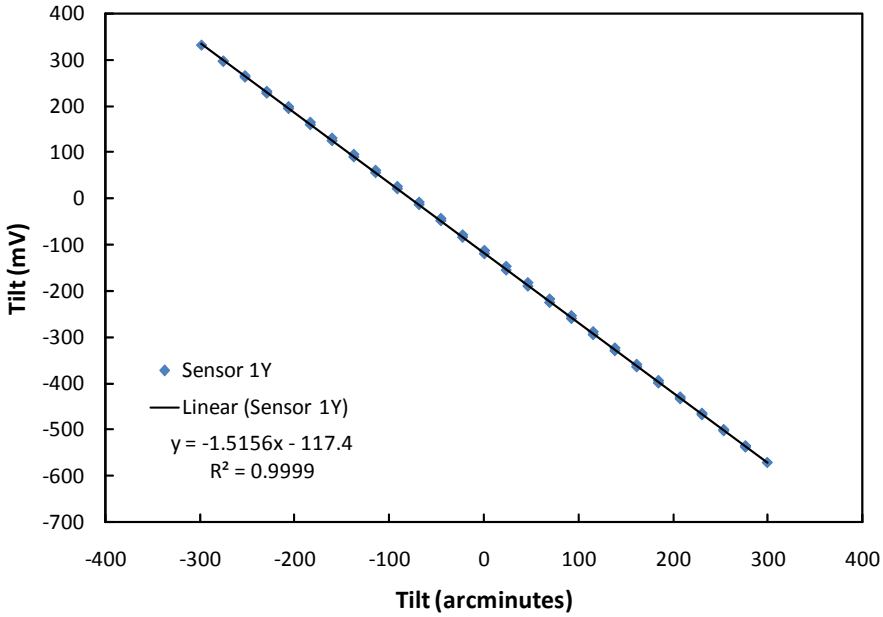

Figure A-2. Graph showing the calibration for Sensor 1, y-axis.

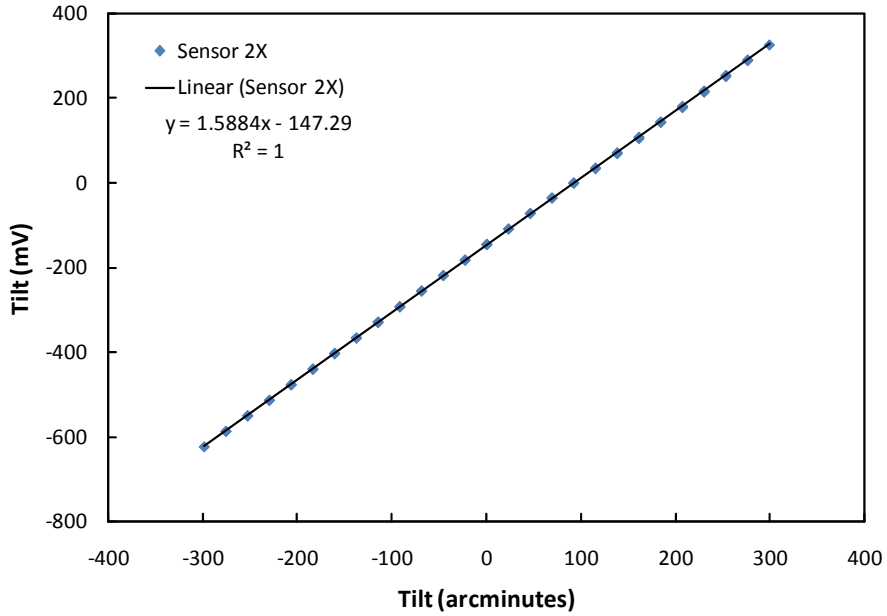

Figure A-3. Graph showing the calibration for Sensor 2, x-axis.

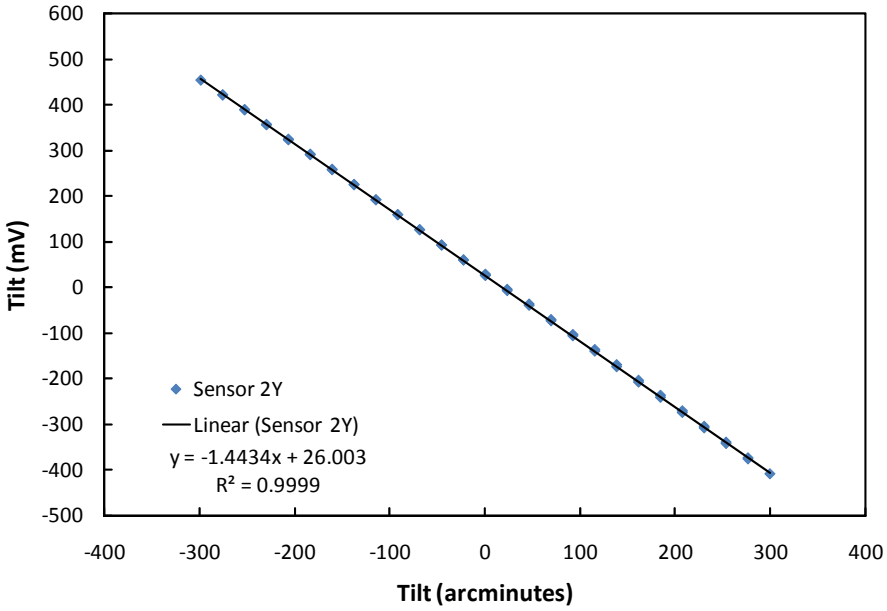

Figure A-4. Graph showing the calibration for Sensor 2, y-axis.

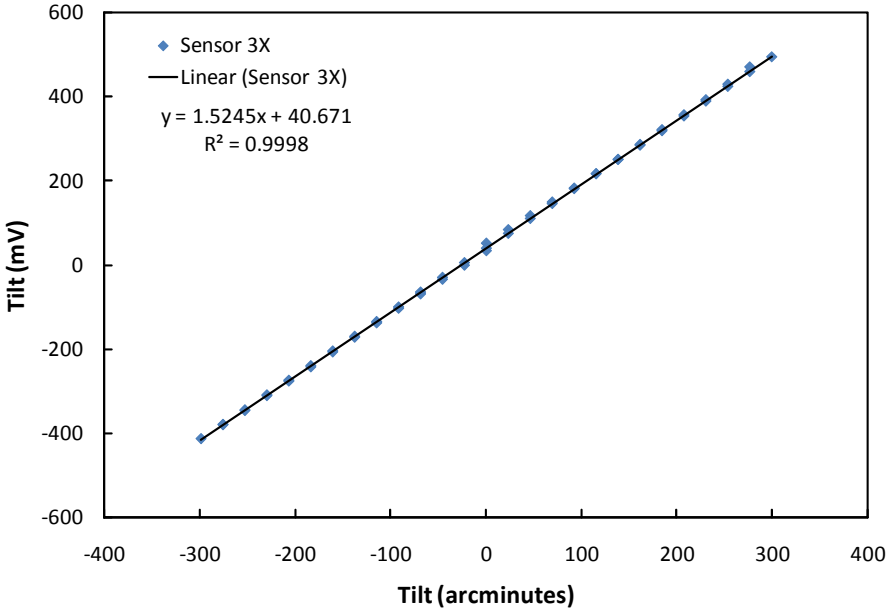

Figure A-5. Graph showing the calibration for Sensor 3, x-axis.

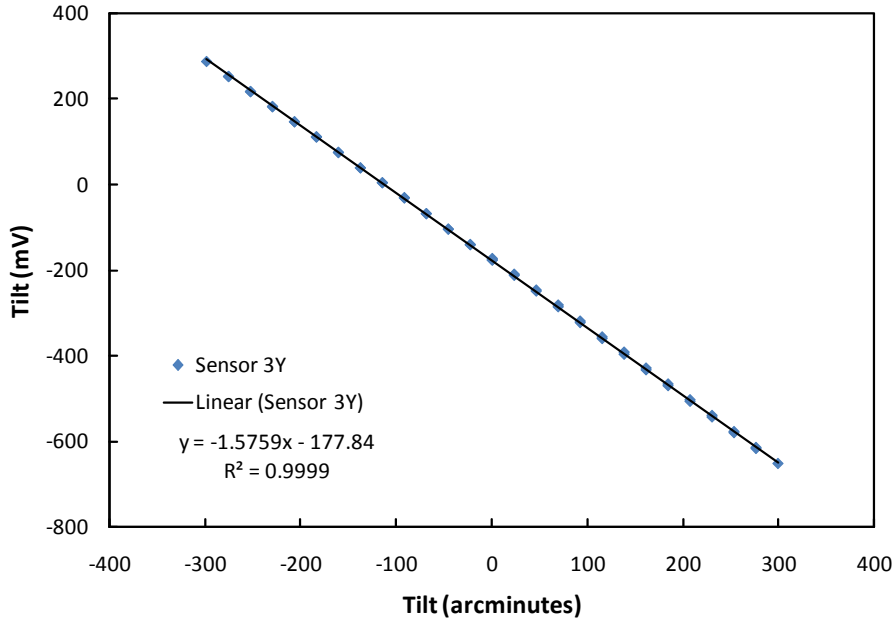

Figure A-6. Graph showing the calibration for Sensor 3, y-axis.

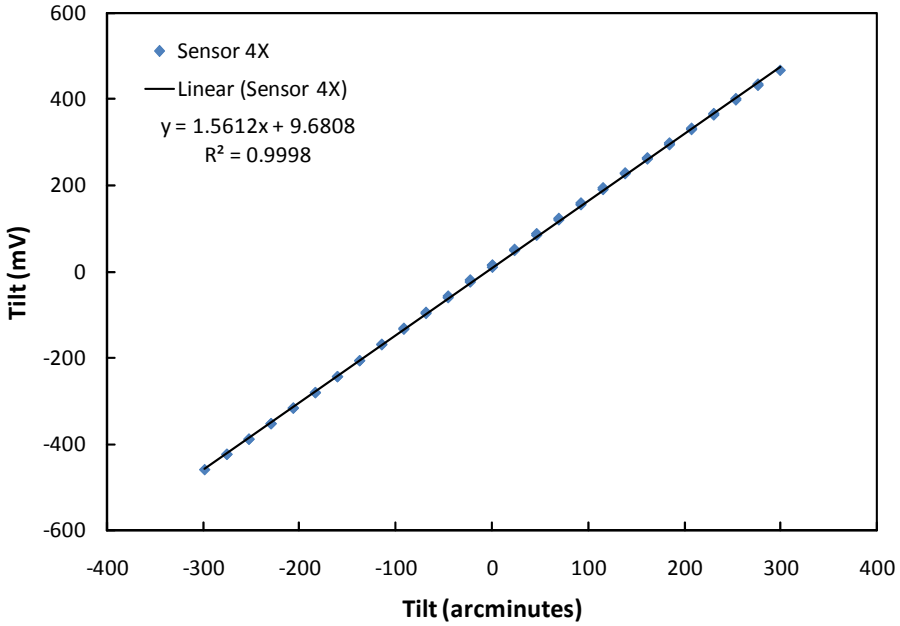

Figure A-7. Graph showing the calibration for Sensor 4, x-axis.

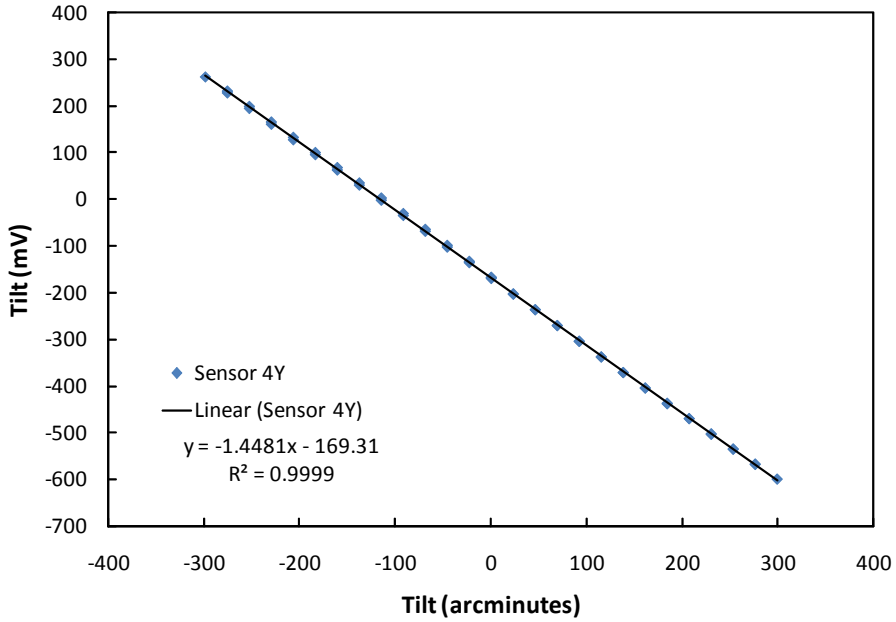

Figure A-8. Graph showing the calibration for Sensor 4, y-axis.

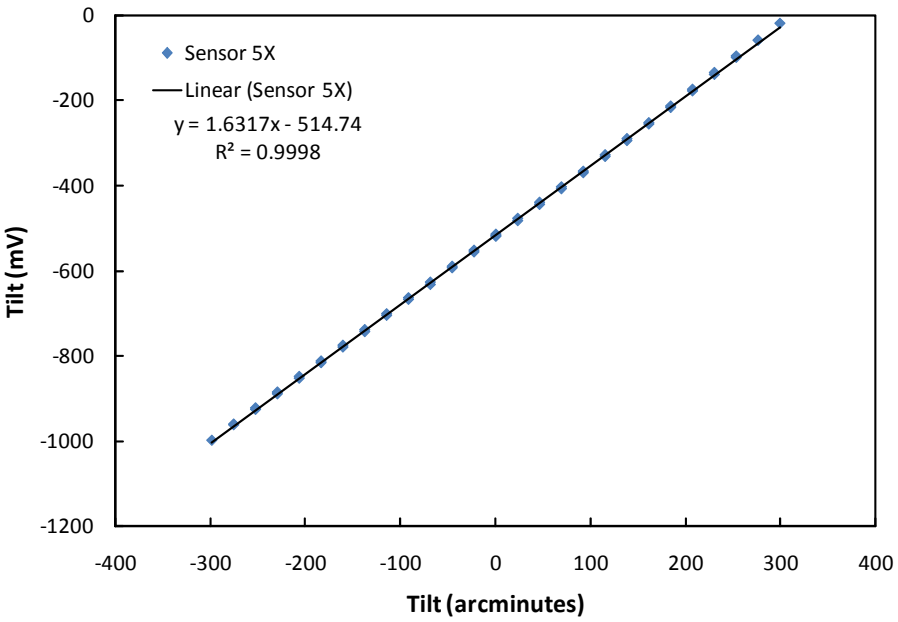

Figure A-9. Graph showing the calibration for Sensor 5, x-axis.

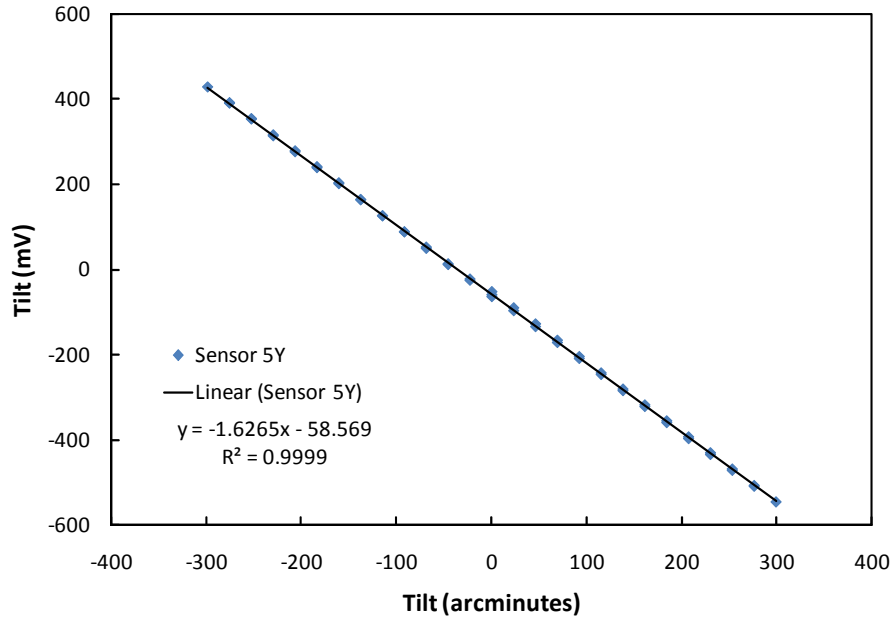

Figure A-10. Graph showing the calibration for Sensor 5, y-axis.

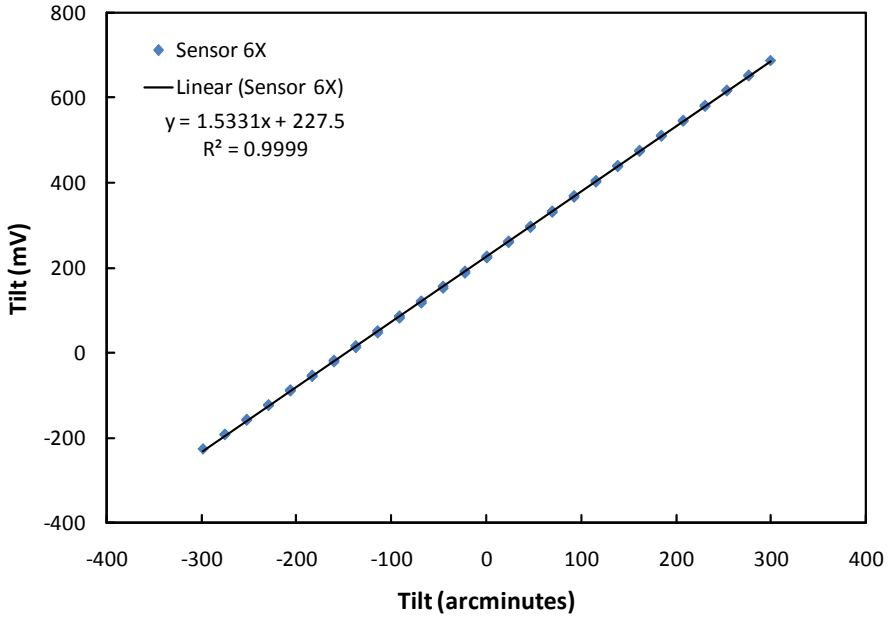

Figure A-11. Graph showing the calibration for Sensor 6, x-axis.

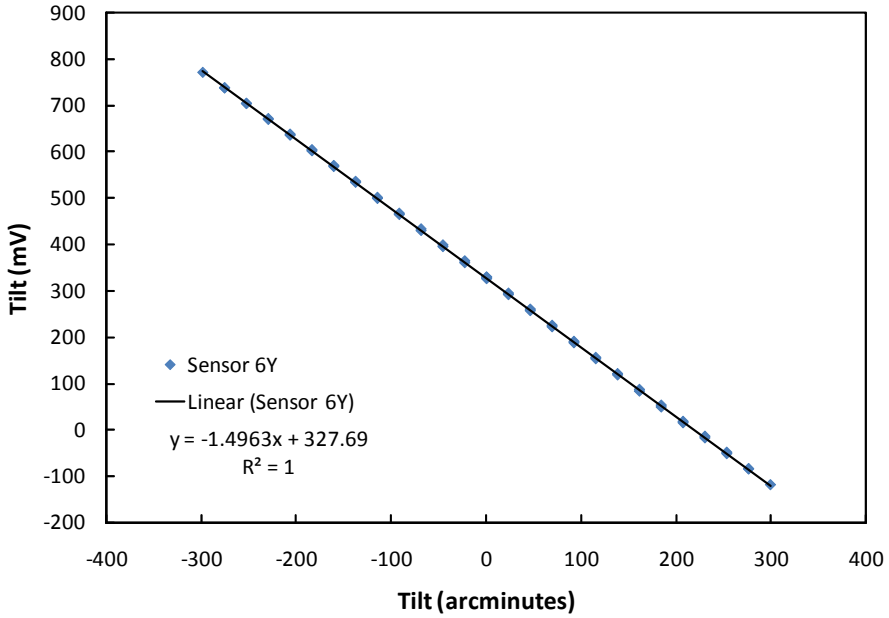

Figure A-12. Graph showing the calibration for Sensor 6, y-axis.

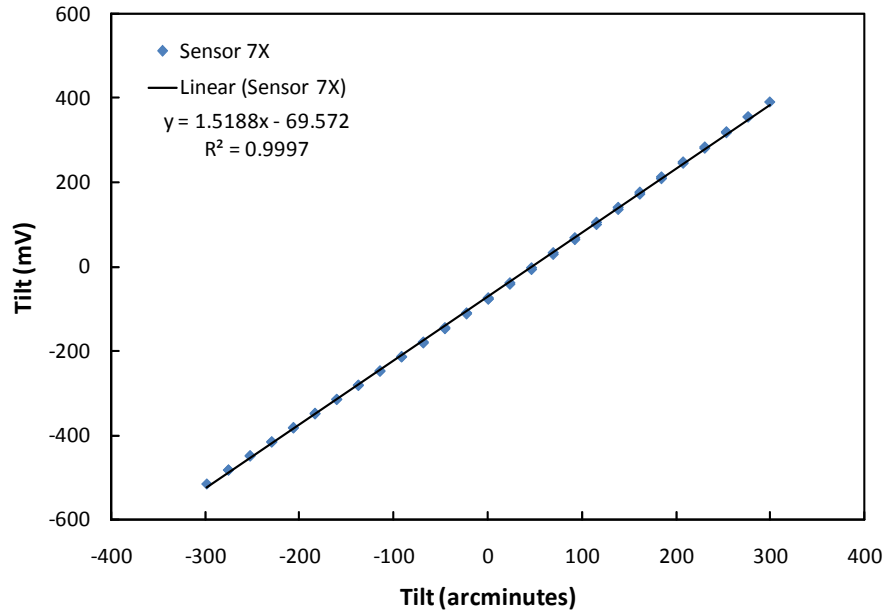

Figure A-13. Graph showing the calibration for Sensor 7, x-axis.

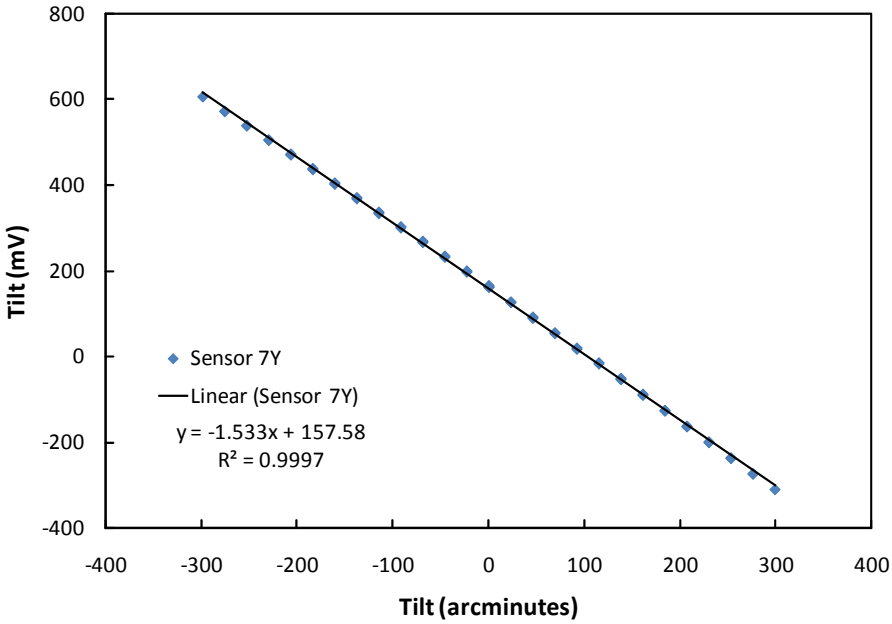

Figure A-14. Graph showing the calibration for Sensor 7, y-axis.

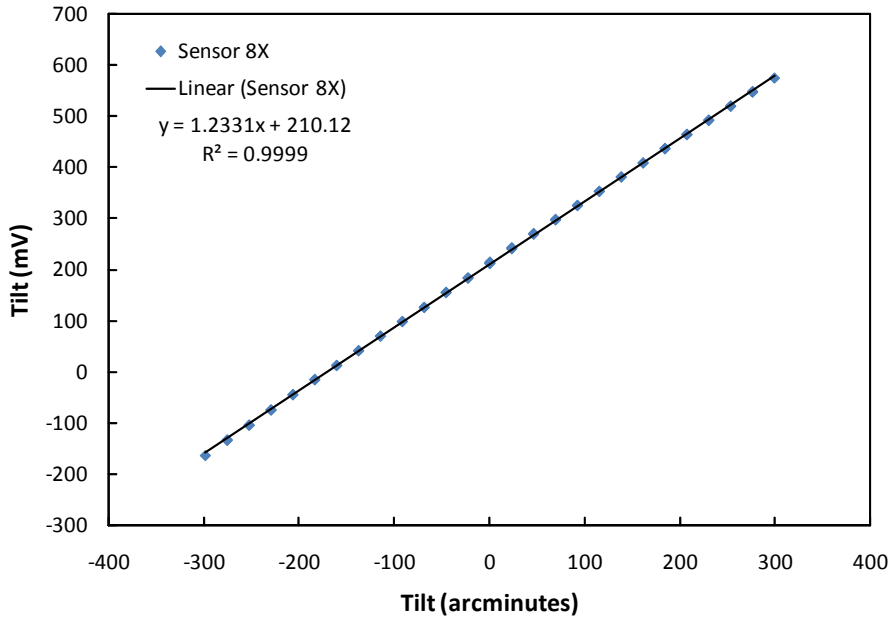

Figure A-15. Graph showing the calibration for Sensor 8, x-axis.

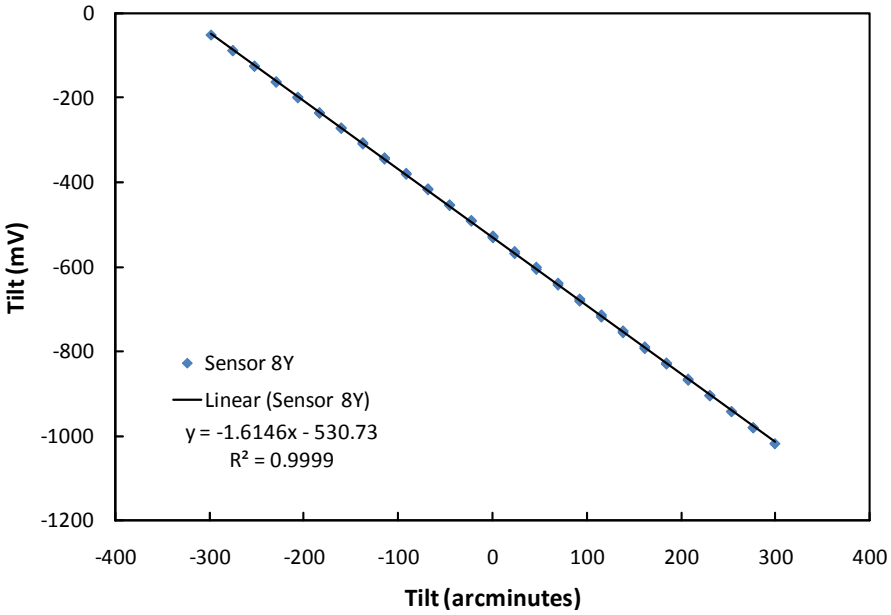

Figure A-16. Graph showing the calibration for Sensor 8, y-axis.

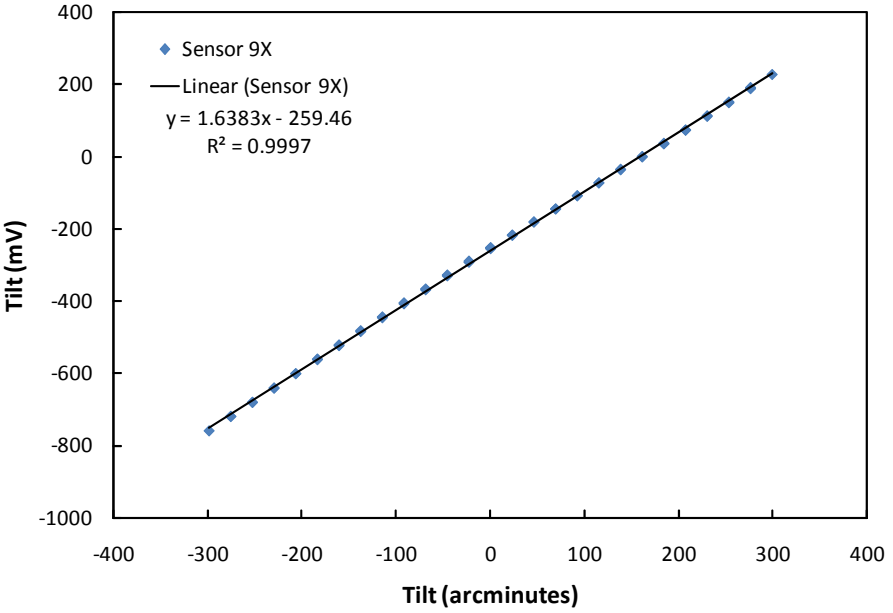

Figure A-17. Graph showing the calibration for Sensor 9, x-axis.

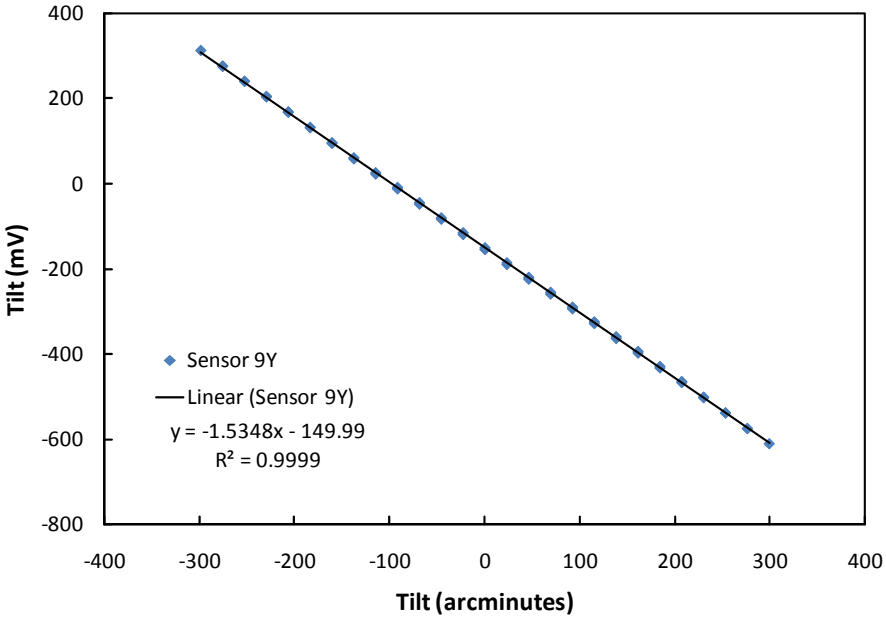

Figure A-18. Graph showing the calibration for Sensor 9, y-axis.

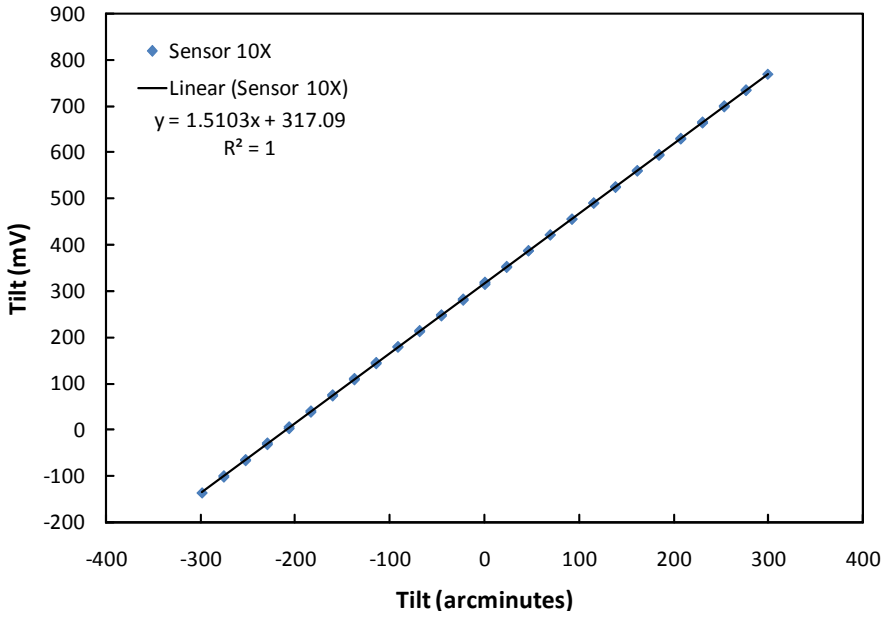

Figure A-19. Graph showing the calibration for Sensor 10, x-axis.

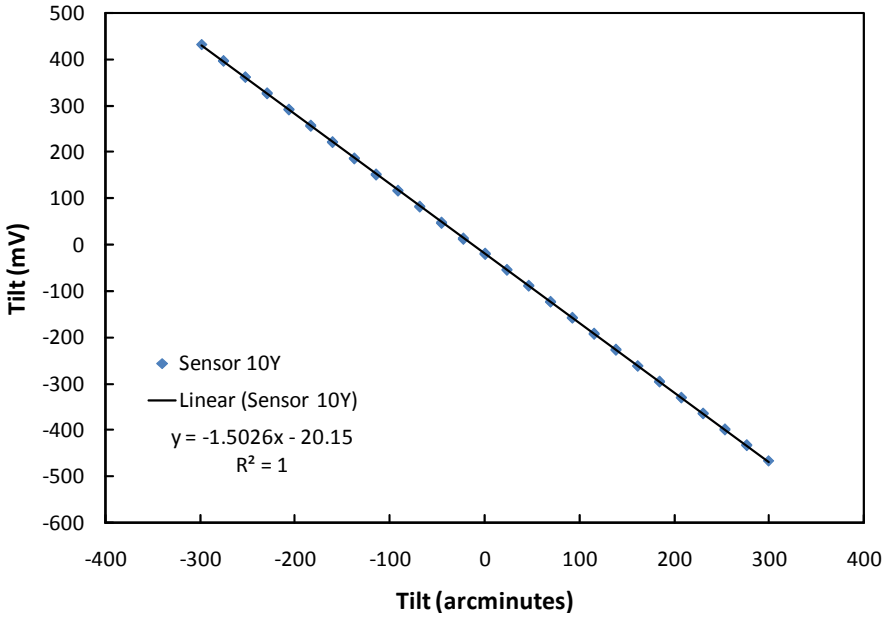

Figure A-20. Graph showing the calibration for Sensor 10, y-axis.

Appendix B. Temperature Compensation Data

Table B-1. X-axis sensor output for x-axis calibration at 20°C.

	Tilt (mV)				
Tilt (arcmin)	**Sensor 1**	**Sensor 2**	**Sensor 3**	**Sensor 4**	**Sensor 5**
276	348.582	478.826	108.995	-1535.592	392.910
207	236.422	376.186	16.044	-1683.169	289.755
138	125.298	272.491	-77.405	-1812.258	189.233
69	14.277	168.880	-172.775	-1928.747	88.425
0	-95.627	65.702	-269.341	-2024.008	-8.696
-69	-208.576	-39.285	-366.902	-2117.325	-118.173
-138	-324.431	-146.742	-464.560	-2208.104	-212.571
-207	-434.466	-255.529	-562.903	-2295.339	-320.414
-276	-544.576	-366.547	-661.776	-2381.459	-432.024

Table B-2. Y-axis sensor output for x-axis calibration at 20°C.

	Tilt (mV)				
Tilt (arcmin)	**Sensor 1**	**Sensor 2**	**Sensor 3**	**Sensor 4**	**Sensor 5**
276	78.992	89.177	-65.288	202.015	1182.450
207	76.565	93.973	-56.649	181.820	1188.362
138	74.932	99.402	-49.447	149.871	1186.354
69	73.547	105.010	-42.716	129.499	1176.911
0	69.939	111.651	-36.550	119.451	1167.127
-69	65.488	118.557	-29.480	107.416	1163.589
-138	61.561	126.268	-22.123	94.916	1151.896
-207	61.550	133.765	-12.471	83.478	1150.412
-276	61.287	141.260	-4.272	75.685	1150.967

Table B-3. X-axis sensor output for x-axis calibration at 30°C.

	Tilt (mV)				
Tilt (arcmin)	**Sensor 1**	**Sensor 2**	**Sensor 3**	**Sensor 4**	**Sensor 5**
-276	-574.337	-377.534	-646.290	-2321.652	-448.021
-207	-461.971	-270.714	-551.639	-2240.778	-337.518
-138	-341.822	-161.149	-457.484	-2146.359	-241.121
-69	-217.872	-52.905	-356.649	-2059.444	-126.948
0	-100.717	53.272	-253.509	-1972.852	-12.713
69	13.734	156.914	-149.140	-1867.023	91.938
138	135.490	257.046	-40.549	-1699.287	194.366
207	248.869	362.630	68.133	-1576.596	300.208
276	364.592	469.598	157.016	-1424.631	409.718

Table B-4. Y-axis sensor output for x-axis calibration at 30°C.

	Tilt (mV)				
Tilt (arcmin)	**Sensor 1**	**Sensor 2**	**Sensor 3**	**Sensor 4**	**Sensor 5**
276	62.216	126.616	-11.166	50.477	1050.859
207	68.984	121.782	-20.356	59.764	1058.469
138	68.641	114.567	-21.002	69.330	1052.708
69	77.169	108.553	-30.268	80.104	1062.251
0	77.823	100.664	-40.829	92.640	1069.018
-69	81.234	95.187	-52.685	106.411	1071.932
-138	82.787	86.710	-58.126	129.368	1042.828
-207	78.697	82.270	-74.145	156.147	1058.238
-276	86.288	80.075	-75.276	179.317	1074.404

Table B-5. X-axis sensor output for x-axis calibration at 40°C.

	Tilt (mV)				
Tilt (arcmin)	**Sensor 1**	**Sensor 2**	**Sensor 3**	**Sensor 4**	**Sensor 5**
276	375.743	469.006	177.528	-1209.809	395.684
207	260.884	373.270	77.074	-1388.152	292.727
138	150.004	268.881	-22.775	-1525.679	188.700
69	41.498	161.875	-128.297	-1650.627	79.159
0	-64.929	51.188	-231.312	-1765.786	-20.345
-69	-175.166	-49.247	-327.213	-1858.201	-125.445
-138	-292.021	-155.081	-425.547	-1953.496	-236.230
-207	-416.468	-251.963	-524.020	-2032.713	-343.922
-276	-519.252	-361.234	-638.425	-2132.415	-450.006

Table B-6. Y-axis sensor output for x-axis calibration at 40°C.

	Tilt (mV)				
Tilt (arcmin)	**Sensor 1**	**Sensor 2**	**Sensor 3**	**Sensor 4**	**Sensor 5**
276	80.535	70.326	-67.803	126.539	888.497
207	83.307	74.848	-56.670	119.363	887.466
138	89.850	78.456	-53.904	96.672	884.063
69	86.589	82.741	-48.174	69.739	875.986
0	85.432	87.260	-34.068	50.644	871.959
-69	81.782	92.976	-25.535	43.271	863.230
-138	74.672	101.476	-21.030	33.584	851.823
-207	66.491	107.160	-12.498	26.469	835.616
-276	78.840	114.928	-7.734	16.449	831.331

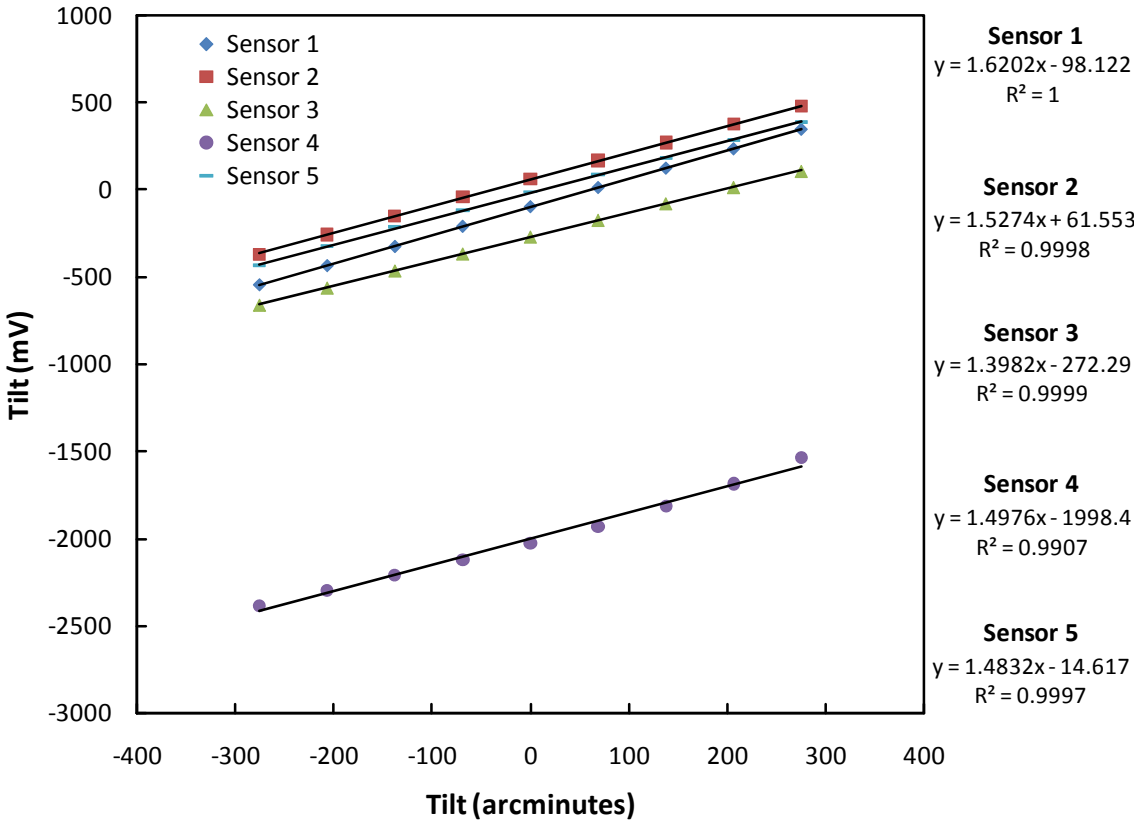

Figure B-1. Graph showing calibration of Sensors 1-5, x-axis at 20°C.

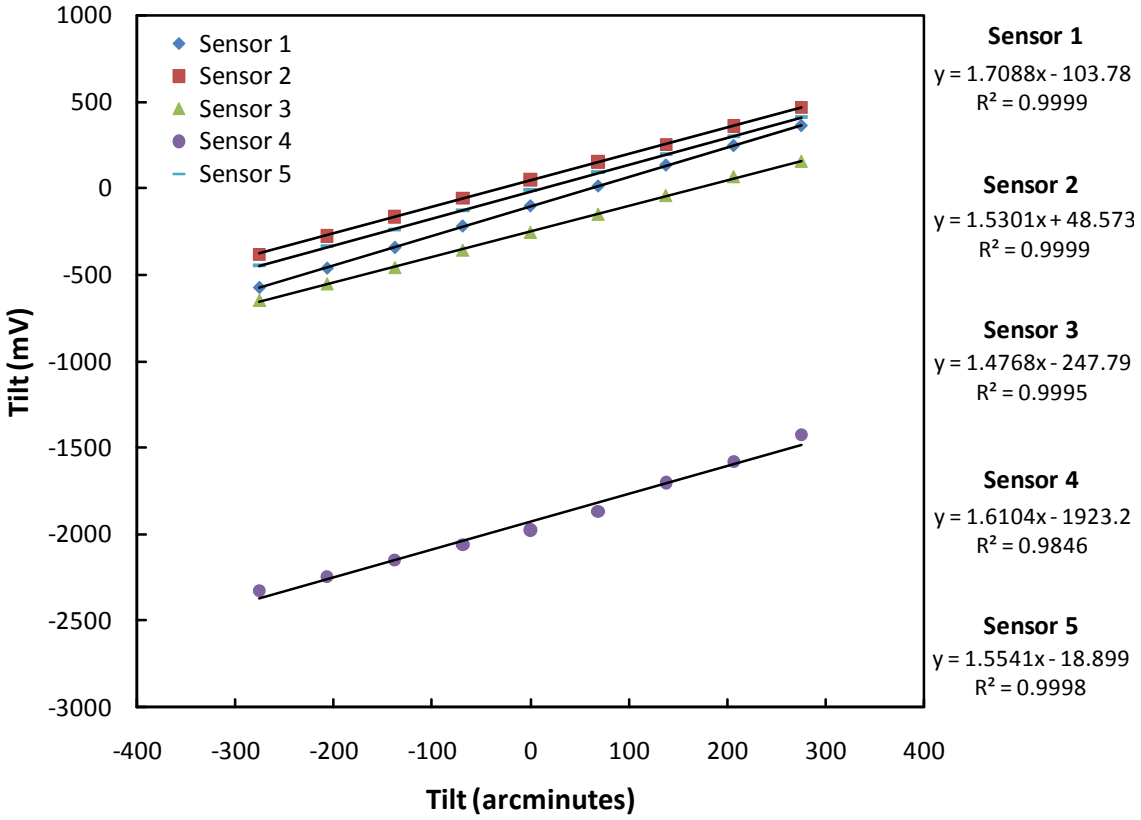

Figure B-2. Graph showing calibration of Sensors 1-5, x-axis at 30°C.

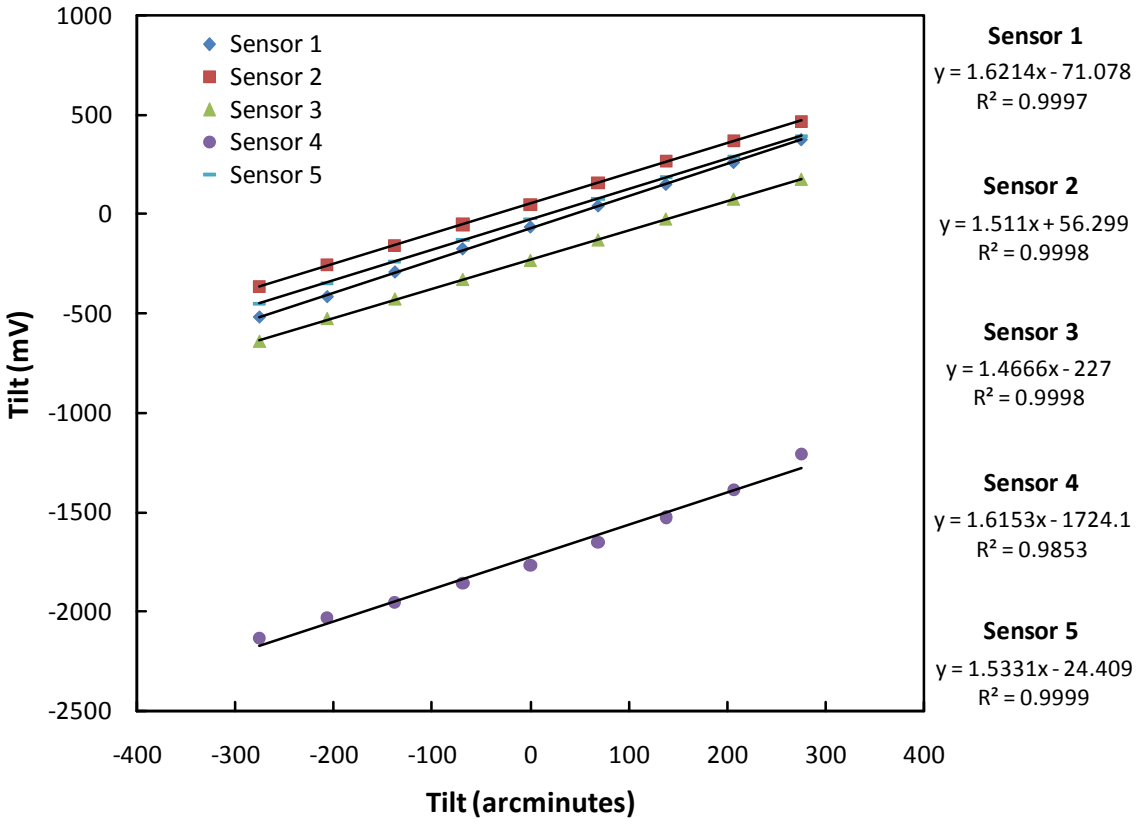

Figure B-3. Graph showing calibration of Sensors 1-5, x-axis at 40°C.

Appendix C. Data from Stationary Drift Tests

Table C-1. Drift per day in mV for Sensors 1-10, x-axis. Daily initial and final half hour averages are shown along with their difference.

		Sensor 1	Sensor 2	Sensor 3	Sensor 4	Sensor 5	Sensor 6	Sensor 7	Sensor 8	Sensor 9	Sensor 10
Day 1	initial	-537.963	-341.647	-663.878	-2356.485	-461.991	215.587	-498.256	435.204	-509.971	465.399
	final	-542.482	-349.675	-670.849	-2335.365	-470.927	219.271	-485.086	440.150	-516.868	485.728
	difference	-4.519	-8.028	-6.972	21.120	-8.936	3.685	13.169	4.946	-6.897	20.329
Day 2	initial	-542.505	-349.766	-670.806	-2334.047	-471.377	219.271	-484.769	440.304	-516.949	485.778
	final	-544.200	-354.936	-670.417	-2328.327	-480.348	218.916	-481.372	448.194	-522.418	488.282
	difference	-1.695	-5.170	0.389	5.720	-8.972	-0.355	3.397	7.890	-5.469	2.504
Day 3	initial	-544.227	-354.958	-670.437	-2329.098	-480.480	218.902	-481.312	448.540	-522.495	488.334
	final	-545.265	-356.582	-669.998	-2329.849	-484.635	215.975	-480.316	459.975	-527.447	490.766
	difference	-1.039	-1.624	0.439	-0.751	-4.156	-2.927	0.995	11.435	-4.952	2.432
Day 4	initial	-544.115	-358.872	-669.848	-2332.080	-491.059	208.556	-486.561	452.484	-533.810	483.057
	final	-545.629	-356.803	-670.167	-2325.928	-487.268	211.670	-480.693	472.821	-533.074	490.091
	difference	-1.514	2.069	-0.320	6.153	3.791	3.114	5.868	20.336	0.736	7.034
Day 5	initial	-545.600	-356.845	-670.134	-2325.226	-487.364	211.548	-480.738	473.271	-533.076	490.276
	final	-547.084	-358.622	-671.416	-2330.395	-490.442	207.012	-481.707	485.253	-537.540	491.538
	difference	-1.485	-1.777	-1.281	-5.170	-3.078	-4.536	-0.969	11.982	-4.464	1.262
Day 6	initial	-546.998	-358.671	-671.496	-2332.054	-490.535	207.007	-481.703	485.473	-537.717	491.490
	final	-547.721	-360.437	-671.846	-2340.606	-495.642	201.516	-486.331	492.630	-545.014	488.650
	difference	-0.723	-1.765	-0.350	-8.552	-5.108	-5.490	-4.628	7.157	-7.297	-2.841
Day 7	initial	-547.763	-360.378	-671.910	-2339.312	-495.440	201.783	-486.174	493.169	-544.996	488.662
	final	-548.282	-361.509	-671.491	-2350.929	-496.451	202.847	-488.360	503.484	-548.847	491.070
	difference	-0.520	-1.130	0.419	-11.618	-1.010	1.064	-2.186	10.315	-3.850	2.407
Day 8	initial	-548.808	-360.256	-671.579	-2349.771	-493.025	206.764	-485.105	507.934	-545.669	495.217
	final	-548.934	-358.807	-670.356	-2353.573	-492.412	208.458	-485.386	516.816	-548.155	495.227
	difference	-0.126	1.449	1.223	-3.802	0.614	1.693	-0.281	8.882	-2.486	0.010
Day 9	initial	-548.984	-358.850	-670.441	-2352.900	-492.309	208.547	-485.434	516.838	-548.156	495.398
	final	-549.314	-358.704	-670.716	-2343.330	-492.786	212.976	-488.015	526.363	-552.165	498.472
	difference	-0.330	0.147	-0.275	9.570	-0.477	4.430	-2.582	9.525	-4.009	3.075
Day 10	initial	-549.275	-358.686	-670.721	-2344.008	-492.730	213.238	-488.029	526.493	-552.209	498.467
	final	-549.980	-360.760	-670.338	-2361.881	-497.075	216.553	-492.645	530.437	-559.228	493.838
	difference	-0.704	-2.074	0.383	-17.874	-4.345	3.316	-4.616	3.943	-7.019	-4.629
Day 11	initial	-550.605	-359.424	-670.289	-2359.733	-493.766	220.599	-489.368	534.590	-556.123	497.935
	final	-551.493	-359.387	-670.017	-2360.782	-494.344	230.072	-490.854	541.819	-559.209	499.154
	difference	-0.888	0.037	0.272	-1.049	-0.579	9.473	-1.486	7.229	-3.086	1.218
Day 12	initial	-551.436	-359.375	-670.141	-2361.751	-494.484	230.166	-490.807	542.603	-559.254	499.038
	final	-552.347	-359.332	-670.228	-2344.160	-494.982	240.395	-493.179	548.968	-562.010	501.256
	difference	-0.911	0.044	-0.087	17.591	-0.497	10.229	-2.371	6.364	-2.756	2.218
Day 13	initial	-551.186	-361.599	-670.019	-2348.172	-501.224	233.464	-499.315	541.344	-568.097	493.447
	final	-552.636	-359.977	-669.601	-2346.797	-505.590	247.765	-498.706	545.062	-565.331	500.274
	difference	-1.450	1.623	0.418	1.375	-4.366	14.301	0.609	3.719	2.766	6.827

Table C-2. Summarized drift per day for Sensors 1-10, x-axis (mV).

	Sensor 1	Sensor 2	Sensor 3	Sensor 4	Sensor 5	Sensor 6	Sensor 7	Sensor 8	Sensor 9	Sensor 10
Day 1	-4.519	-8.028	-6.972	21.120	-8.936	3.685	13.169	4.946	-6.897	20.329
Day 2	-1.695	-5.170	0.389	5.720	-8.972	-0.355	3.397	7.890	-5.469	2.504
Day 3	-1.039	-1.624	0.439	-0.751	-4.156	-2.927	0.995	11.435	-4.952	2.432
Day 4	-1.514	2.069	-0.320	6.153	3.791	3.114	5.868	20.336	0.736	7.034
Day 5	-1.485	-1.777	-1.281	-5.170	-3.078	-4.536	-0.969	11.982	-4.464	1.262
Day 6	-0.723	-1.765	-0.350	-8.552	-5.108	-5.490	-4.628	7.157	-7.297	-2.841
Day 7	-0.520	-1.130	0.419	-11.618	-1.010	1.064	-2.186	10.315	-3.850	2.407
Day 8	-0.126	1.449	1.223	-3.802	0.614	1.693	-0.281	8.882	-2.486	0.010
Day 9	-0.330	0.147	-0.275	9.570	-0.477	4.430	-2.582	9.525	-4.009	3.075
Day 10	-0.704	-2.074	0.383	-17.874	-4.345	3.316	-4.616	3.943	-7.019	-4.629
Day 11	-0.888	0.037	0.272	-1.049	-0.579	9.473	-1.486	7.229	-3.086	1.218
Day 12	-0.911	0.044	-0.087	17.591	-0.497	10.229	-2.371	6.364	-2.756	2.218
Day 13	-1.450	1.623	0.418	1.375	-4.366	14.301	0.609	3.719	2.766	6.827

Table C-3. Drift per day in mV for Sensors 1-10, y-axis. Daily initial and final half hour averages are shown along with their difference.

		Sensor 1	Sensor 2	Sensor 3	Sensor 4	Sensor 5	Sensor 6	Sensor 7	Sensor 8	Sensor 9	Sensor 10
Day 1	initial	61.944	146.535	0.764	29.380	1083.395	357.285	601.375	-770.387	-289.140	-64.161
	final	66.735	151.175	-0.534	54.893	1012.242	353.896	588.023	-761.802	-291.062	-64.885
	difference	4.790	4.639	-1.298	25.513	-71.153	-3.389	-13.352	8.585	-1.922	-0.724
Day 2	initial	66.735	151.140	-0.581	52.765	1011.510	353.898	587.867	-761.845	-291.073	-64.887
	final	67.354	151.483	-1.421	64.530	993.409	352.446	582.775	-769.284	-293.535	-64.286
	difference	0.619	0.344	-0.840	11.765	-18.101	-1.452	-5.092	-7.438	-2.462	0.601
Day 3	initial	67.422	151.200	-1.448	65.488	993.322	352.419	582.675	-769.557	-293.572	-64.282
	final	66.800	151.092	-2.901	70.291	987.946	349.031	580.827	-781.904	-295.145	-64.191
	difference	-0.622	-0.107	-1.453	4.803	-5.376	-3.388	-1.848	-12.347	-1.574	0.091
Day 4	initial	62.191	150.004	-3.487	69.114	981.258	347.686	580.291	-781.645	-293.926	-64.866
	final	68.008	151.179	-3.102	89.134	988.096	347.660	581.143	-797.493	-295.268	-62.957
	difference	5.817	1.174	0.385	20.020	6.839	-0.026	0.852	-15.848	-1.342	1.910
Day 5	initial	68.052	151.188	-3.090	90.460	988.450	347.633	581.191	-798.238	-295.394	-62.904
	final	69.429	152.525	-2.732	95.941	997.021	345.731	581.304	-814.699	-296.787	-62.931
	difference	1.377	1.337	0.358	5.481	8.571	-1.902	0.114	-16.461	-1.393	-0.027
Day 6	initial	69.422	152.528	-2.766	95.522	997.173	345.734	581.323	-814.911	-296.655	-62.861
	final	66.996	151.944	-3.286	102.875	1003.705	344.814	581.099	-829.576	-298.242	-63.743
	difference	-2.425	-0.584	-0.520	7.353	6.532	-0.920	-0.224	-14.665	-1.588	-0.883
Day 7	initial	67.154	151.982	-3.259	103.418	1004.184	344.898	581.203	-829.824	-298.259	-63.754
	final	66.869	152.159	-4.821	99.916	1012.344	345.044	581.435	-844.595	-300.896	-65.435
	difference	-0.284	0.177	-1.562	-3.501	8.160	0.146	0.232	-14.771	-2.636	-1.681
Day 8	initial	69.355	152.781	-4.527	100.452	1015.650	345.850	581.833	-845.195	-301.586	-65.036
	final	69.202	152.578	-5.418	106.863	1022.198	349.892	583.138	-854.367	-301.544	-63.168
	difference	-0.153	-0.203	-0.891	6.411	6.548	4.042	1.305	-9.172	0.043	1.868
Day 9	initial	69.188	152.578	-5.467	107.384	1022.264	350.021	583.107	-854.385	-301.577	-63.224
	final	69.939	153.898	-5.757	124.853	1034.389	355.847	586.192	-864.400	-301.814	-62.264
	difference	0.751	1.320	-0.290	17.469	12.124	5.826	3.085	-10.015	-0.238	0.960
Day 10	initial	70.110	153.899	-5.747	125.285	1034.581	356.034	586.239	-864.573	-301.780	-62.255
	final	68.996	154.653	-5.011	120.091	1043.410	360.659	587.397	-874.402	-302.148	-62.358
	difference	-1.114	0.754	0.736	-5.194	8.830	4.626	1.158	-9.829	-0.368	-0.104
Day 11	initial	71.632	155.263	-4.676	120.263	1046.679	361.618	587.736	-874.726	-302.834	-61.938
	final	71.754	155.389	-5.626	132.657	1057.557	367.495	588.793	-883.871	-304.551	-62.912
	difference	0.122	0.126	-0.950	12.394	10.877	5.877	1.057	-9.145	-1.716	-0.973
Day 12	initial	71.871	155.396	-5.663	132.366	1057.779	367.734	588.867	-884.480	-304.575	-62.825
	final	71.406	155.261	-6.720	152.618	1066.709	374.708	589.144	-892.719	-305.994	-63.380
	difference	-0.466	-0.135	-1.057	20.252	8.930	6.973	0.277	-8.239	-1.419	-0.555
Day 13	initial	66.743	154.119	-7.330	150.963	1061.231	373.422	588.522	-892.419	-304.650	-64.183
	final	69.515	154.649	-7.664	159.353	1086.100	382.832	592.341	-889.401	-305.272	-61.897
	difference	2.772	0.530	-0.334	8.390	24.869	9.410	3.819	3.019	-0.621	2.286

Table C-4. Summarized drift per day for Sensors 1-10, y-axis (mV).

	Sensor 1	Sensor 2	Sensor 3	Sensor 4	Sensor 5	Sensor 6	Sensor 7	Sensor 8	Sensor 9	Sensor 10
Day 1	4.790	4.639	-1.298	25.513	-71.153	-3.389	-13.352	8.585	-1.922	-0.724
Day 2	0.619	0.344	-0.840	11.765	-18.101	-1.452	-5.092	-7.438	-2.462	0.601
Day 3	-0.622	-0.107	-1.453	4.803	-5.376	-3.388	-1.848	-12.347	-1.574	0.091
Day 4	5.817	1.174	0.385	20.020	6.839	-0.026	0.852	-15.848	-1.342	1.910
Day 5	1.377	1.337	0.358	5.481	8.571	-1.902	0.114	-16.461	-1.393	-0.027
Day 6	-2.425	-0.584	-0.520	7.353	6.532	-0.920	-0.224	-14.665	-1.588	-0.883
Day 7	-0.284	0.177	-1.562	-3.501	8.160	0.146	0.232	-14.771	-2.636	-1.681
Day 8	-0.153	-0.203	-0.891	6.411	6.548	4.042	1.305	-9.172	0.043	1.868
Day 9	0.751	1.320	-0.290	17.469	12.124	5.826	3.085	-10.015	-0.238	0.960
Day 10	-1.114	0.754	0.736	-5.194	8.830	4.626	1.158	-9.829	-0.368	-0.104
Day 11	0.122	0.126	-0.950	12.394	10.877	5.877	1.057	-9.145	-1.716	-0.973
Day 12	-0.466	-0.135	-1.057	20.252	8.930	6.973	0.277	-8.239	-1.419	-0.555
Day 13	2.772	0.530	-0.334	8.390	24.869	9.410	3.819	3.019	-0.621	2.286

REFERENCES

1. Barker, R. M. *Manuals for the Design of Bridge Foundations: Shallow Foundations, Driven Piles, Retaining Walls and Abutments, Drilled Shafts, Estimating Tolerable Movements, Load Factor Design Specifications, and Commentary*. Washington, D.C.: Transportation Research Board, National Research Council, 1991.

2. Iskander, M., W. Aboumoussa, and P. Gouvin. "Instrumentation and Monitoring of a Distressed Multi-story Underground Parking Garage", *Journal of Performance of Constructed Facilities*, 15(3), August 2001.

3. Marron, D. "Remote Monitoring of Structural Stability Using Electronic Inclinometers", *Structural Materials Technology IV - An NDT Conference*, 2000.

4. Mueller, D. S. and C.R. Wagner. "Field Observations and Evaluations of Streambed Scour at Bridges", DTFH61-93-Y-00050. Washington, D.C., Federal Highway Administration, 2005.

5. Näsi, J., A. Sorsa, and K. Leiviskä. "Sensor Validation and Outlier Detection Using Fuzzy Limits", *Proceedings of the 44th IEEE Conference on Decision and Control, and the European Control Conference*, Seville, Spain, 2005.

6. NYSDOT. Structural Forensic Investigation Report: BIN 109299A, Ramp AC, Dunn Memorial Bridge Interchange. Albany, New York, 2005.

7. Pheifer, David and William B. Powell. "Sensors – The Electrolytic Tilt Sensor", *Sensors Magazine,* May 1, 2000.

8. Richardson, E. V., J. E. Pagan-Ortiz, J. D. Schall, and G. R. Price. "Monitoring and Plans for Action for Bridge Scour: Instruments and State Departments of Transportation Experiences", *9th International Bridge Management Conference, IBMC03-029*, 2003.

9. Richardson, E. V. and S. R. Davis. *Hydraulic Engineering Circular No. 18: Evaluating Scour at Bridges, Fourth Edition.* Report FHWA NHI 01-001. FHWA, U.S. Department of Transportation, 2001.

10. Schall, J. and G. Price. "Portable Scour Monitoring Equipment", *NCHRP Report 515,* 2004.

11. Schuyler, J. N. and F. Gularte. "Automated Tiltmeter Monitoring of Bridge Response To Compaction Grouting", *Proceedings of SPIE's 7th Annual International Symposium on Smart Structures and Materials*, Newport Beach, California, March 2000.

12. “Tiltmeter Temperature Coefficients: Source, Definition and Use to Improve Accuracy”, *Applied Geomechanics Inc. B-95-1005, Rev.C.* <http://www.geomechanics.com/pdf/apps/Tempco_B95_1005C.pdf>, 2008.

13. Warren, Linda P. “Stream Stability and Scour Assessment at Bridges in Massachusetts”, *U.S. Geological Survey Open-File Report 93–480*, 2007.